Johannes Gutenberg-Universität Mainz - Institut für Physik

Realization and characterization of a phase locked laser system for coherent spectroscopy of fiber-coupled cesium atoms

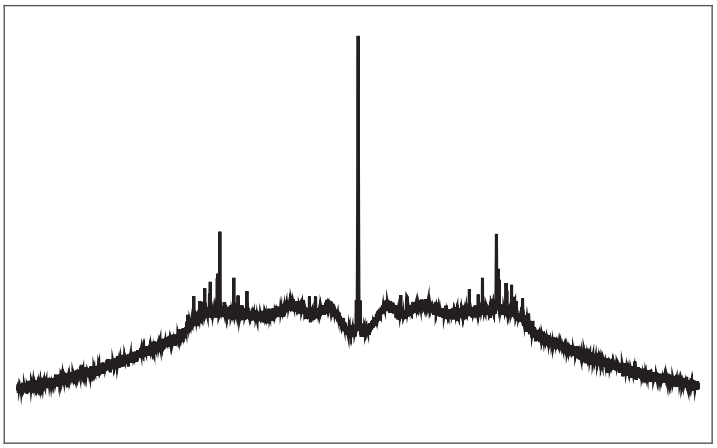

Diplomarbeit von **Melanie Müller**

Vorgelegt am **13. Juli 2010**
bei **Prof. Dr. Arno Rauschenbeutel**

JG|U
JOHANNES GUTENBERG UNIVERSITÄT MAINZ

Contents

1. Introduction

Coherent phenomena in atoms and molecules have been investigated since the invention of the laser in the early 1960's [1]. Since then the laser has become an indispensable tool in many fields of today's physics, and opened the route towards many new research areas such as laser spectroscopy and quantum optics. In the spectral range of many atomic transitions, diode lasers are especially convenient for applications in atomic spectroscopy, which is why research in modern physics laboratories cannot be imagined without them. Diode lasers are part of the electronic revolution that began in the last half of the twentieth century and still continues today. Their high reliability, the small size and the low price are the reason, why they marked a cornerstone in the development of modern communication systems and even found their way into our everyday life.
The laser became a prerequisite to study the properties of matter and its interaction with light. For a long time the resolution in optical spectroscopy was limited due to Doppler-broadening, and the introduction of nonlinear laser spectroscopy allowed to perform precision spectroscopy with a highly increased resolution. Besides the investigation of the atomic structure using high resolution spectroscopy, the laser also offers the possibility for coherent excitation of atoms. This allows one to coherently couple different atomic states, meaning that there is a definite phase relation between the atomic states induced by the laser field. Whereas in incoherent spectroscopy one measures the total intensity, i.e., the populations of the atomic states, coherent spectroscopy allows to measure the coherences of the system.
In the continuously expanding field of nonlinear spectroscopy, three level systems and their preparation in coherent superposition states attracted a lot of interest. Alzetta et. al. were the first who observed a reduction of absorption as a "dark line" in the fluorescence spectrum of sodium atoms [2]. This effect is known as coherent population trapping, a "process [which] remained a sort of amusing scientific curiosity for some time" [3]. Today this phenomenon is well understood and forms the basis for many quantum interference effects such as lasing without inversion [4]. Another one of these "strange" interactions of light with matter is that of electromagnetically induced transparency (EIT). It was Steven Harris in 1989 [4, 5] who laid the foundations of EIT, a phenomenon that causes an otherwise opaque medium to be transparent to resonant light in the presence of a second additional light field.
Experiments on coherent interaction of light with matter require the involved laser fields to be coherently coupled. This implies that their phase and frequency difference has to be stabilized to a high degree. The most versatile method for the preparation of coherent light fields is that of optical phase locking. An optical phase locked loop stabilizes the phase and frequency of a slave laser so that its phase follows that of a second master laser. The pioneering work on optical phase locked loops has been done in the 1960's [6], and they have become a well established tool to obtain phase coherent lasers, not only for the generation of coherently prepared media, but also for coherent optical communication systems, precision spectroscopy and high accurate frequency stabilization of lasers.
A three level system as it is required for EIT can be realized by many alkali atoms which provide a suitable energy level structure. Those systems form the basis for applications

such as slow light [7, 8], the storage of light pulses [9], quantum memories [10] and quantum repeater [11], which attracted a lot of interest in the last decade by many groups. An essential requirement for many of these applications is the cooling and trapping of cold atoms in order to minimize decoherences in the atomic system. A novel method is to trap atoms close to the surface of an optical nanofiber [12], which has firstly been implemented in our group [13]. The evanescent field of an ultrathin optical nanofiber is used to trap cesium atoms using a two-color dipole trap [14, 15]. This system is particular attractive for nonlinear optics such as EIT due to its high optical density and its direct integration of laser-cooled atomic ensembles within fiber networks. These outstanding properties make this system perfectly suitable for the investigation of electromagnetically induced transparency and related phenomena with fiber coupled atoms.

The focus of this work lies on the implementation of an optical phase locked loop specifically designed for coherent spectroscopy on cesium atoms using two diode lasers. The phase locked loop is characterized and analyzed in detail. Moreover, it is shown that it significantly improves the properties of the EIT signal.

The first chapter gives an introduction to coherent optics using electromagnetically induced transparency. The phenomenon of quantum interference is investigated and the optical response of an ideal three level Λ-system is determined using the density matrix. In the second chapter the general properties of diode lasers, their response to frequency modulation and the frequency stabilization of diode lasers is described. The theory of optical phase locked loops is explained in detail in chapter 3. At first the fundamental idea of optical phase locking is investigated, and afterwards a general introduction to control theory and to the characterization of phase noise is given in this chapter. The experimental realization of the optical phase locked loop is then explained in chapter 4, and the laser system is characterized according to its relative phase stability. The last chapter shows the applicability of the laser system for EIT experiments on cesium atoms, where first EIT measurements on a vapor cell are performed.

2. Coherent optics with electromagnetically induced transparency

The interaction of an atom with an incident light field is a function of the wavelength of the light. In general, the optical response of a medium gets highly enhanced if the frequency of the photons matches an atomic transition frequency, leading to high absorption at the resonance frequency accompanied by strong dispersion. However, a coherent superposition of the atomic states formed by an additional light field can cause transparency of an atom to an incident light field even in the vicinity of a resonant transition. This effect of eliminating the absorption of an otherwise opaque medium to resonant light is called electromagnetically induced transparency (EIT). The term EIT was first introduced by Harris and coworkers in 1990, where they performed the first measurement of EIT in strontium vapor [16].
The phenomenon of EIT is based on light-induced atomic coherence which leads to destructive quantum interference between the involved excitation pathways. The result is a modified optical response, which shows highly suppressed absorption in a very narrow spectral range together with a dramatic modification of the refractive properties. The typical behavior of high absorption with a high change in refractive index is no longer seen and the transmitted light experiences a steep dispersion within a transparent window. This can, e.g., allow one to slow down light pulses [7, 8] and even store light in atomic ensembles [9].

2.1. The physical understanding of EIT

EIT is an effect of quantum interference based on the light-induced coupling of atomic states. In order to understand the physics of EIT, it is necessary to initially understand the phenomenon of quantum interference and coherence in atomic systems. The concept of EIT is investigated by introducing the dressed state picture of the atom-light interaction based on the related phenomenon of coherent population trapping (CPT).

2.1.1. Quantum interference and coherence in atomic systems

Quantum interference describes the interference of probability amplitudes which represent different alternative pathways, e.g. of a single photon in an interferometer. In the case of coherent preparation of atomic ensembles, the interference of different transition pathways is referred to as quantum interference. Two energy states of an atom can be coupled via different transition processes, which are all described by a quantum mechanical probability amplitude. As these amplitudes are summed and can be positive or negative in sign, they can interfere either constructively or destructively leading to enhancement or cancellation of the total transition amplitude.
The interference of different excitation pathways can be demonstrated by Fano interference, which was the first quantum interference introduced by Fano in 1961 [17]. It can be observed for multi-electron atoms with an autoionizing state $|2\rangle$; see figure 2.1 (a). This

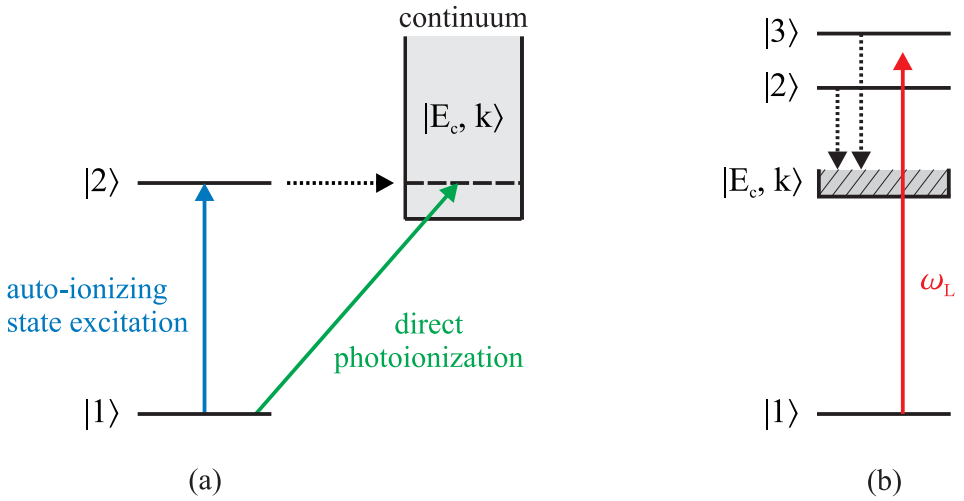

Figure 2.1.: Examples of quantum interference: Fano interference (a) and level structure for lasing without inversion (b). In (a), the two excitation pathways to the continuum state $|E_c, k\rangle$ of an atom with an autoionizing resonance can interfere: the ground state $|1\rangle$ is coupled to the continuum either by direct photoionization or via excitation to a bound state $|2\rangle$ and subsequent spontaneous decay to the continuum via interelectronic Coulomb interaction. In (b) the interference is caused by the close spacing of the resonances $|2\rangle$ and $|3\rangle$, which both decay to the same continuum $|E_c, k\rangle$ if they are excited by a light field ω_L.

is a neutral, doubly excited state which decays naturally to some ionized continuum of states $|E_c, k\rangle$ due to the interaction of the excited electrons. An atom prepared in $|1\rangle$ can get excited to the continuum via two possible pathways: either by direct photoionization $|1\rangle \rightarrow |E_c, k\rangle$ or indirectly by exciting the atom to the bound state $|2\rangle$, which subsequently decays to the continuum. These two pathways can interfere constructively or destructively depending on the energy of the exciting photon[1]. This leads to frequency dependent enhancement and reduction of absorption in the vicinity of the autoionizing resonance. As a consequence, one observes characteristically asymmetric line shapes in the absorption profiles of these autoionizing states [18].

This type of quantum interference can also be observed in the case of two discrete lifetime-broadened energy levels as depicted in figure 2.1 (b). Consider two closely spaced[2] upper states $|2\rangle$ and $|3\rangle$ which both spontaneously decay to the continuum $|E_c, k\rangle$. If an atom initially in state $|1\rangle$ gets excited by a laser field with frequency ω_L which is scanned across $|2\rangle$ and $|3\rangle$, the absorption profile will exhibit a Fano-like interference. This arises due to quantum interference between the two possible pathways of the atom to get to the continuum, either via state $|2\rangle$ or state $|3\rangle$. This leads to an effect known as lasing without inversion (LWI) which closely related to EIT [4].

Quantum interference can also be induced intentionally by applying a laser field to an atomic medium with well separated energy states [19]; see figure 2.2. If a strong resonant

[1] In multi-electron systems different electronic configurations are mixed due to the so called "configuration interaction". Thus, the state $|E_c, k\rangle$ is actually an admixture of $|2\rangle$ and all possible continuum states and likewise $|2\rangle$ gets modified by the continuum states. The probability for excitation to $|E_c, k\rangle$ is then given by the transition matrix dipole element $\langle E_c, k|H_{\text{int}}|1\rangle$ which contains the terms $\langle 2^*|H_{\text{int}}|1\rangle$, due to excitation to the modified state $|2^*\rangle$, and $\langle E_c, k|H_{\text{int}}|1\rangle$, where H_{int} is the transition operator. The coefficients of these terms vary sharply as the energy traverses the resonance of $|E_c, k\rangle$ and interfere with opposite phase on both sides of the resonance, see [17].

[2] The frequency difference of the energy states is comparable to or less than their linewidths.

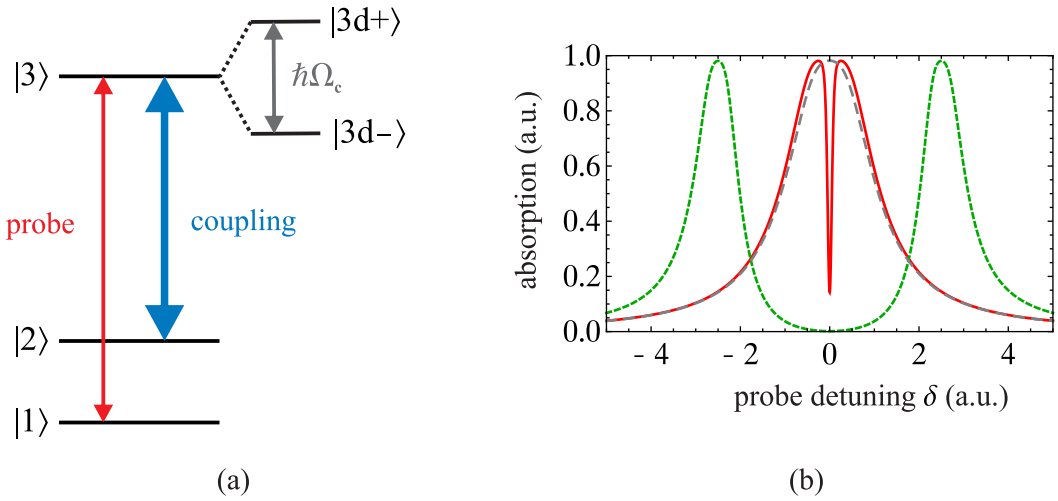

Figure 2.2.: Autler-Townes-Doublet in the absorption profile of an atom: (a) The states $|2\rangle$ and $|3\rangle$ are coupled by a strong coupling laser with Rabi frequency Ω_c, leading to the dressed states $|3d+\rangle$ and $|3d-\rangle$. Figure (b) shows the absorption profile of the probe laser dependent on the detuning δ from resonance: In the case of high coupling strength Ω_c, two separated lines spaced by $\hbar\Omega_c$ are observed (green dashed line). In the case of the red solid line quantum interference causes a reduced absorption at $\delta = 0$. The gray dashed curve shows the non-coupled Lorentzian absorption line.

laser field with Rabi frequency Ω_c is applied to the transition $|2\rangle \rightarrow |3\rangle$, the states $|2\rangle$ and $|3\rangle$ will be coherently coupled. As a result, these states will be replaced by the new shifted states $|3d+\rangle$ and $|3d-\rangle$ spaced by $\hbar\Omega_c$ which are called the dressed states. These are the eigenstates of the time-independent Hamiltonian of the combined atom-light system. If a probe light resonant to the $|1\rangle \rightarrow |3\rangle$ transition is applied and scanned across the upper level, the absorption profile will show a characteristic line splitting called the Autler-Townes-Doublet [20]. If the splitting $\hbar\Omega_c$ exceeds the natural linewidth of the atomic states, the cancellation of absorption is simply due to the fact that the spectral overlap between the dressed states and the spectral profile of the laser is zero at resonance $\delta = 0$. The absorption profile then shows two distinct line shapes spaced by $\hbar\Omega_c$ as depicted by the green dashed line in figure 2.2 (b). However, if the coupling Ω_c is small enough so that the splitting is comparable or less than the natural linewidths, the absorption will cancel due to quantum interference between the two dressed states. In this case, the observed line shape shown by the red solid line in figure 2.2 (b) is not simply the sum of two single lines but has a more complicated structure, in which a narrow dip at $\delta = 0$ appears.

2.1.2. EIT in a 3-level Λ-system

The effect of EIT is closely related to the concept of coherent population trapping (CPT). They can both be explained by the same physics and EIT can be considered as a special case of CPT. In either case the atoms get trapped in a dark state, which is created by external laser fields and is called dark since it is decoupled from the light fields [2]. Thus, it is convenient to first consider CPT and introduce the concept of dark states in the dressed state picture to understand the underlying physics of these phenomena.
The observation of EIT and CPT usually requires a three-level atomic system, in which one transition is dipole forbidden whilst the other two transitions are dipole coupled. In

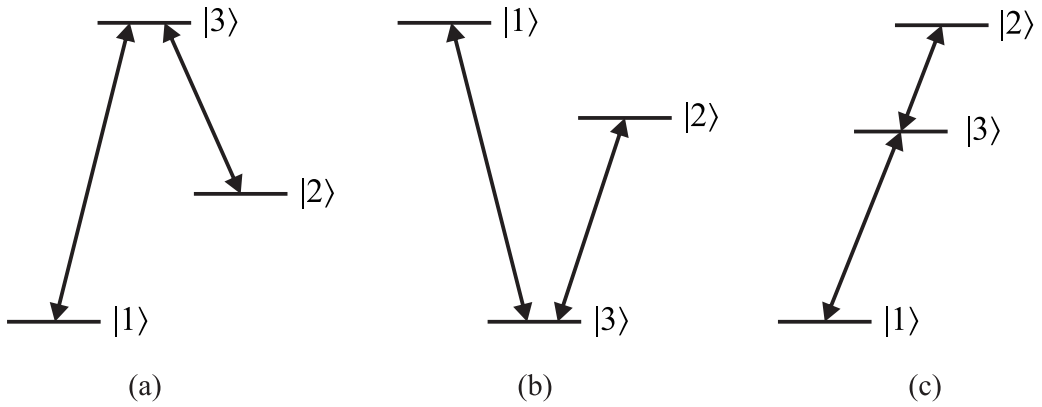

Figure 2.3.: Three basic configurations for a 3-level-system interacting with two light fields: (a) Λ-system, (b) V-system, (c) ladder-system. In all cases, the $|1\rangle \rightarrow |2\rangle$ transition is dipole forbidden and the states $|1\rangle$ and $|2\rangle$ are coupled to $|3\rangle$.

figure 2.3 the three basic level schemes called the Λ-, V- and ladder-system are shown. In all schemes, $|1\rangle \rightarrow |2\rangle$ is the dipole forbidden transition and $|1\rangle$ is a ground state, whereas for the Λ-system $|2\rangle$ is typically a meta-stable state. In the following the focus lies on the Λ-scheme and CPT and EIT for this system are investigated. Thus, consider the Λ-system shown in figure 2.4, in which the two dipole-allowed transitions are driven by two laser fields with Rabi frequencies Ω_p of the probe laser and Ω_c of the coupling laser, respectively. The Rabi frequencies are determined by the field amplitudes E_p and E_c as

$$\Omega_p = \frac{d_{13}\, E_p}{\hbar} \qquad \text{and} \qquad \Omega_c = \frac{d_{23}\, E_c}{\hbar} \tag{2.1}$$

in which d_{13} and d_{23} are the dipole transition elements of the corresponding transitions. The field detunings from resonance are given by $\delta_p = \omega_p - \omega_{31}$ and $\delta_c = \omega_c - \omega_{32}$, respectively, where ω_p and ω_c are the laser frequencies and ω_{31} and ω_{32} are the frequencies of the dipole allowed transitions. For now, the radiative decay rates Γ_{31} and Γ_{32} and the dephasing rate γ_{21} of state $|2\rangle$ will be ignored in the dressed state picture. They are introduced in the next chapter where the optical response of the system is determined using the density matrix formalism.
If the coupling laser is close to the atomic resonance, i.e. δ_c is small, atoms which are initially in state $|2\rangle$ will be excited to state $|3\rangle$ and afterwards can decay to either of the states $|2\rangle$ or $|1\rangle$. Thus the atoms are optically pumped into $|1\rangle$. Likewise the probe field Ω_p will pump atoms from state $|1\rangle$ into state $|2\rangle$. Usually optical pumping enhances the absorption of a light field which excites the pumped state, since there is an increased population in this state. However, since both fields couple to the same excited state, destructive quantum interference causes a decreased absorption of both fields.
Consider the total Hamiltonian of the system given by the sum of the Hamiltonian H_0 of the bare atom and the term H_{int} which describes the interaction of the atom with the light fields:

$$H = H_0 + H_{\text{int}}\,, \tag{2.2}$$

where the interaction term using the rotating wave approximation (RWA) is given by

$$H_{\text{int}} = -\frac{\hbar}{2}\left[\Omega_p e^{-i\omega_p t}|3\rangle\langle 1| + \Omega_c e^{-i\omega_c t}|3\rangle\langle 2| + c.c.\right]\,. \tag{2.3}$$

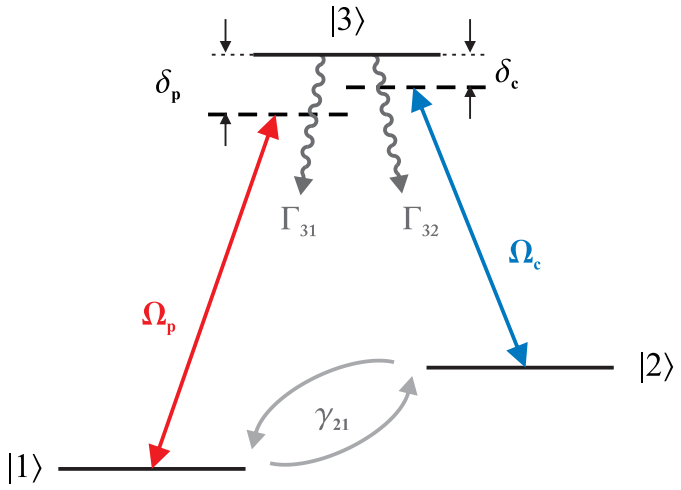

Figure 2.4.: Λ-system used for CPT. The dipole allowed transitions $|1\rangle \rightarrow |3\rangle$ and $|2\rangle \rightarrow |3\rangle$ are driven by two laser fields with strength Ω_p and Ω_c, which are detuned from the resonance by δ_p and δ_c, respectively. Γ_{31} and Γ_{32} are the decay rates out of state $|3\rangle$ and γ_{21} is the dephasing rate between the two ground states.

The eigenstates of the complete system described by H are the dressed states. They are a linear superposition of the bare atomic states $|1\rangle$, $|2\rangle$ and $|3\rangle$ induced by the two laser fields. With time dependent amplitudes $c_1(t)$, $c_2(t)$ and $c_3(t)$ they can be written in the form

$$|\Psi\rangle = c_1(t)\,|1\rangle + c_2(t)\,|2\rangle + c_3(t)\,|3\rangle\,. \tag{2.4}$$

To understand the origin of the quantum interference, it is useful to consider the superposition states $|+\rangle$ and $|-\rangle$ rather than the ground states $|1\rangle$ and $|2\rangle$:

$$|+\rangle(t) = \frac{\Omega_p}{\Omega'} e^{-i\omega_1 t}|1\rangle + \frac{\Omega_c}{\Omega'} e^{-i\omega_2 t}|2\rangle \tag{2.5}$$

$$|-\rangle(t) = \frac{\Omega_c}{\Omega'} e^{-i\omega_1 t}|1\rangle - \frac{\Omega_p}{\Omega'} e^{-i\omega_2 t}|2\rangle \tag{2.6}$$

with $\Omega' = (|\Omega_p|^2 + |\Omega_c|^2)^{1/2}$ and the frequencies ω_1 and ω_2 of the states $|1\rangle$ and $|2\rangle$, respectively [21]. The important feature of these states is that they do not contain the upper level $|3\rangle$. The transition dipole matrix elements which describe the excitation into state $|3\rangle$ are given by $\langle 3|H_{\text{int}}|-\rangle$ and $\langle 3|H_{\text{int}}|+\rangle$, yielding

$$\langle 3|H_{\text{int}}|+\rangle = -\frac{\hbar}{2\Omega'}\left(\Omega_p^2\, e^{-i(\omega_p+\omega_1)t} + \Omega_c^2\, e^{-i(\omega_c+\omega_2)t}\right) \tag{2.7}$$

$$\langle 3|H_{\text{int}}|-\rangle = -\frac{\hbar}{2\Omega'}\,\Omega_p\Omega_c\, e^{-i(\omega_p+\omega_1)t}\left(1 - e^{i(\omega_p-\omega_c-\omega_2+\omega_1)t}\right) \tag{2.8}$$

The state $|-\rangle$ is especially interesting since its transition dipole element vanishes in the case of two-photon resonance $\omega_p - \omega_c = \omega_2 - \omega_1$:

$$\langle 3|H_{\text{int}}|-\rangle = 0 \tag{2.9}$$

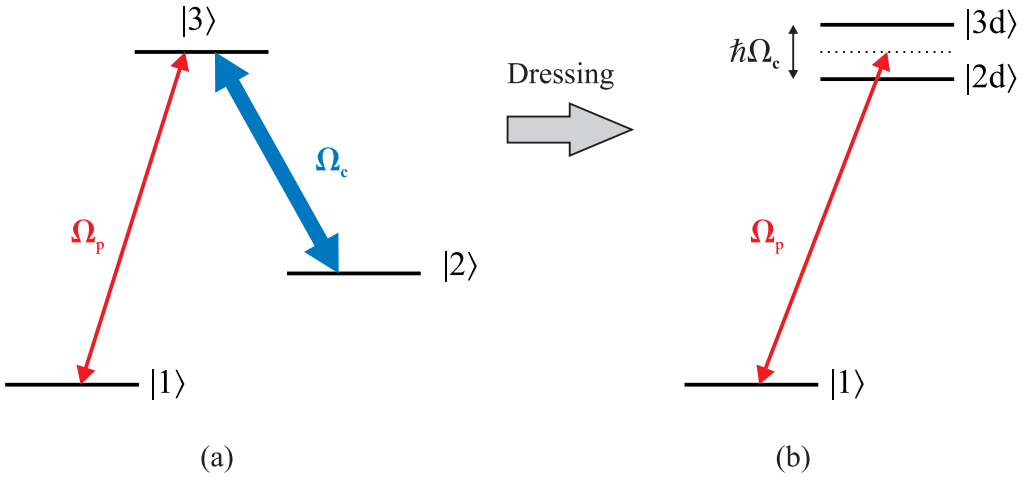

Figure 2.5.: Dressing of the atomic states in the case of EIT of a 3-level Λ-system as shown in (a): The coupling of the states $|2\rangle$ and $|3\rangle$ with a strong laser field leads to dressed states $|3d\rangle$ and $|2d\rangle$ as pictured in (b) (right side). The destructive interference of these two dressed states leads to EIT when probing the $|1\rangle \rightarrow |3\rangle$ transition with a weak probe field.

Hence, this state is decoupled from the electromagnetic field and no excitation to state $|3\rangle$ can occur. Therefore, $|-\rangle$ is known as a dark state, since an atom prepared in $|-\rangle$ will not absorb or emit any light and is thus trapped in that state. This phenomenon is called coherent population trapping and its origin is the destructive interference between the transition amplitudes $|1\rangle \rightarrow |3\rangle$ and $|2\rangle \rightarrow |3\rangle$.
In CPT the two laser fields have comparable strengths $\Omega_p \approx \Omega_c$. In the special case of EIT the coupling field Ω_c is much stronger than the probe field, i.e. $\Omega_p \ll \Omega_c$. In this situation only the stronger coupling field will induce coherent superposition states, whilst the probe laser will be treated as a weak perturbative field which does not influence the atomic states. Under this condition, the dark state $|-\rangle$ in equation (2.6) approaches the ground state $|1\rangle$, in which the population is stored:

$$|-\rangle_{\mathrm{EIT}} = |1\rangle \tag{2.10}$$

In figure 2.5 the dressing of the atomic states is illustrated for the case of EIT. The dressed states $|2d\rangle$ and $|3d\rangle$ are given by the coherent superposition of the upper bare atomic states $|2\rangle$ and $|3\rangle$ caused by the coupling field. The ground state $|1\rangle$ is not included in the coupling and thus becomes the dark state. For two-photon resonance $\delta_p = \delta_c = \delta$, the dressed eigenstates can be written as [22]

$$|2d\rangle = \cos\theta|2\rangle - \sin\theta|3\rangle \tag{2.11}$$
$$|3d\rangle = \sin\theta|2\rangle + \cos\theta|3\rangle \tag{2.12}$$

where the mixing angle θ is given by

$$\tan 2\theta = \frac{\Omega_c}{\delta}\,. \tag{2.13}$$

In the case of a resonant coupling field $\delta = 0$, the mixing angle approaches $\theta \to \pi/2$ and thus the dressed states have the form

$$|2d\rangle = \frac{1}{\sqrt{2}}(|2\rangle - |3\rangle) \tag{2.14}$$

$$|3d\rangle = \frac{1}{\sqrt{2}}(|2\rangle + |3\rangle)\,. \tag{2.15}$$

Thus, for $\delta_p = \delta_c = 0$ the transition probability amplitudes for exciting an atom from state $|1\rangle$ by the probe field are equal in amplitude but have opposite signs

$$\langle 2d|H_{\text{int}}|1\rangle = -\langle 3d|H_{\text{int}}|1\rangle\,. \tag{2.16}$$

Therefore, the total transition amplitude vanishes and the medium becomes transparent to the probe field. In the case of an off-resonant coupling field $\delta_c \neq 0$, the bare states $|2\rangle$ and $|3\rangle$ contribute with different amplitudes to the dressed states, and the situation of a vanishing transition amplitude will arise at the two-photon resonance $\delta_p = \delta_c$.

2.2. Semiclassical theory of light-matter interaction using the density matrix

The interaction of an atomic system with coherent light fields can be described by different theoretical models. One approach is to use the dressed state picture as introduced in the previous chapter, i.e. the new eigenstates of the system obtained by diagonalization of the total Hamiltonian. However, to account for the non-perturbative coupling field and additional damping terms, a general density matrix approach will be used in this chapter to determine the optical response of the medium. In this model the time evolution of the populations of the atomic levels as well as the atomic coherences between those levels is determined by using the master equation. Damping processes like spontaneous emission and decoherences are introduced phenomenologically by adding an extra damping term and thus using the master equation in the Lindblad form.
The linear optical response of an atom is given by the linear susceptibility, which is closely related to the atomic coherences and thus can be determined by the steady state solutions of the master equation. For this purpose a semiclassical approach is used in which the atom is treated quantum mechanically and the light fields are considered as classical fields. In the case of single photons and the propagation of quantized fields in EIT[3], the fully quantized treatment including dark-state polaritons would be required [25, 10].

2.2.1. Atomic susceptibility and density matrix

An atomic ensemble such as used in EIT experiments can be described by the density matrix ρ, whose elements in the case of the pure state in equation (2.4) are given by the amplitudes

$$\rho_{ij} = c_i\, c_j^*\,, \tag{2.17}$$

with $i, j = 1,2,3$. The populations are given by $\rho_{ii} = |c_i|^2$ and the off-diagonal elements $\rho_{ij} = c_i\, c_j^*$ with $i \neq j$ are the coherences of the system, which can be related to the optical

[3]For example EIT in resonators, where the atom couples to the cavity modes of the resonator [23], or in experiments of squeezed light with EIT [24].

response of the atoms.
The atomic polarization p_{at} of an atom induced by the laser field driving the transition $|i\rangle \rightarrow |j\rangle$ can be written in terms of the coherence term ρ_{ij} as [26]

$$p_{\mathrm{at}} = d_{ij}\,\rho_{ij} \tag{2.18}$$

in which d_{ij} is the dipole matrix element of the atomic transition. Thus, for an ensemble of N atoms the macroscopic polarization P due to the light field is given by

$$P = N\,d_{ij}\,\rho_{ij}\,. \tag{2.19}$$

The linear response of a medium to near-resonant light is given by the linear susceptibility $\chi^{(1)}$. It relates the induced polarization to the incident electrical field E

$$P = \epsilon_0 \chi^{(1)} E \tag{2.20}$$

where ϵ_0 is the vacuum permittivity. Combining equations (2.20) and (2.19) and introducing the Rabi frequency $\Omega = d_{ij}\,E/\hbar$ leads to the relation between the linear susceptibility and the off-diagonal element ρ_{ij} of the density matrix

$$\chi^{(1)} = \frac{N}{\epsilon_0 \hbar}\,\frac{d_{ij}^2}{\Omega}\,\rho_{ij}\,. \tag{2.21}$$

The linear susceptibility is a complex quantity whose real part $\mathrm{Re}\{\chi^{(1)}\}$ describes the refractive properties of the medium, whilst the imaginary part $\mathrm{Im}\{\chi^{(1)}\}$ determines the absorption. In the absence of any magnetic field, $\chi^{(1)}$ is related to the complex refractive index $n = n_r + i\kappa$ by

$$n = \sqrt{1+\chi^{(1)}} \approx 1 + \frac{\chi^{(1)}}{2}\,. \tag{2.22}$$

The real part of n is the refraction index n_r of the medium and the imaginary part κ is related to the absorption coefficient α by $\kappa = \alpha c/2\omega$, in which ω is the frequency of the light field. Thus, refraction and absorption of the atomic ensemble can be expressed as

$$n_r = 1 + \frac{1}{2}\,\mathrm{Re}\{\chi^{(1)}\} \tag{2.23}$$

$$\alpha = \frac{\omega}{c}\,\mathrm{Im}\{\chi^{(1)}\}\,. \tag{2.24}$$

Since in equation (2.21) the complex character of $\chi^{(1)}$ is contained in the complex coherence term ρ_{ij}, one can rewrite the refractive index and absorption coefficient in terms of the coherences of the density matrix:

$$n_r = \frac{N d_{ij}^2}{2\epsilon_0 \hbar \Omega_{ij}}\,\mathrm{Re}\{\rho_{ij}\} + 1 \tag{2.25}$$

$$\alpha = \frac{N d_{ij}^2 \omega}{\epsilon_0 \hbar \Omega_{ij} c}\,\mathrm{Im}\{\rho_{ij}\}\,. \tag{2.26}$$

These relations demonstrate that one obtains the optical response of a medium to a light field from the coherences ρ_{ij}, which can be determined using the master equation.

2.2.2. Density matrix formalism for EIT in a Λ-system

In order to investigate EIT using the density matrix elements, the optical response of a 3-level Λ-system to a coupling and a probe field is determined. Therefore, we consider the three-level system introduced in chapter 2.1.2, see figure 2.4. The Hamiltonian H_0 of the bare atom and H_{int} describing the interaction can be obtained by a generalization of the Hamiltonian of a two-level system interacting with a single laser field to the 3-level system. Therefore, H_0 and H_{int}, which was given in the last chapter using the RWA, can be expressed by

$$\begin{aligned} H_0 &= \hbar\omega_1|1\rangle\langle 1| + \hbar\omega_2|2\rangle\langle 2| + \hbar\omega_3|3\rangle\langle 3| \\ H_{\text{int}} &= -\frac{\hbar}{2}\left[\Omega_p e^{-i\omega_p t}|3\rangle\langle 1| + \Omega_c e^{-i\omega_c t}|3\rangle\langle 2| + c.c.\right] \end{aligned} \tag{2.27}$$

in which $\hbar\omega_1$, $\hbar\omega_2$ and $\hbar\omega_3$ are the energies of the states $|1\rangle$, $|2\rangle$ and $|3\rangle$. The terms $|i\rangle\langle i| = \sigma_{ii}$ are the atomic projection operators and $\sigma_{ij} = |i\rangle\langle j|$ are the atomic ladder operators describing transitions from $|j\rangle$ to $|i\rangle$. As in the last chapter, Ω_p and Ω_c are the Rabi frequencies of the probe and coupling field, respectively, and the detunings from resonance are given by δ_p and δ_c.
The time evolution of the density matrix elements is given by the master equation [27]:

$$\frac{d}{dt}\rho_{ij} = -\frac{i}{\hbar}\langle i|\left[H,\rho\right]|j\rangle\,. \tag{2.28}$$

In this chapter the quantity of interest is the optical response of a medium to resonant light, which is determined by the off-diagonal elements ρ_{21}, ρ_{31} and ρ_{32} of the density matrix, for which $\rho_{ij} = \rho^*_{ji}$ holds. In the master equation approach the effect of decoherence is taken into account by including damping terms, where it is assumed that the off-diagonal matrix elements ρ_{ij} decay with the respective rates γ_{ij}. In the case of ρ_{32} and ρ_{31}, this contains spontaneous emission from state $|3\rangle$ to $|1\rangle$ or $|2\rangle$, respectively, with the total spontaneous emission rate $\Gamma_3 = \Gamma_{31} + \Gamma_{32}$. Furthermore, the off-diagonal decay rates are determined by dephasing processes like collisions in an atomic vapor. In the presence of damping, the time evolution of the coherences is then given by the Lindblad equations [27]

$$\frac{d}{dt}\rho_{31} = -\frac{i}{\hbar}\langle 3|\left[H,\rho\right]|1\rangle - \frac{\gamma_{31}}{2}\langle 3|\left(2\sigma_{13}\rho\sigma_{31} - \sigma_{33}\rho - \rho\sigma_{33}\right)|1\rangle \tag{2.29}$$

$$\frac{d}{dt}\rho_{32} = -\frac{i}{\hbar}\langle 3|\left[H,\rho\right]|2\rangle - \frac{\gamma_{32}}{2}\langle 3|\left(2\sigma_{23}\rho\sigma_{32} - \sigma_{33}\rho - \rho\sigma_{33}\right)|2\rangle \tag{2.30}$$

$$\frac{d}{dt}\rho_{21} = -\frac{i}{\hbar}\langle 2|\left[H,\rho\right]|1\rangle - \frac{\gamma_{21}}{2}\langle 2|\left(2\sigma_{12}\rho\sigma_{21} - \sigma_{22}\rho - \rho\sigma_{22}\right)|1\rangle\,. \tag{2.31}$$

This leads to the following time dependences of the coherences:

$$\frac{d}{dt}\rho_{31} = -\left[i\omega_{31} - \frac{\gamma_{31}}{2}\right]\rho_{31} + i\frac{\Omega_p}{2}e^{-i\omega_p t}(\rho_{11} - \rho_{33}) + i\frac{\Omega_c}{2}e^{-i\omega_c t}\rho_{21} \tag{2.32}$$

$$\frac{d}{dt}\rho_{32} = -\left[i\omega_{32} - \frac{\gamma_{32}}{2}\right]\rho_{32} + i\frac{\Omega_c}{2}e^{-i\omega_c t}(\rho_{22} - \rho_{33}) + i\frac{\Omega_p}{2}e^{-i\omega_p t}\rho_{12} \tag{2.33}$$

$$\frac{d}{dt}\rho_{21} = -\left[i\omega_{21} - \frac{\gamma_{21}}{2}\right]\rho_{21} - i\frac{\Omega_p}{2}e^{-i\omega_p t}\rho_{23} + i\frac{\Omega_c^*}{2}e^{i\omega_c t}\rho_{31} \tag{2.34}$$

with the transition frequencies $\omega_{31} = \omega_3 - \omega_1$, $\omega_{32} = \omega_3 - \omega_2$ and $\omega_{21} = \omega_2 - \omega_1$ of the atomic states, respectively. So far no assumptions regarding the field strengths of probe and coupling fields have been made. In EIT the coupling is much stronger than the

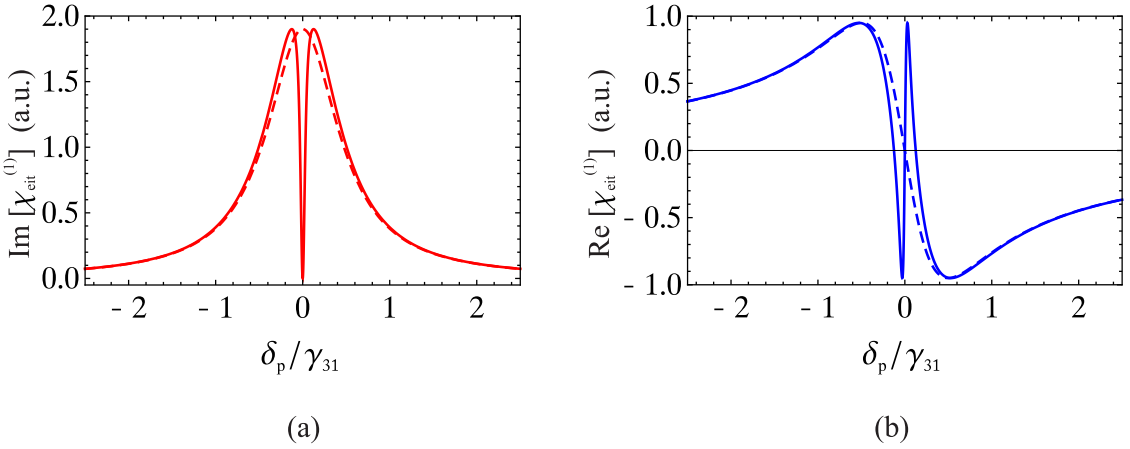

Figure 2.6.: The solid lines show the real part (a) and imaginary part (b) of the dressed susceptibility of EIT, plotted against the probe detuning δ_p which is normalized to the decay rate γ_{31}. The dashed lines show the case of no coupling, which is the same as that of a two-level atom.

perturbative probe field, i.e., $\Omega_p \ll \Omega_c$. Thus, the off-diagonal elements can be evaluated to the lowest order in Ω_p, but all orders of the strong field Ω_c must be kept. In addition it is assumed that all atoms are initially in the ground state $|1\rangle$, i.e. $\rho_{22}(0) = \rho_{33}(0) = 0$ and $\rho_{11}(0) = 1$. Evaluating the density matrix elements in orders of Ω_p leads to

$$\begin{aligned} \rho_{11} &\approx 1 \\ \rho_{22} = \rho_{33} = \rho_{32} &\approx 0 \end{aligned} \tag{2.35}$$

where the terms in the second line are set to zero because they contain only higher orders of Ω_p, whereas ρ_{11} includes a term $1-O(|\Omega_p|^2)$, which means that for all times the population stays in $|1\rangle$. However, the terms ρ_{31} and ρ_{21} contain only first order terms and can be expressed by

$$\frac{d}{dt}\rho_{31} = -\left(i\omega_{31} + \frac{\gamma_{31}}{2}\right)\rho_{31} + i\frac{\Omega_p}{2}e^{-i\omega_p t} + i\frac{\Omega_c}{2}e^{-i\omega_c t}\rho_{21} \tag{2.36}$$

$$\frac{d}{dt}\rho_{21} = -\left(i\omega_{21} + \frac{\gamma_{21}}{2}\right)\rho_{21} + i\frac{\Omega_c^*}{2}e^{i\omega_c t}\rho_{31}\,. \tag{2.37}$$

By introducing new variables $\widetilde{\rho}_{31} = \rho_{31}e^{i\omega_p t}$ and $\widetilde{\rho}_{21} = \rho_{21}e^{i(\omega_p-\omega_c)t}$ and including the probe detuning $\delta_p = \omega_p - \omega_{31}$ and the two-photon detuning $\Delta = \delta_p - \delta_c = (\omega_p - \omega_c) - \omega_{21}$ one obtains

$$\frac{d}{dt}\widetilde{\rho}_{31} = i\left(\delta_p + i\frac{\gamma_{31}}{2}\right)\widetilde{\rho}_{31} + i\frac{\Omega_p}{2} + i\frac{\Omega_c}{2}\widetilde{\rho}_{21} \tag{2.38}$$

$$\frac{d}{dt}\widetilde{\rho}_{21} = i\left(\Delta + i\frac{\gamma_{21}}{2}\right)\widetilde{\rho}_{21} + i\frac{\Omega_c^*}{2}\widetilde{\rho}_{31}\,. \tag{2.39}$$

These can now be solved in the adiabatic regime, i.e. $\dot{\widetilde{\rho}}_{31} = 0$ and $\dot{\widetilde{\rho}}_{21} = 0$. The optical response of the atoms to the weak probe field resonant to the $|1\rangle \rightarrow |3\rangle$ transition is the quantity of interest for EIT. Therefore only the susceptibility induced by the coherence term ρ_{31} is considered here. Using equation (2.39) the solution of equation (2.38) is

$$\widetilde{\rho}_{31} = \frac{\Omega_p(2\Delta + i\gamma_{21})}{|\Omega_c|^2 - (2\delta_p + i\gamma_{31})(2\Delta + i\gamma_{21})}\,. \tag{2.40}$$

As described in chapter 2.2.1, the susceptibility can be calculated from the coherences via the macroscopic polarization that is induced. In the case of the probe field, the complex linear susceptibility is given by

$$\chi_p^{(1)} = \frac{N}{\epsilon_0 \hbar} \frac{d_{13}^2}{\Omega_p} \widetilde{\rho}_{31} \tag{2.41}$$

with the dipole matrix element d_{13}^2 of the probe transition. This is the relevant susceptibility for describing the EIT effect, and $\chi_{\mathrm{EIT}}^{(1)}$ is given by $\chi_p^{(1)}$. The linear susceptibility describing EIT is thus

$$\chi_{\mathrm{EIT}}^{(1)} = \frac{N d_{13}^2}{\epsilon_0 \hbar} \frac{2(2\Delta + i\gamma_{21})}{|\Omega_c|^2 - (2\delta_p + i\gamma_{31})(2\Delta + i\gamma_{21})} \,. \tag{2.42}$$

Separating this into its real and imaginary parts finally gives one the absorptive and dispersive line shapes for EIT:

$$\text{Refraction:} \qquad \mathrm{Re}\{\chi_{\mathrm{EIT}}^{(1)}\} = \frac{N d_{13}^2}{\epsilon_0 \hbar} \frac{4\Delta \left(|\Omega_c|^2 - 4\delta_p \Delta\right) - 4\delta_p \gamma_{21}^2}{\left||\Omega_c|^2 + (\gamma_{21} + 2i\Delta)(\gamma_{31} + 2i\delta_p)\right|^2} \tag{2.43}$$

$$\text{Absorption:} \qquad \mathrm{Im}\{\chi_{\mathrm{EIT}}^{(1)}\} = \frac{N d_{13}^2}{\epsilon_0 \hbar} \frac{8\gamma_{31}\Delta^2 + 2\gamma_{21}\left(|\Omega_c|^2 + \gamma_{21}\gamma_{31}\right)}{\left||\Omega_c|^2 + (\gamma_{21} + 2i\Delta)(\gamma_{31} + 2i\delta_p)\right|^2} \,. \tag{2.44}$$

The latter determines the transmission as [22]

$$T = e^{-\alpha z} = \exp\left(-\mathrm{Im}\{\chi_{\mathrm{EIT}}^{(1)}\} \frac{\omega_{31}}{c} z\right) \,. \tag{2.45}$$

The line shapes of the real and the imaginary parts of the "dressed" susceptibility are plotted in figure 2.6 as a function of the normalized probe detuning δ_p/γ_{31} from resonance. The plot shows the ideal case of a perfect metastable state $|2\rangle$, i.e. $\gamma_{21} = 0$, and a resonant coupling field $\Delta = \delta_p$ is assumed, whereby the normalized coupling strength is set to $\Omega_c/\gamma_{31} = 0.25$. If the coupling is switched on, the imaginary part is zero at resonance and the medium becomes totally transparent for the probe light. At the same time, the real part of the susceptibility is still zero at resonance but exhibits steep anomalous dispersion in a region of high transparency. This can, e.g., lead to anomalous slow group velocities, since the group velocity at resonance depends on the change of the refraction index $n_r = \sqrt{1 + \mathrm{Re}\{\chi^{(1)}\}}$ with frequency, i.e. $dn_r/d\omega_p$, as [22]

$$v_g = \frac{c}{n + \omega_p \frac{dn}{d\omega_p}} \tag{2.46}$$

Usually, in normal media a change in the group velocity is always associated with high absorption. In EIT, the group velocity can be controlled by the strength of the coupling field, which determines the width of the EIT resonance and the slope of the real part of the susceptibility, i.e. $dn/d\omega_p$, while the medium stays transparent. This steepness of the dispersion function is the key parameter in order to obtain small group velocities of the probe light, and it is directly related to the transmission width.

2.2.3. Critical parameters in EIT

The shape of the EIT resonance and the transparency at the two-photon resonance depends highly on parameters like the atomic coherences and the coupling strength. Since it is necessary for the experimental observation of EIT to take care in choosing an appropriate level system and in setting the experimental parameters, the dependence of the EIT resonance on these parameters is investigated.
In the case of a resonant coupling laser $\omega_c = \omega_{32}$ there are two parameters which mainly determine the shape and depth of the transparency window: the coupling strength Ω_c and the dephasing rate γ_{21} of the dipole-forbidden $|1\rangle \rightarrow |2\rangle$ transition. The amount of transparency itself does not change with coupling strength, but depends highly on the decoherence between the two lower states $|1\rangle$ and $|2\rangle$. In figure 2.7 (a) the influence of the dephasing rate γ_{21} on the linear susceptibility is shown. In the case of $\gamma_{21} = 0$ perfect transparency is obtained, but the amount of transparency decreases rapidly with increasing γ_{21}. If $\gamma_{21} \gg \Omega_c$, the EIT resonance will vanish due to insufficient ground state coherence, but it can be recovered by increasing the coupling strength Ω_c.
The coupling strength Ω_c mainly affects the width of the EIT resonance, and in figure 2.7 (b) the EIT line shape is shown for different values of Ω_c. In the limit $\Omega_c \ll \gamma_{31}$ a single absorption profile with a narrow transparency window at resonance is observed. The linewidth of this window is much narrower than the width γ_{31} of the total absorption peak. With increasing coupling power the width of the EIT resonance becomes broader. In the limit of $|\Omega_c| > \gamma_{31}$, the spectral profile shows two distinct lines corresponding to the two dressed states from section 2.1.2.
The condition for observing EIT depending on the parameters Ω_c, γ_{31} and γ_{21} is given as [22]

$$|\Omega_c|^2 \gg \gamma_{31}\gamma_{21} \,. \tag{2.47}$$

The transmission width of the EIT resonance depends not only on the coupling power, but also on the coherences, and it is directly related to the steepness of the real part of the susceptibility at resonance. In the case of a homogeneously broadened system with the width Γ_3 of the upper state[4], the EIT linewidth scales quadratically with the coupling strength Ω_c if $\Omega_c \ll \Gamma_3$ [28]:

$$\Gamma_{eit} \propto \frac{\Omega_c^2}{\Gamma_3} \,. \tag{2.48}$$

The quadratic dependence on Ω_c indicates power broadening in this regime. When performing EIT on hot atomic gases the effect of Doppler broadening on the EIT linewidth has to be considered. For a Λ-system, the condition for the two-photon resonance including the Doppler shifts of the atoms is given by

$$\omega_{21} = (\omega_p - \vec{k}_p \cdot \vec{v}) - (\omega_c - \vec{k}_c \cdot \vec{v}) \tag{2.49}$$

where $\vec{k}_p$ and $\vec{k}_c$ are the wave vectors of the fields and $\vec{v}$ is the velocity of the atoms. For co-propagating beams the Doppler shift becomes negligible if the residual Doppler shift $(\omega_p - \omega_c)v/c$ is small enough, which is typically fulfilled since the optical frequencies of the lasers are comparable. Thus, the two-photon resonance is in principle independent

[4] Γ_3 usually denotes the lifetime broadened width of the atomic resonance. In the presence of collisional broadening it must be replaced by $\Gamma_3 + \gamma_{coll}$.

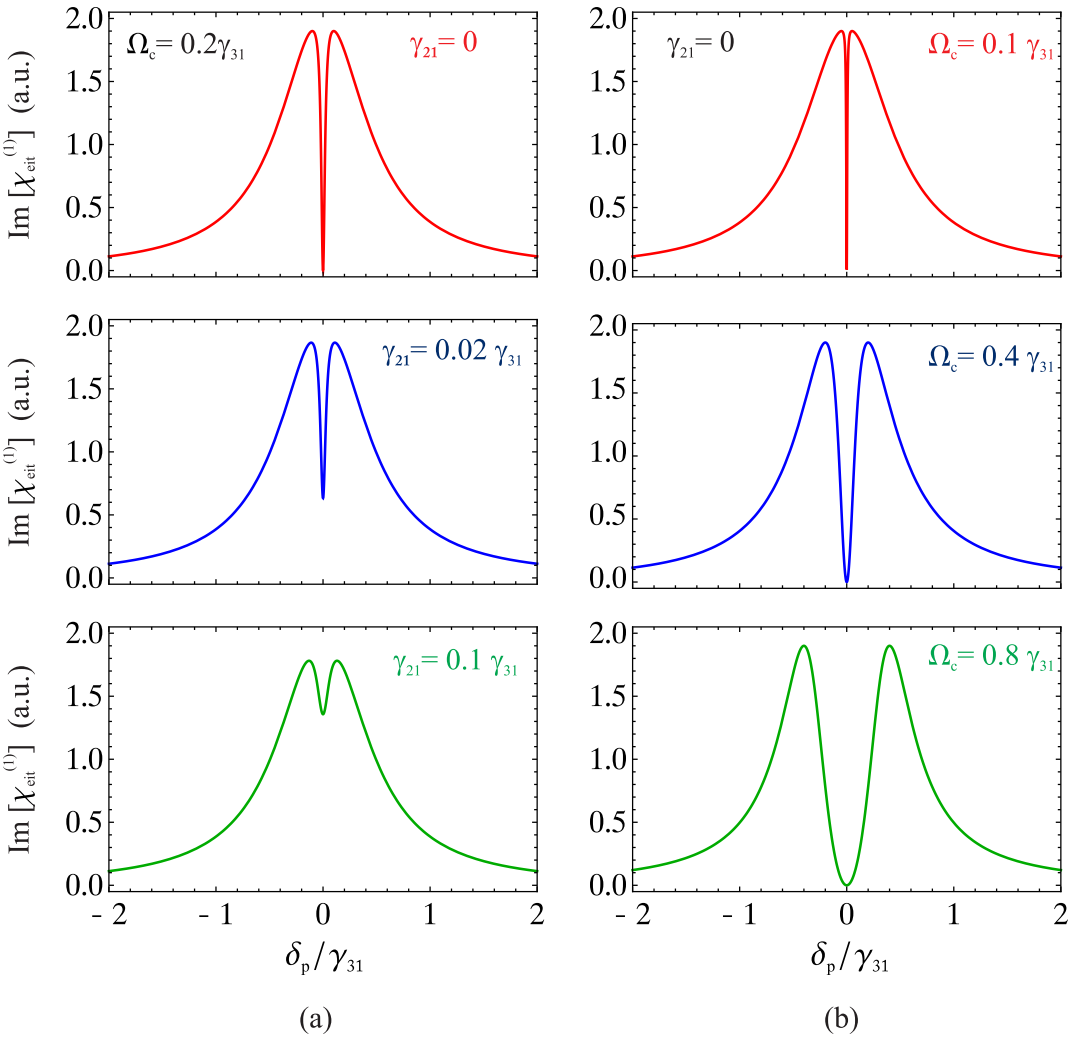

Figure 2.7.: Dependency of the imaginary part of the susceptibility on the decoherence rate γ_{21} (a) and the coupling strength Ω_c (b).

of Doppler broadening in this special case. However, only small deviations in the angle of the beams are sufficient to cause a considerable residual Doppler shift. Assuming a Doppler broadened resonance with linewidth Γ_D, and also a non-vanishing ground state decoherence γ_{21}, an expression for the EIT width depending on Ω_c can be estimated [28]:

$$\Gamma_{\text{eit}} \approx \frac{\Omega_c^2}{\Gamma_D} \qquad \text{if} \qquad \Omega_c^2 \gg \frac{2\gamma_{21}\Gamma_D^2}{\Gamma_3} \tag{2.50}$$

$$\Gamma_{\text{eit}} \approx \sqrt{\frac{2\gamma_{21}}{\Gamma_3}}\Omega_c \qquad \text{if} \qquad \Omega_c^2 \ll \frac{2\gamma_{21}\Gamma_D^2}{\Gamma_3}\,. \tag{2.51}$$

In the first situation the EIT width is proportional to the intensity Ω_c^2 of the coupling field, and in contrast to the homogeneous broadened system, this occurs if the coupling is strong enough so that the EIT linewidth exceeds the Doppler broadening of the resonance[5]. In this regime the width is dominated by power broadening due to the coupling field. In the second case the EIT linewidth scales linear with the coupling strength and it is independendt of the Doppler width Γ_D.

The model for EIT presented in this chapter is a basic model which assumes a simple three level structure without any substructure. In experiments on EIT, sublevels like m_F sub-states must be taken into account, including their relative strength and selection rules. As an example it is possible to observe multiple EIT resonances inside one absorption line, corresponding to the different Λ-schemes formed by the m_F-states, by applying a strong magnetic field [21]. resonant coupling laser and a two-photon detuning $\Delta = \delta_p - \delta_c \neq 0$ the absorption profile becomes asymmetric. For small detunings $\Delta \ll \gamma_{31}$ one observes an EIT resonance which is slightly off-resonance from the probe transition inside the broad absorption line. However, if the detuning is large compared to the width γ_{31} of the upper state, the absorption profile shows absorption line of a single two-level system plus an additional narrow peak at the two photon resonance $\delta_p = \delta_c$.

[5] Assuming that $\Gamma_D \gg \Gamma_3$.

3. Frequency control and stabilization of diode lasers

Basov et. al. [29] suggested in 1961, that stimulated emission of radiation could occur in semiconductors by the recombination of charge carriers injected in a pn-junction. The first lasing action of a semiconductor was then observed in 1962 [30]. Henceforward a remarkable development in the field of laser diodes has been made and they have become a key element in a variety of areas of science and technology. Semiconductor lasers have particular advantages compared to other laser types: they are extremely compact and small in size, can easily be operated by injecting a small current at low voltages, and their frequency can simply be modulated by modulating the injection current. Thus, they are particularly attractive for locking techniques such as phase locking of two optical oscillators.
This chapter describes the basic principles of semiconductor lasers and their frequency modulation via the injection current. Furthermore, the phase noise characteristics of semiconductor lasers are investigated. Finally, in the last section, the stabilization of the laser frequency via optical feedback and using the approach of polarization spectroscopy is explained.

3.1. Fundamentals of diode lasers

Lasers are optical oscillators which are based on **L**ight **A**mplification by **S**timulated **E**mission of **R**adiation. The important process for the laser to operate as a coherent light source is that of stimulated emission of photons out of an atomic (or molecular) state. The three basic components required to build a laser are the gain medium for amplification of the light, an energy source which pumps the gain medium and an optical resonator, which provides frequency selective optical feedback of the emitted photons.
In order to achieve amplification of light, it is necessary to have population inversion in the gain medium, so that more atoms are in the upper than in the lower state of the laser transition. However, in thermal equilibrium the energy levels are occupied according to the Boltzmann distribution, and there is always more population in the lower energy states. Population inversion corresponds to a non-equilibrium situation and is achieved by actively pumping the laser medium, so that for energies $E_2 > E_1$ one obtains

$$N_2 - N_1 > 0\,, \tag{3.1}$$

where N_1 and N_2 are the populations of the corresponding energy levels.

Semiconductor lasers

In the case of diode lasers, the semiconductor material has energy bands instead of discrete energy levels. At zero temperature the valence band is fully occupied and no electron is

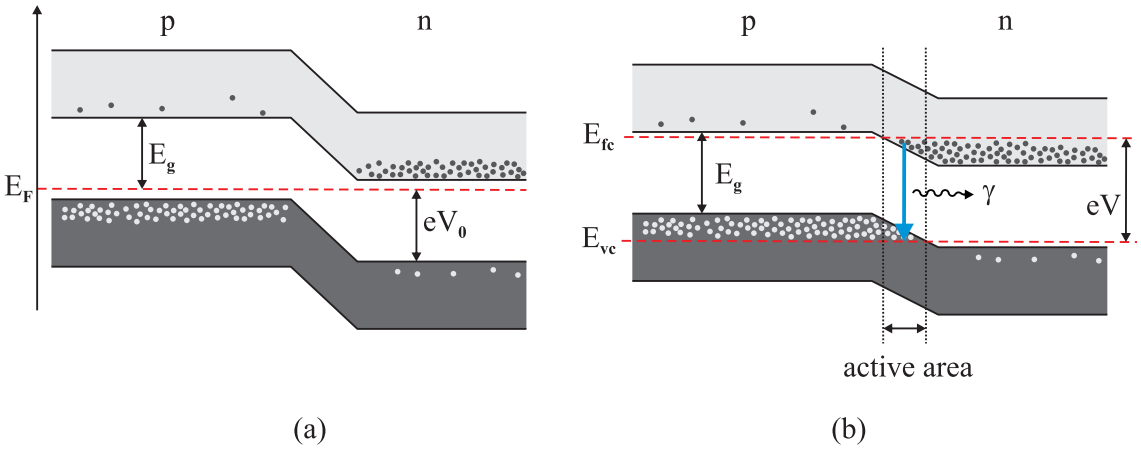

Figure 3.1.: (a) Band structure of a pn-junction in thermal equilibrium with the fermi energy E_F and the potential difference V_0 due to the diffusion of charge carriers. (b) Forward biased pn-junction with the external voltage V. The fermi levels for electrons, E_fc, and holes, E_fv are separated by eV, which leads to population inversion in the active area.

excited to the conduction band. The probability for a given energy state to be occupied by an electron is described by the Fermi-Dirac statistic

$$f(E) = \frac{1}{1 + \exp\left(\frac{E - E_\mathrm{F}}{k_\mathrm{B} T}\right)} \tag{3.2}$$

with the Fermi energy E_F, which is the maximum electron energy at $T = 0$, and the Boltzmann constant k_B. The probability for an energy level in the valence band to be empty, i.e., to be occupied by a hole, is thus given by $1 - f(E)$.
In a semiconductor laser, population inversion is achieved by pumping electrons in the active region of a forward biased pn-junction. Figure 3.1 (a) shows the band structure of a pn-junction in thermal equilibrium. The two different Fermi levels of the p- and the n-regions must align in the case of thermal equilibrium, and no charge carriers are present in the transition region. If an external forward biased voltage V is applied, the equilibrium is violated and the charge carrier distribution is now described by the two quasi-fermi levels E_fv and E_fc for the valence and the conduction band, respectively. This situation is illustrated in figure 3.1 (b), where due to the separation between E_fv and E_fc there is a net number of charge carriers in the active region. The occupation probabilities for an energy level in the conduction and in the valence band are given as [31]

$$f_\mathrm{v}(E) = \frac{1}{1 + \exp\left(\frac{E - E_\mathrm{fc}}{k_\mathrm{B} T}\right)} \qquad f_\mathrm{c}(E) = \frac{1}{1 + \exp\left(\frac{E - E_\mathrm{fv}}{k_\mathrm{B} T}\right)}\,. \tag{3.3}$$

The probabilities that a photon with energy $E = h\nu = E_2 - E_1$ is absorbed or emitted in the active region are thus

$$\begin{aligned} f_\mathrm{ab} &= f_\mathrm{v}(E_1)[1 - f_\mathrm{c}(E_2)] \\ f_\mathrm{em} &= f_\mathrm{c}(E_2)[1 - f_\mathrm{v}(E_1)]\,. \end{aligned}$$

The transition rates for spontaneous emission, $r_{\mathrm{sp}}(E)$, and that for stimulated emission and absorption, $r_{\mathrm{em}}(E)$ and $r_{\mathrm{ab}}(E)$,can be determined by

$$\begin{aligned} r_{\mathrm{sp}}(E) &= A_{21}\ \rho_{\mathrm{c}}(E_2)\rho_{\mathrm{v}}(E_1)\ f_{\mathrm{c}}(E_2)[1-f_{\mathrm{v}}(E_1)] \\ r_{\mathrm{em}}(E) &= B_{21}\ \rho_{\mathrm{c}}(E_2)\rho_{\mathrm{v}}(E_1)\ f_{\mathrm{c}}(E_2)[1-f_{\mathrm{v}}(E_1)] \\ r_{\mathrm{ab}}(E) &= B_{12}\ \rho_{\mathrm{c}}(E_2)\rho_{\mathrm{v}}(E_1)\ [1-f_{\mathrm{c}}(E_2)]f_{\mathrm{v}}(E_1)\,, \end{aligned}$$

where $\rho_{\mathrm{v}}(E)$ and $\rho_{\mathrm{c}}(E)$ are the respective density of states in the valence and the conduction band, and the proportionality constants A_{21} and $B_{21} = B_{12}$ are the Einstein coefficients [31]. For lasing operation one is mostly interested in the net stimulated emission rate $r_{\mathrm{st}}(E)$, which is given by

$$\begin{aligned} r_{\mathrm{st}}(E) &= r_{\mathrm{em}}(E) - r_{\mathrm{ab}}(E) && (3.4)\\ &= A_{21}\ \rho_{\mathrm{c}}(E_2)\rho_{\mathrm{v}}(E_1)\ [f_{\mathrm{c}}(E_2) - f_{\mathrm{v}}(E_1)]\,. && (3.5) \end{aligned}$$

In order to obtain population inversion, $r_{\mathrm{st}}(E)$ has to be positive, which leads to the inversion condition

$$f_{\mathrm{c}}(E_2) > f_{\mathrm{v}}(E_1)\,, \tag{3.6}$$

which is the equivalent to equation (3.1), and according to which the occupancy probability in the conduction band has to be larger than that of the valence band. The strong pumping of carriers into the active area by the injection current, as illustrated in figure 3.1 (b), leads to a shift of the quasi-fermi levels E_{fv} and E_{fc}, and condition (3.6) is fulfilled in the active area if the separation between the quasi-fermi levels is larger than the photon energy $h\nu$ [31],

$$E_{\mathrm{fc}} - E_{\mathrm{fv}} > h\nu\,. \tag{3.7}$$

The optical resonator of a laser diode is realized by the cleaved rear end facet of the semiconductor. Since semiconductor materials typically have large refractive indices ($n \approx 3.6$), there is a substantial back reflection due to the mismatch between the semiconductor refractive index and that of the surrounding air. If R_1 and R_2 are the reflectivities of the laser diode end facets, L the cavity length and α_l the constant losses inside the cavity, the threshold gain g_{th} has to be equal to the total losses in order to obtain laser oscillations. Additionally, the phase shift κL which the light experiences in one round trip has to be a multiple integer of π. Thus, the lasing condition can be written as

$$g_{\mathrm{th}} = \alpha_l + \frac{1}{2L}\ln\left(\frac{1}{R_1 R_2}\right) \tag{3.8}$$

with $\kappa L = m\pi$ and m an integer. The lifetime of the photons is proportional to the inverse of the total loss rate given by the right side of equation (3.8), which yields

$$\tau_{\mathrm{ph}} = \frac{1}{g_{\mathrm{th}} c}\,. \tag{3.9}$$

The dynamic behavior of a laser diode is characterized by investigating the propagation of the optical field inside the semiconductor medium. Thereby, one can introduce a normalized complex field amplitude $E_0(t)$ which is related to the photon number S by [31]

$$E_0(t) = \sqrt{S(t)}\exp(i\varphi(t)) \tag{3.10}$$

with the phase $\varphi(t)$ of the slowly varying amplitude $\sqrt{S(t)}$ of the traveling wave. The purpose of rate equations is to determine the temporal response of a laser diode. For the photon number $S(t)$, the carrier density $n(t)$ and the phase $\varphi(t)$ one can write the rate equations

$$\frac{dS}{dt} = \frac{S}{\tau_{\mathrm{ph}}}(G-1) + R_{\mathrm{sp}} \tag{3.11}$$

$$\frac{dn}{dt} = \frac{i-i_{\mathrm{th}}}{eV} - \frac{1}{\tau_e}(n-n_{\mathrm{th}}) - \frac{GS}{V\tau_{\mathrm{ph}}} \tag{3.12}$$

$$\frac{d\varphi}{dt} = \frac{\alpha}{2\tau_{\mathrm{ph}}}\frac{\partial G}{\partial n}(n-n_{\mathrm{th}})\,, \tag{3.13}$$

following the procedure in [31]. Here, R_{st} and R_{sp} are the effective stimulated and spontaneous emission rates taking into account the confinement of the light in the waveguide formed by the structure of the laser diode. The normalized gain of the laser diode is defined as $G = R_{\mathrm{st}}\,\tau_{\mathrm{ph}}$, and the lifetime of the charge carriers is given by τ_e. Furthermore, e is the electron charge, V defines the volume of the active medium, i is the injected current and i_{th} denotes the threshold current for laser operation. In relation (3.13) describing the phase variations, the term $\partial G/\partial n$ describes the dependence of the normalized gain $G = R_{\mathrm{st}}\,\tau_{\mathrm{ph}}$ on the carrier density, and n_{th} is the carrier density at the threshold gain g_{th}. The parameter α depends on the complex refractive index $\mu = \mu' + i\mu''$ of the medium and relates changes of the real part of the refractive index, μ', to changes in its complex part μ'', i.e.

$$\alpha = \frac{\Delta\mu'}{\Delta\mu''}\,. \tag{3.14}$$

This parameter plays an important role in the phase noise characteristics of laser diodes, as will be explained in section 3.3. Equations (3.11) to (3.13) are the basic relations to describe the dynamic behavior of the laser diode and they can be used to study its modulation response.

3.2. Theory of frequency modulation

In locking techniques such as optical phase locked loops, fast control of the laser frequency is required. In the case of diode lasers this demands modulation of its injection current, which causes a modulation of the output intensity as well as of the lasing frequency. This section gives a short introduction to the general theory of frequency modulation, and afterwards the modulation properties of semiconductor lasers are investigated in more detail.

3.2.1. Introduction to frequency modulation

In order to describe the modulation of the frequency of an oscillator signal, consider the carrier signal

$$v_{\mathrm{c}}(t) = V_{\mathrm{c}}\cos(\omega_{\mathrm{c}}t + \phi(t)) \tag{3.15}$$

with amplitude V_{c}, frequency ω_{c} and the time varying phase $\phi(t)$. Frequency modulation (FM) uses a modulation signal, $u_{\mathrm{m}}(t)$, to vary the carrier frequency within a small range

about its original value, i.e. the instantaneous output frequency of the oscillator is varied proportionally to the modulation signal. The instantaneous frequency of the signal is

$$\omega(t) = \omega_\mathrm{c} + \frac{d\phi(t)}{dt} = \omega_\mathrm{c} + \Delta\omega(t)\,, \tag{3.16}$$

where $\Delta\omega(t) = \frac{d\phi(t)}{dt}$ is the instantaneous frequency deviation. The latter is an important quantity in understanding the concept of frequency modulation, and it is proportional to the modulation signal $u_\mathrm{m}(t)$,

$$\Delta\omega(t) = k_\mathrm{FM}\, u_\mathrm{m}(t)\,, \tag{3.17}$$

where k_FM is the modulation sensitivity. The maximum (temporal) change of the carrier frequency is the peak frequency deviation

$$\Delta\Omega = |\Delta\omega_\mathrm{max}|\ . \tag{3.18}$$

Considering a sinusoidal modulation signal

$$u_\mathrm{m}(t) = U_\mathrm{m}\cos(\omega_\mathrm{m} t)\,, \tag{3.19}$$

the peak frequency deviation is directly proportional to the modulation amplitude U_m,

$$\Delta\Omega = k_\mathrm{FM}\, U_\mathrm{m}\,. \tag{3.20}$$

One should note that $\Delta\Omega$ is time independent and thus a real frequency, which has no Fourier component in the output spectrum. It is rather a measure of the maximum amplitude of the modulation signal.
The modulation index β is an important parameter in the characterization of FM spectra, and it is defined as the ratio between the peak frequency deviation and the modulation frequency:

$$\beta = \frac{\Delta\Omega}{\omega_\mathrm{m}}\,. \tag{3.21}$$

Thus, according to relation (3.20), the modulation index is a function of both the amplitude and the frequency of the modulating signal.
Using relations (3.16) and (3.17), the frequency modulated signal can be written in the form

$$v_\mathrm{FM}(t) = V_\mathrm{c}\cos\left(\omega_\mathrm{c} t + k_\mathrm{FM}\int u_\mathrm{m}(t)dt\right)\ . \tag{3.22}$$

With the definition of β this leads to the following expression for the FM signal:

$$v_\mathrm{FM}(t) = V_\mathrm{c}\cos\left(\omega_\mathrm{c} t + \beta\sin(\omega_\mathrm{m} t)\right)\ . \tag{3.23}$$

This equation describes how the modulated signal varies with time. In order to obtain the output spectrum in the frequency domain one can rewrite $v_\mathrm{FM}(t)$ in the complex form [32]

$$v_\mathrm{FM}(t) = V_\mathrm{c}\,\mathrm{Re}\left\{\exp(i\beta\sin(\omega_\mathrm{m} t))\,\exp(i\omega_\mathrm{c} t)\right\}\ . \tag{3.24}$$

The complex envelope contains the modulation frequency ω_m and the modulation index, and thus all information about the modulation. It can be written in terms of the Bessel functions J_n [32], yielding

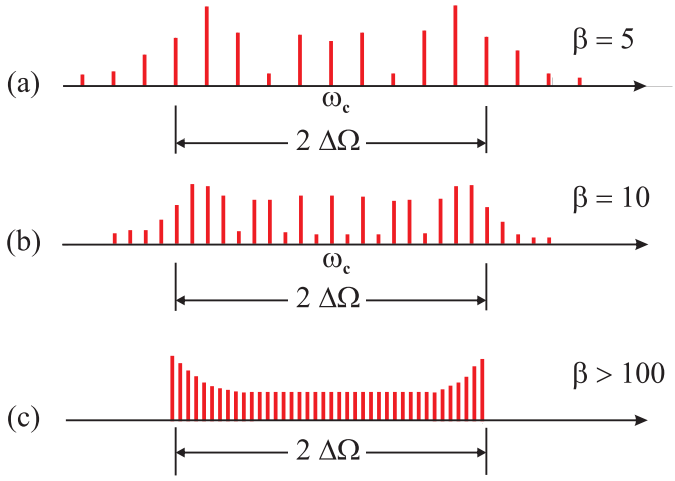

Figure 3.2.: Illustration of the spectra of a frequency modulated signal for different modulation indices β. The modulation amplitude U_m is held constant and the modulation frequency is varied. As β increases, the number of sidebands increases, and for very large modulation indices the number of sidebands cannot be resolved.

$$v_\mathrm{FM}(t) = V_\mathrm{c}\,\mathrm{Re}\left\{(i)^n \sum_{n=-\infty}^{\infty} J_n(\beta)\exp[i(\omega_\mathrm{c}+n\omega_\mathrm{m})t]\right\}. \tag{3.25}$$

The FM output spectrum in the frequency domain is given by the Fourier transform of equation (3.25). This relation indicates that the FM signal contains an infinite number of sideband pairs symmetrically distributed around the carrier frequency, where the separation between neighbouring sidebands is given by the modulation frequency[1]. The amplitude of the nth pair of sidebands is thereby given by the Bessel function coefficient $J_n(\beta)$. In practice, however, only a finite number of sidebands within a certain bandwidth are significant, depending on the modulation index β.
In order to obtain the peak frequency deviation $\Delta\Omega$ from the FM spectrum, its dependence on the modulation index β has to be considered. Figure 3.2 shows the theoretical FM spectra for different values of β in the case of a constant modulation amplitude, i.e. a constant $\Delta\Omega$, and increasing modulation frequency [33]. The number of sidebands increases with larger modulation indices. In the case of small β only a few sidebands are obtained and $\Delta\Omega$ is smaller than the range of significant sidebands. However, for very large modulation indices the number of sidebands cannot be resolved, but the envelope determines the peak frequency deviation $\Delta\Omega$, which in this limit can be obtained by measuring the edges of the FM spectrum envelope.

3.2.2. Frequency modulation of laser diodes

The FM spectrum of a laser diode whose injection current is modulated by a sinusoidal signal is investigated in this section. A variation in the injection current leads to a change of the laser intensity and also of the optical frequency. Two main effects determine the modulation response of a laser diode. First of all, a modulation of the charge carrier density causes a modulation of the photon number and of the refractive index, which in

[1] This can be seen more obvious by writing equation (3.25) in the explicit form.

turn changes the frequency. Furthermore, temperature variations of the laser diode also lead to a change in the emission frequency due to a modulation of the cavity length.
In order to determine the FM response of the laser diode, the intensity modulation (IM) characteristics have to be considered first. If a step-current pulse above threshold is applied to the laser diode, the current pulse increases the carrier density above the lasing threshold n_{th}. This consequently causes an increased photon number S, since the normalized gain $G = R_{\mathrm{st}}\,\tau_{\mathrm{ph}}$ in equation (3.11) includes the stimulated emission rate, which depends on the charge carrier density. The additional photons in turn lead to an enhanced rate of generated photons due to stimulated emission. However, this large number of photons "consumes" a lot of charge carriers, which again leads to a reduction of n below n_{th}. This on the other hand causes the photon number S to decrease rapidly again, which also increases the carrier density again and so on. These relaxation oscillations are damped due to spontaneous emission and a steady state is reached after a certain time (typically 1 ns). The occurrence of relaxation oscillations is due to the fact that the photon lifetime is typically much shorter than the lifetime of the charge carriers, i.e. $\tau_{\mathrm{ph}} \ll \tau_e$.
In order to obtain the response to a sinusoidal modulation signal rather than a step function, consider the modulated current

$$i(t) = \langle i \rangle + \Delta i \cos(\omega_{\mathrm{m}} t)\,, \tag{3.26}$$

with the amplitude Δi of the modulation signal, the modulation frequency ω_{m} and the mean value of the injection current $\langle i \rangle$. In the case of small modulation amplitudes $|\Delta i| \ll \langle i \rangle$, this leads to a sinusoidal variation of the photon number S and the carrier density n with deviations ΔS and Δn, respectively. One can derive an expression which connects the current changes to the changes of the photon number, which, as described in [31], yields

$$\frac{\Delta S}{\Delta i}\left(\frac{e}{\tau_{\mathrm{ph}}}\right) = \frac{1}{1 + \frac{i\omega_{\mathrm{m}}}{\omega_{\mathrm{d}}} + \left(\frac{i\omega_{\mathrm{m}}}{\omega_{\mathrm{r}}}\right)^2}\,. \tag{3.27}$$

Here, ω_{r} is the relaxation resonance frequency and ω_{d} is the damping frequency. They are given by [31]

$$\omega_{\mathrm{r}} = \frac{1}{\tau_{\mathrm{ph}}}\sqrt{\frac{\langle S \rangle\, \partial G/\partial n}{V}} \qquad\qquad \omega_{\mathrm{d}} \cong \frac{\omega_{\mathrm{r}}^2\,\tau_{\mathrm{ph}}}{\gamma}\,, \tag{3.28}$$

where ω_{r} depends on the average photon number $\langle S \rangle$ and the partial derivative of the normalized gain G with respect to the carrier density. The frequency ω_{d} describes the damping of the relaxation oscillations, in which the term γ is related to the spontaneous emission and nonlinearities of the gain G such as the effect of gain compression [34]. Depending on the operating current the relaxation damping is dominated by spontaneous emission, in the case of small photon numbers, whereas for larger photon numbers the gain compression becomes more relevant.
Based on equation (3.27) the frequency response of a laser diode can be calculated. For this purpose, one has to find an expression which connects the frequency changes $\Delta\nu$ to the photon number variations ΔS. A change in the optical frequency is related to the phase changes given in equation (3.13), since $\Delta\omega = \omega - \omega_{\mathrm{th}} = d\varphi/dt$. By expanding G from equation (3.11) in terms of $n = n_{\mathrm{th}}$ and combining this with the phase rate equation (3.13),

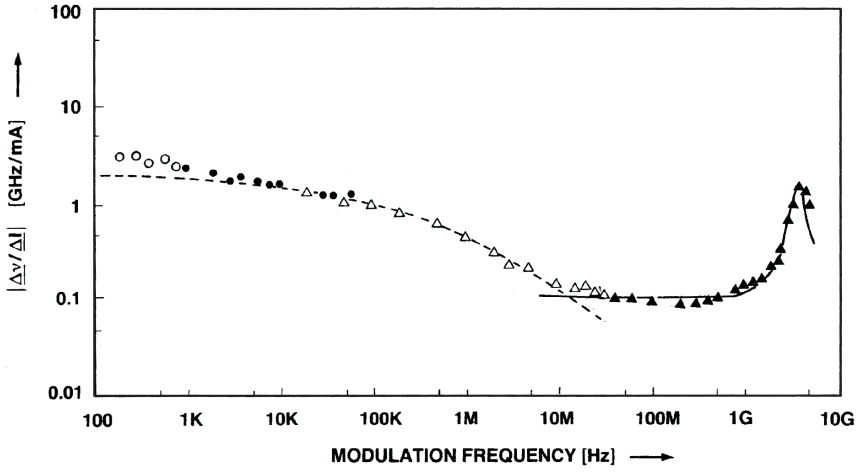

Figure 3.3.: Typical frequency response $\Delta\nu/\Delta i$ of a laser diode whose injection current is modulated. The graph shows the response of a GaAlAs laser diode and is obtained from reference [31].

a relation $\Delta\nu/\Delta S$ can be derived for the case of a small sinusoidal modulation, yielding [31]

$$\frac{\Delta\nu}{\Delta i} = \frac{\Delta\nu}{\Delta S}\,\frac{\Delta S}{\Delta i} = \frac{\alpha\,\tau_{\mathrm{ph}}\,\omega_{\mathrm{c}}}{4\pi e\,\langle S\rangle}\,\underbrace{\frac{1+i(\omega_{\mathrm{m}}/\omega_{\mathrm{c}})}{1+(i\omega_{\mathrm{m}}/\omega_{\mathrm{r}})^2+i(\omega_{\mathrm{m}}/\omega_{\mathrm{d}})}}_{\text{carrier density effect}} + \underbrace{C_{\mathrm{t}}\,\frac{1}{1+i(\omega_{\mathrm{m}}/\omega_{\mathrm{t}})}}_{\text{thermal effect}}\,. \tag{3.29}$$

The first term due to carrier density modulation is similar to that for intensity modulation, but additionally contains the characteristic frequency ω_{c}, which describes the relation between intensity and frequency modulation. The thermal effects were not incorporated in the considerations of the intensity modulations, and they are additionally included by the second term. This describes the response similar to that of a low pass filter, where the cutoff is here given by the thermal cutoff frequency ω_{t} which is typically in the range of 100 kHz...1 MHz. The thermal constant C_{t} depends on the thermal resistance and the temperature sensitivity of the laser diode.
In figure 3.3 the typical FM response of a laser diode is shown. The pronounced peak in the frequency range above 1 GHz corresponds to the relaxation oscillations, and the carrier density effect dominates at large frequencies of more than 10 MHz (solid line). For low modulation frequencies the FM response is mainly determined by the thermal effects and starts to decrease in the range of 10 kHz, dependent on the thermal cutoff frequency (dashed line).
The correlation between intensity and frequency modulation is described by the characteristic frequency ω_{c}, and for low modulation frequencies (< 1 GHz) the FM response is proportional to the IM response, with the proportionality determined by ω_{c}. It is expedient to describe the relation between FM and IM by their modulation indices β_{FM} and β_{IM}, respectively. For frequency modulation β_{FM} is given by equation (3.21), and in the case of amplitude modulation the modulation index is defined as the maximum deviation of the photon number from the mean value, i.e.,

$$\beta_{\mathrm{FM}} = \left|\frac{2\pi\Delta\nu}{\omega_{\mathrm{m}}}\right| \qquad \beta_{\mathrm{IM}} = \left|\frac{\Delta S}{\langle S\rangle}\right|\,. \tag{3.30}$$

The ratio between the two modulation indices can be written as [31]

$$\frac{\beta_{\mathrm{FM}}}{\beta_{\mathrm{IM}}} = \frac{\alpha}{2}\sqrt{1+\left(\frac{\omega_{\mathrm{c}}}{\omega_{\mathrm{m}}}\right)^2}\,. \tag{3.31}$$

The factor α is given in equation (3.14) and typically takes values between $3\ldots7$. The characteristic frequency lies in the low GHz-range, dependent on the optical intensity. Thus, for slow modulation frequencies below 10 MHz we find $\beta_{\mathrm{FM}} \gg \beta_{\mathrm{IM}}$. If the laser diode is modulated at low modulation currents (in amplitude) one can thus have a significant frequency shift in conjunction with negligible intensity modulation.

3.3. Phase and frequency noise of laser diodes

The linewidth of a laser is broadened due to phase and frequency noise of the optical field. Schawlow and Townes predicted a fundamental limit for the laser linewidth which originates from spontaneous emission in the laser medium [35]. Whereas photons generated by stimulated emission have the same phase, the phase of spontaneously emitted photons is random, and each spontaneously emitted photon is further multiplied by stimulated emission. This leads to considerable phase fluctuations of the lasing field, and the resulting linewidth has a Lorentzian shape.
However, in semiconductor lasers it was found that the linewidth is significantly larger than that predicted by Schawlow and Townes [36], and typical values are in the range of 100 MHz. It was Henry who realized that a correction factor is required, whose origin is the strong coupling between amplitude and phase noise in semiconductor lasers [37]. Spontaneous emission in diode lasers leads to fluctuations of the refraction index μ,

$$\Delta\mu = \Delta\mu' + i\Delta\mu''\,, \tag{3.32}$$

within the duration of the relaxation oscillations. During this time, until the oscillations are damped, there will be a net change in the laser gain $\Delta G \propto \Delta\mu''$ due to changes in the absorptive part μ'' of the refractive index. The origin of $\Delta\mu''$ is a fluctuation of the charge carrier density n. Since the real and imaginary part of μ are related by the Kramers-Kroning relations, this also leads to fluctuations of the dispersive part $\Delta\mu'$. Hence, there is a coupling between the phase and the amplitude of the laser field, which is described by the factor α given in equation (3.14). The resulting modified Schawlow-Townes linewidth is given by [37]

$$\Delta\nu = \frac{2\pi h\nu(\Delta\nu_{\mathrm{c}})^2}{P}(1+\alpha)^2\,. \tag{3.33}$$

This formula describes the linewidth due to spontaneous emission, which corresponds to white frequency noise and results in a Lorentzian line shape of the laser spectrum. However, there can be a significant contribution of $1/f$-frequency noise to the spectral broadening of lasers. In semiconductor lasers fluctuations in the charge carriers and in temperature, due to technical noise of the injection current, can lead to a $1/f$-dependence of the frequency noise spectrum. It can be shown [31, 38] that the spectral line shape for $1/f$-frequency noise is linked to a Gaussian line shape. Usually one has to consider both white and $1/f$-frequency noise, and the frequency noise spectrum is given by the sum of both noise processes. The resulting laser line shape is a convolution of the Lorentzian and the Gaussian spectrum, i.e. in this case the laser line shape is described by a Voigt profile.

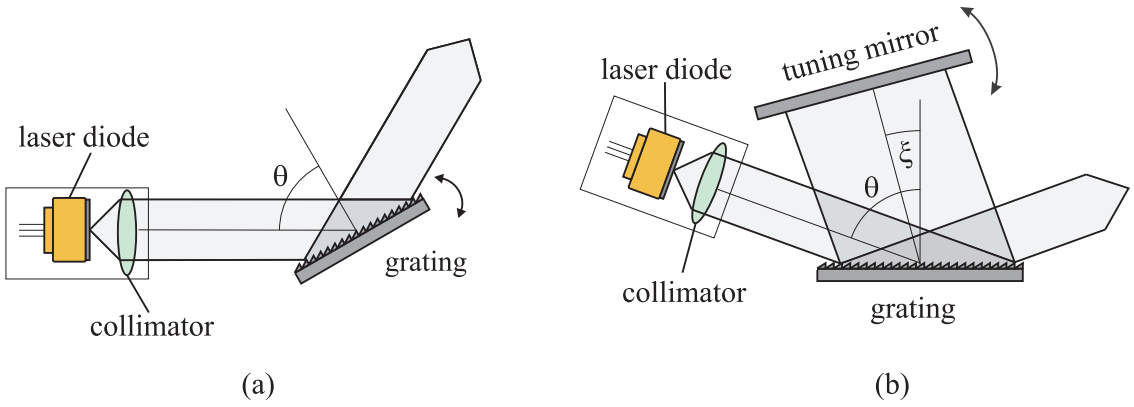

Figure 3.4.: Littrow (a) and Littman-Metcalf configuration (b) for implementation of an external cavity diode laser.

Finally, one should note that the relaxation oscillations also contribute to the frequency noise of a diode laser, and they cause a large peak in the frequency noise spectrum at the relaxation oscillation frequency ω_r, equivalent to the peak in the modulation response in figure 3.3. As long as the linewidth is considerably smaller than relaxation resonance frequency, the linewidth can be estimated by formula (3.33), or in the case of significant $1/f$-noise by the Voigt profile.

3.4. Frequency stabilization

3.4.1. Optical feedback

The linewidth of semiconductor lasers can be reduced by passive stabilization of the optical frequency via optical feedback. An external resonator which is build around the laser diode does not only reduce the laser linewidth but also improves frequency tuning.
An effective way to implement optical feedback is by using a diffraction grating which reflects the emitted light back into the laser diode. The external resonator is then formed by the rear end facet of the laser diode and the external grating, resulting in an external cavity diode laser (ECDL). In this configuration the laser frequency is determined by the overlap of the two resonator modes. The selected wavelength λ is determined by the grating equation

$$m\lambda = d\,(\sin\theta + \sin\xi)\,, \tag{3.34}$$

where d is the grating constant, m the diffraction order and θ and ξ are the incident angle of the laser beam to the grating and the diffraction angle, respectively [39]. Two common configurations to implement optical feedback are often used, which are the Littrow configuration as shown in figure 3.4 (a) and the Littman-Metcalf configuration illustrated in figure 3.4 (b).
In the Littrow arrangement the grating reflects the first diffraction order back into the laser diode, and the zeroth order provides the output laser beam. Here, the angle of incidence is equal to the diffraction angle, i.e. $\theta = \xi$, and the laser wavelength is thus determined by

$$m\lambda = 2d\sin\theta\,. \tag{3.35}$$

The Littrow setup is easily implemented and the wavelength can be adjusted by tilting the grating and thus changing the diffraction angle. However, it has the disadvantage that tilting of the grating also changes the angle of the output beam.
The Littman configuration in contrast circumvents this problem by using an extra mirror, which reflects the diffracted beam back into the laser diode and thus forms the external resonator. Here, the angle ξ between the first diffraction order and the grating is adjusted by tuning the mirror in order to select the laser wavelength according to the grating equation (3.34). As in the Littrow setup, the zeroth order is used to couple out the laser beam. The double pass configuration of the Littman-Metcalf setup leads to an increased selectivity and the incidence angle θ can be chosen independently of the wavelength. This allows one to illuminate most grooves of the grating by choosing a large angle θ.

3.4.2. Polarisation spectroscopy

In order to actively stabilize the laser frequency to an atomic transition, an error signal proportional to the frequency difference from resonance is required. The method of polarization spectroscopy can be used to overcome the Doppler-broadening of the spectral line shapes by detecting the change in the polarization state of a probe laser caused by a second counter-propagating pump beam [40, 41]. The obtained polarization spectrum is an ideal error signal for frequency stabilization.
The basic idea of polarization spectroscopy is to induce a birefringence in an atomic gas by selectively pumping the m_F-states of an atomic transition. The schematic setup is shown in figure 3.5 (a). The circularly polarized pump beam enters the gas cell and the optically pumped atoms are probed with a weak counter-propagating probe beam, where both beams are assumed to originate from the same laser. According to the transition rules and in the case of degenerate sublevels, the strong pump beam only excites transitions with $\Delta m_F = +1$, as shown in figure 3.5 (b) for a transition $J = 1 \rightarrow J = 2$, where the quantization axes is chosen in the direction of the pump beam. This leads to an unbalance in the population of the m_F-states and hence a net spatial orientation, resulting in an optical anisotropy of the atomic ensemble.
If a 45°-linearly polarized weak probe beam passes through the pumped atomic ensemble, its polarization state is rotated due to the induced birefringence. To see the origin of this effect, the probe beam can be decomposed into two σ^+- and σ^--circularly polarized beams. Due to the anisotropy, the refractive indices n_+ and n_- for the two counter-rotating waves are different, and so are the absorption coefficients α_+ and α_-. For an interaction region with length L, the phase shift caused by the difference in the refractive indices, $\Delta n = n_+ - n_-$, and the absorption difference are given by [40]

$$\Delta\phi = \frac{\omega L}{c}\Delta n \qquad\qquad \Delta\alpha = \frac{\Delta\alpha_0}{1 + (\frac{\omega-\omega_0}{\gamma})^2}\,. \tag{3.36}$$

Here $\omega - \omega_0$ is the detuning from resonance, γ is the power broadened linewidth of the atomic transition, and $\Delta\alpha_0$ is the absorption difference at resonance $\omega = \omega_0$. The absorption difference of the two circularly polarized components is a Lorentzian function and causes an ellipticity of the transmitted probe light, an effect also known as circular dichroism. The difference in the refraction index Δn causes a rotation of the polarization axes, which is the important effect in order to obtain the error signal. As an important point, one should note that the atoms are probed Doppler-free, since the counter-propagating pump and probe beams interact with a different velocity class of atoms as long as their

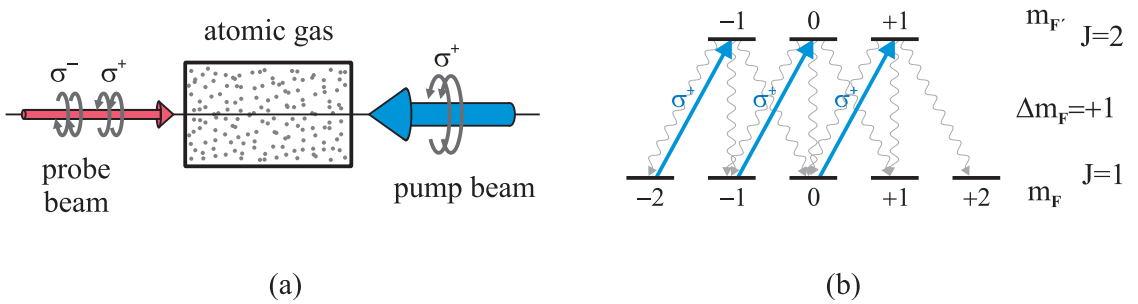

Figure 3.5.: (a) Basic setup for polarization spectroscopy using a circular polarized pump beam and a linear counter-propagating probe beam, which can be written as a superposition of σ^+- and σ^- polarized light. (b) m_F-state selective optical pumping by a σ^+-polarized pump beam for a transition $J = 1 \rightarrow J = 2$.

frequency difference is larger than the natural linewidth of the probed transition.
In order to use the birefringence for frequency locking, the difference in the power of the s- and p-polarized components of the probe field, i.e. the rotation $\delta\phi$, has to be detected. This dispersive signal gives the derivative of the Lorentzian line shape, which then provides the error signal for frequency locking. The advantage of this differential error signal is that one can lock to the center of the atomic transition, whereas e.g. in saturation absorption spectroscopy one has to lock to the side of the saturated absorption dip. Furthermore, the steepness of the slope can be adjusted carefully by adjusting the power and polarization of the laser beam.

4. Optical phase locked loops

Optical phase locked loops (OPLL) are an essential element of phase-coherent lasers, which form the basis for coherent quantum optic experiments such as EIT, lasing without inversion (LWI) or stimulated Raman adiabatic passage (STIRAP). The principle operation of an OPLL is the same as that of a standard PLL used in many electrical systems to provide phase stable signals. This chapter gives an introduction to phase locked loops and discusses the fundamental theory of optical PLLs and their characterization. The experimental realization of an OPLL will be discussed in chapter 4.

4.1. Introduction to phase locked loops

4.1.1. What is a phase locked loop?

In a phase locked loop the phase of an oscillator is compared with the phase of a reference signal, also called local oscillator (LO). The detected phase difference is converted into a voltage, which can be used as the error signal to control the phase difference of the two oscillators. In the locked condition they will have a fixed phase relation, and since frequency is the time derivative of phase, this implies that the frequency of the slave oscillator, which is the one which is stabilized by the loop, will be exactly proportional to that of the LO.

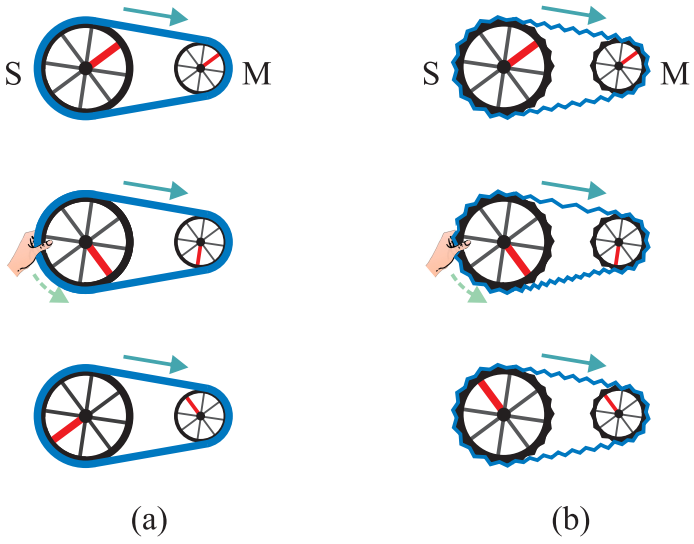

Figure 4.1.: Mechanical analogy of (a) a frequency lock and (b) a phase lock adopted from [42]. Initially the wheels rotate with the same frequency (top), then the slave wheel gets temporarily slowed down (center) and afterwards they rotate again with the same frequency (bottom), but only in (b) the phase relation is recovered.

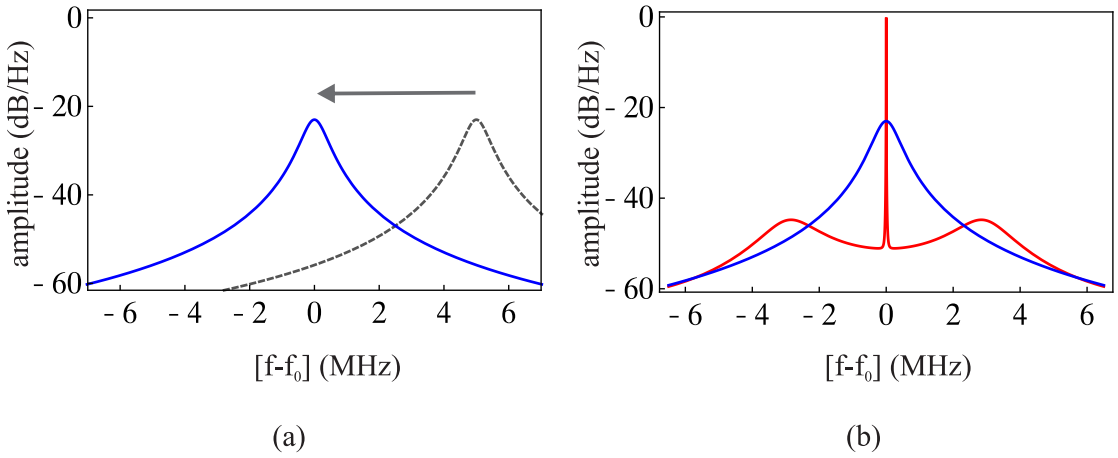

Figure 4.2.: Power spectra on a logarithmic scale of a noisy signal in the case of frequency locking (a) and phase locking (b). In (a) the frequency lock only corrects the center frequency to the reference value f_0, and in (b) the phase lock additionally reduces the noise around the carrier frequency.

In figure 4.1 the difference between phase and frequency locking is illustrated using a mechanical analogy adopted from reference [42]. Consider two wheels which are both rotating with a certain angular frequency given by the "master wheel" (M). As long as there is no influence from outside, the "slave wheel" (S) follows this frequency because both wheels are coupled with a belt. In the case of frequency stabilization, the belt is represented by an inelastic v-belt. If an external force changes the frequency of the slave wheel (e.g. by slowing down the wheel with the hand), the v-belt will continue to slip over it with the frequency of the master wheel. After the disturbance the frequency will again be the same as that of the master, but the original phase relation will be lost. In contrast, if one considers two cog wheels instead which are coupled by an elastic chain, a short change of the slave wheel's frequency will cause stretching of the chain on one side of the wheel and compression on the other side. Afterwards, the chain will recover the original phase relation by forcing the slave wheel to rotate with a higher frequency for a short time, until the stretching and compression caused by the disturbance is compensated. Thus, the original phase relation between the two wheels is preserved.
To demonstrate the effect of a PLL on the slave signal which gets stabilized, it is convenient to consider the power spectrum of the signal. As depicted in figure 4.2 (a), a frequency lock sets the frequency of the signal to some reference value f_0 but does not change its shape, i.e. a frequency lock does not suppress the noise which causes broadening of the signal. In contrast, a phase lock will not only correct the signal's center frequency but will additionally decrease its spectral width, that is it suppresses the noise so that one obtains only a narrow peak at the center frequency, which is given by the LO.

4.1.2. Optical phase locking of two lasers

An optical phase locked loop is a special kind of PLL in which the two oscillators are represented by lasers. Their frequencies or phases, respectively, are either locked so that they have the same frequency (homodyne optical phase locking), or their phase difference is locked to a stable reference oscillator (heterodyne optical phase locking). Lasers are coherent optical oscillators which are characterized by their long coherence time, which

is due to the stimulated emission of radiation in the lasing process. The coherence of a laser is limited by spontaneous emission also inherent in the laser medium, which causes a random walk of the phase of the laser field. In this sense, the coherence time can be regarded as the time during which no phase fluctuations of the light field are present. However, the phases of two independent lasers are uncorrelated and there is no coherence between the two light fields. In order to couple those coherently, the frequency of the slave laser has to be controlled with a servo loop relative to the frequency of the second master laser.
The electric fields of the lasers can be expressed as [21]

$$E_1(t) = E_{01} \exp\left[i(\omega_1 t + \varphi_1(t))\right] \tag{4.1}$$
$$E_2(t) = E_{02} \exp\left[i(\omega_2 t + \varphi_2(t))\right] \tag{4.2}$$

where E_{01} and E_{02} are the field amplitudes. The fields oscillate with frequencies ω_1 and ω_2, respectively, and $\varphi_1(t)$ and $\varphi_2(t)$ denote the phase fluctuations of the lasers. The instantaneous phases of the light fields are given by

$$\phi_1(t) = \omega_1 t + \varphi_1(t) \qquad \text{and} \qquad \phi_2(t) = \omega_2 t + \varphi_2(t)\,, \tag{4.3}$$

which leads to the instantaneous frequency difference

$$\Delta\omega = \frac{d}{dt}\Delta\phi = \frac{d}{dt}[\phi_1(t) - \phi_2(t)] = (\omega_1 - \omega_2) + [\dot{\varphi}_1(t) - \dot{\varphi}_2(t)]\,. \tag{4.4}$$

If there are no phase fluctuations between the two light fields, i.e. if

$$\dot{\varphi}_1(t) - \dot{\varphi}_2(t) = 0 \tag{4.5}$$

and thus the phase difference $\Delta\varphi(t) = \varphi_1(t) - \varphi_2(t)$ is constant in time, the lasers are perfectly coherently coupled and the instantaneous frequency difference has a fixed value $\Delta\omega = \omega_1 - \omega_2$. Therefore, stabilization of the lasers' phase difference leads to a constant frequency difference between the lasers.
Figure 4.3 shows the basic setup for heterodyne optical phase locking. It is composed of a master laser, a slave laser, two local oscillators and the feedback loop. In order to perform phase locking of two lasers at a large frequency difference, their beat signal has to be detected by superimposing the two light fields on a fast photodiode. The intensity on the photodiode is then given by

$$\begin{aligned} I(t) =& \frac{1}{2}\epsilon_0 c\,|E_1(t) + E_2(t)|^2 \\ =& I_1 + I_2 + 2\sqrt{I_1 I_2}\cos[\Delta\omega t + \Delta\varphi(t)]\,, \end{aligned} \tag{4.6}$$

where I_1 and I_2 are the intensities of the two laser fields and ϵ_0 is the vacuum permittivity. Since only the oscillating term is needed, the dc-terms I_1 and I_2 are ignored. By detecting the beat signal oscillating at $\Delta\omega$, the frequency gets down-converted at the photodiode from the THz-range to the microwave range, meaning that the master laser acts as a reference oscillator. The resulting beat signal is an electrical quantity which can be processed by the control loop.
In our specific case the frequency of the beat signal lies in the GHz-range, but most phase detectors work in the MHz-range. Thus it is necessary to down-convert the beat signal further at a second conversion stage. For this purpose the beat signal can be compared

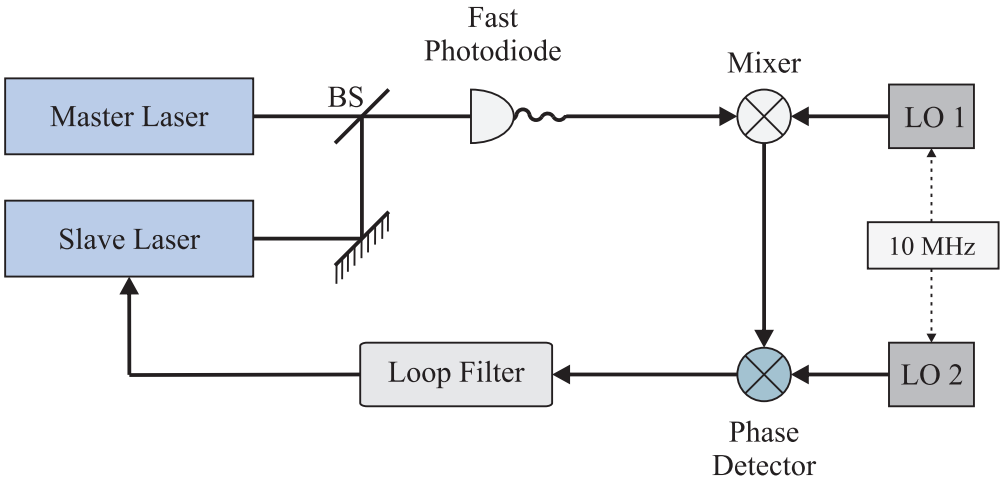

Figure 4.3.: Basic scheme of heterodyne optical phase locking at large frequency offsets. The beat signal of the lasers is detected with a photodiode and mixed with a local oscillator (LO1). The phase is then compared with the phase of a second oscillator (LO2) at the phase detector. Both oscillators are phase stabilized to the same 10 MHz reference. The loop filter converts the output of the PD into a control voltage and thus provides the feedback to the slave laser.

with a stable radio frequency (RF) signal from a local oscillator (LO1) at a mixer[1]. The analog mixer multiplies the two input signals and its output oscillates at the sum and difference frequency of the beat signal and the LO1. After suppressing the unwanted fast oscillating part with a low pass filter, the output of the mixer is given by

$$v_{\mathrm{mixer}}(t) \propto \cos[(\omega_{\mathrm{LO1}} - \Delta\omega)t - (\varphi_{\mathrm{LO1}}(t) - \Delta\varphi(t))] \tag{4.7}$$

with the phase $\varphi_{\mathrm{LO1}}(t)$ and frequency ω_{LO1} of LO1. The phase of this signal is then compared with the phase $\varphi_{\mathrm{LO2}}(t)$ of a second local oscillator LO2, set to the desired frequency of the down-converted signal, using a phase frequency detector whose output voltage represents the phase difference of the two input signals within a certain phase range. The output of an analog phase detector (APD), after filtering out the high frequency part, can be written as [43]

$$v_{\mathrm{APD}}(t) \propto \cos[\Delta\varphi(t) - \varphi_{\mathrm{LO1}}(t) + \varphi_{\mathrm{LO2}}(t)]\,. \tag{4.8}$$

In order to ensure a stable PLL it is necessary that the phase difference of the two local oscillators, $\Delta\varphi_{\mathrm{LO}}(t) = \varphi_{\mathrm{LO1}}(t) - \varphi_{\mathrm{LO2}}(t)$, does not change in time. Therefore they must be phase locked to the same frequency reference, e.g., a GPS disciplined oscillator or a stable 10 MHz reference signal typically provided by signal generators. As a last step, the output of the phase detector, that is the error signal, is adjusted by a loop filter. This filter is necessary to process the error voltage and to provide an appropriate control voltage to the slave laser which causes a frequency change in a direction so that the phase error $\Delta\varphi(t) - \Delta\varphi_{\mathrm{LO}}(t)$ is reduced.
Phase locking two lasers is typically challenging due to the high amount of phase noise inherent in the lasers compared to noise in electronic signal sources. For this reason, a large loop bandwidth on the order of the combined linewidths of the lasers is required in order to strongly suppress the low and high frequency noise. Even in the locked condition the

[1] Another way would be to use a frequency divider to divide the signal down by the desired factor.

instantaneous frequency difference $\Delta\omega$ is not a perfect single frequency but still contains some residual phase noise. In order to build a stable phase locked system, the remaining phase error at the output of the phase detector should not exceed the dynamic range of the detector, otherwise "cycle slips" occur and disturb the phase coherence of the lasers.

4.2. Theoretical analysis of optical phase locked loops

Since optical phase locking can be described by the same theory as that of normal PLLs, the basic principles of PLLs are discussed in this chapter. Subsequently, the special case of an optical PLL, in which the VCO is represented by a laser diode, is covered in more detail. Furthermore, a general introduction to phase noise characteristics is given and the power spectrum of a phase locked beat signal is calculated. Thereupon the propagation of phase noise in OPLLs is specified further.

4.2.1. Fundamentals of control theory

Control systems are mostly negative feedback circuits used to control the output of a dynamical system depending on its input. The actual value of the output signal is compared with a desired reference signal and the control loop provides feedback of the error signal. A PLL is a special feedback system which consists essentially of a voltage controlled oscillator (VCO), a phase detector (PD) and a loop filter (LF) [44]. Here, the loop controls the phase of the VCO (slave) with respect to the phase of the master oscillator. This is the simplest form of a PLL, but in general, such as for an optical phase locked loop, the PLL can contain several other components like mixers or frequency dividers. For simplicity and because other components can be easily included afterwards, at first only the basic PLL is considered.
The most important tool to analyze PLLs is the concept of transfer functions and that of the related Laplace transform, which is widely used in signal processingt [45]. For linear time-invariant systems the transfer function K describes the relation between the output and the input of the system. In the time domain, the output of a system is given by the convolution of the pulse response of the system with the input signal. In the frequency domain it is simply the product of the transfer function K and the system input:

$$v_{\mathrm{out}} = K \cdot v_{\mathrm{in}} \,. \tag{4.9}$$

If the system consists of several components, the overall transfer function is simply the product of all the transfer functions of the components. A PLL can be treated as a linear system if one considers only small phase errors, so that one can neglect any non-linearity of the components such as the phase detector. In this situation the concept of transfer functions can be applied to PLLs. In the following, small letters $v(t)$ and $\phi(t)$ are used for signals in the time domain, and capital letters $V(s) = \mathcal{L}\{v(t)\}$ and $\Phi(s) = \mathcal{L}\{\phi(t)\}$ for the frequency domain, in which $\mathcal{L}\{\cdot\}$ denotes the Laplace transform and s is the complex Laplace variable related to the frequency by $s = i\omega$.
In figure 4.4 the block diagram of a PLL is shown. The input signal is the phase $\phi_{\mathrm{r}}(t)$ of the reference oscillator, which is compared with the output signal given by the phase $\phi_{\mathrm{o}}(t)$ of the slave oscillator (VCO) at the phase detector. In a PLL phase is transferred to voltage at the phase detector and back into frequency at the VCO. In the time domain the linearized output of the phase detector is given by the error voltage [44]

$$v_{\mathrm{err}}(t) = K_{\mathrm{d}}(\phi_{\mathrm{r}} - \phi_{\mathrm{o}})(t) \,, \tag{4.10}$$

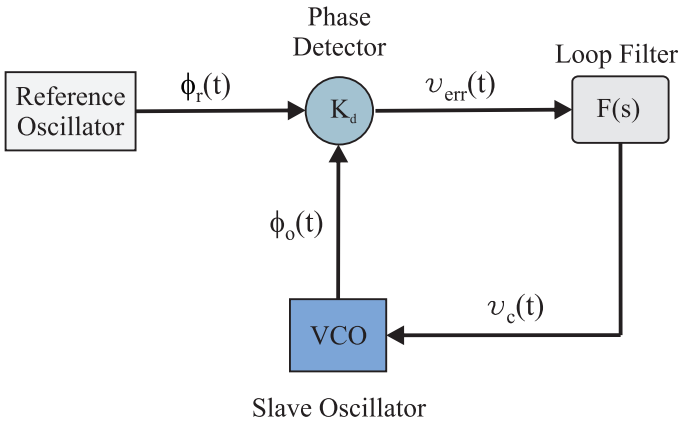

Figure 4.4.: Block diagram of the PLL: ϕ_r and ϕ_o are the phases of the reference and slave oscillator, $F(s)$ is the loop filter transfer function and $v_{\mathrm{err}}(t)$ and $v_c(t)$ are the error and control voltages, respectively.

where K_d denotes the linear sensitivity of the phase detector and $\phi_\mathrm{err} = \phi_\mathrm{r} - \phi_\mathrm{o}$ describes the phase error between the input and the output signal. Similarly, one can express this relation in the frequency domain as

$$V_\mathrm{err}(s) = K_\mathrm{d}(\Phi_\mathrm{r} - \Phi_\mathrm{o})(s)\,. \tag{4.11}$$

The error voltage provided by the phase detector is the input of the loop filter, whose output is the control voltage

$$V_\mathrm{c}(s) = F(s)V_\mathrm{err}(s)\,, \tag{4.12}$$

in which the transfer function of the loop filter is given by $F(s)$.
The control voltage provided by the loop filter is applied to the VCO, which is an oscillator whose output frequency can be controlled by the input voltage. Thus, the control voltage $v_\mathrm{c}(t) = \mathcal{L}^{-1}\{V_\mathrm{c}(s)\}$ leads to a frequency deviation $\Delta\omega_\mathrm{o}(t)$ of the VCO from its mean value,

$$\Delta\omega_\mathrm{o}(t) = K_\mathrm{o}v_\mathrm{c}(t)\,, \tag{4.13}$$

where K_o describes the constant proportional gain of the VCO. This equation describes the frequency output of the VCO, however, the phase output $\Phi_\mathrm{o}(s)$ is the desired quantity, and it can be determined using the relation

$$\frac{d}{dt}\phi_\mathrm{o}(t) = \Delta\omega_\mathrm{o}(t) = K_\mathrm{o}v_\mathrm{c}(t)\,. \tag{4.14}$$

The relation between the output phase and the input voltage in the frequency domain is obtained using the Laplace transform, which yields

$$\mathcal{L}\{\frac{d}{dt}\phi_\mathrm{o}(t)\} = s\,\Phi_\mathrm{o}(s) = K_\mathrm{o}V_\mathrm{c}(s)\,. \tag{4.15}$$

The transfer function of the VCO is thus given as the product of the linear gain K_o and an integral term $1/s$, representing the conversion from frequency to phase:

$$\Phi_\mathrm{o}(s) = \frac{K_\mathrm{o}}{s}V_\mathrm{c}(s)\,. \tag{4.16}$$

The open-loop gain $G(s)$ describes how a phase error $\Phi_{\mathrm{err}}(s)$ transforms to the output of the VCO in the open-loop condition. It is defined as the product of the transfer functions of all the components in the loop [44]:

$$G(s) = \frac{\Phi_{\mathrm{o}}(s)}{\Phi_{\mathrm{err}}(s)} = \frac{K_{\mathrm{d}} K_{\mathrm{o}} F(s)}{s} \,. \tag{4.17}$$

When feedback is implemented (i.e. in the closed-loop condition), the steady state solution yields the closed-loop gain $H(s)$ and the error transfer function $E(s)$, which describe how an input signal $\Phi_{\mathrm{r}}(s)$ appears at the output $\Phi_{\mathrm{o}}(s)$ and at the phase error $\Phi_{\mathrm{err}}(s)$, respectively [44]:

$$H(s) = \frac{\Phi_{\mathrm{o}}(s)}{\Phi_{\mathrm{r}}(s)} = \frac{G(s)}{1 + G(s)} \tag{4.18}$$

$$E(s) = \frac{\Phi_{\mathrm{err}}(s)}{\Phi_{\mathrm{r}}(s)} = \frac{1}{1 + G(s)} \,. \tag{4.19}$$

On the basis of the Bode plot of a transfer function one can easily get insight to several characteristics of the system like stability and bandwidth. The shape of the closed-loop gain is usually similar to that of a common low pass filter. It has unity gain for lower frequencies and for higher frequencies the gain decreases, i.e. the feedback is "perfectly" matched to the reference signal within the locking bandwidth. In contrast, $E(s)$ performs a high pass filtering operation, and it has negative gain in the frequency range where $|H(s)| = 1$ in order to suppress the noise, whereas outside the loop bandwidth its magnitude is $|E(s)| = 1$, meaning that the loop is not able to suppress any noise at frequencies larger than the loop bandwidth.
The stability of the system is a key consideration in feedback systems, and by inspection of equations (4.18) and (4.19) one can see that both transfer functions have a pole at $G(s) = -1$. The denominator $1 + G(s) = 0$ is called the characteristic equation, and it is satisfied if the following two conditions are fulfilled:

$$|G(s)| = 1 \tag{4.20}$$

$$\mathrm{Arg}[G(s)] = 180^{\circ} \,. \tag{4.21}$$

In this situation the system will be completely unstable. Furthermore, instead of suppressing the noise one will get noise enhancement if the denominator in equations (4.18) and (4.19) meets the following criterion:

$$|1 + G(s)| < 1 \,. \tag{4.22}$$

Hence, servo bumps appear in the output spectrum of the VCO at frequency for which this condition is met, e.g. if the phase comes close to -180° and $|G(s)| < 1$, indicating the bandwidth of the loop.
When phase locking two diode lasers, it makes sense to have a closer look on the shape of the transfer function K_{o} of the VCO, i.e. the slave laser diode in this case. In chapter 3.2.2 it is explained that for modulation frequencies below 10 MHz, a change in the laser diode temperature is the dominant effect which causes a change in the laser frequency, whereas carrier density modulation can be neglected. Since the desired loop bandwidth is typically less than 10 MHz, it is reasonable to assume that the transfer function of the laser diode is

determined only by this effect, and in this case the gain of the laser diode can approximately be written as [46]

$$K_{\mathrm{o}} = K_{\mathrm{ld}} \frac{\alpha}{\alpha + s} \tag{4.23}$$

where K_{ld} denotes the sensitivity of the laser diode and α is a factor which has to be measured experimentally. Equation (4.23) describes a one-pole transfer function with a pole at $\alpha = i\omega$ and α typically lies between 100 kHz and 1 MHz, corresponding to the thermal cutoff frequency as explained in section 3.2.2. Thus, already at frequencies of several 100 kHz the system can become unstable due to the phase shift of the laser diode. Since the desired bandwidth of an OPLL is typically of the order of several MHz, the loop must be able to compensate for this phase shift.
Another issue in designing OPLLs can be due to delay times in the feedback loop. A substantially large delay time causes a significant phase shift at higher frequencies and thus can limit the bandwidth of the loop. To account for that, an extra factor describing the loop delay τ can be included in equation (4.17), which leads to the following open-loop gain for the OPLL:

$$G(s) = \frac{K_{\mathrm{d}} K_{\mathrm{ld}} F(s)}{s} \, e^{-s\tau} \, \frac{\alpha}{\alpha + s} \, . \tag{4.24}$$

With this equation, the loop bandwidth is limited by the phase shift due to the delay τ and the factor α of the laser diode transfer function.

4.2.2. Characterization of phase noise

The performance of an OPLL is typically quantified by measuring the residual phase noise or, equivalently, by measuring the frequency noise. In the time domain, the frequency stability of a signal is often characterized using the Allan variance. Alternatively one can characterize the phase noise of a signal in the frequency domain by measuring its power spectral density (PSD). In metrology and for long term measurements, the Allan variance is the favored quantity to measure frequency stability. However, the OPLL in this thesis will be used for experiments performed on short time scales, in which case the PSD is the more convenient method for measuring the quality of the phase lock. This chapter gives an introduction to the properties of phase noise in oscillator signals and its characterization with power spectral densities.
Ideally, the output of a signal source would be a purely sinusoidal signal without any unwanted modulation in amplitude, phase or frequency. The total power of this ideal signal would be contained in one single frequency. However, no practical oscillator provides such a pure spectral signal and noise is always present at the output. Thus, the output voltage of an oscillator containing noise can be written as

$$v(t) = [A + a(t)] \cos\left(2\pi f_0 t + \phi(t)\right) \, , \tag{4.25}$$

in which $a(t)$ represents the amplitude noise and $\phi(t)$ denotes the phase noise [47]. It is assumed that $\phi(t)$ describes a stationary random process and all phase fluctuations and frequency deviations from the carrier frequency f_0 are contained in $\phi(t)$. Amplitude noise is usually neglected in the analysis of phase noise, and for small phase fluctuations $\phi(t) < 1$, the oscillator signal can be expressed as [47]

$$v(t) \approx A \cos(2\pi f_0 t) - A \, \phi(t) \sin(2\pi f_0 t) \, . \tag{4.26}$$

The second term indicates the phase noise for frequencies $f \neq f_0$ outside the carrier frequency,

$$v_{f\neq f_0}(t) = A\,\phi(t)\sin(2\pi f_0 t)\,. \tag{4.27}$$

The power spectral density is a very useful tool to characterize oscillator signals, and it describes how the power of a time series is distributed with frequency. If noise is considered, the noise power spectral density identifies the noise power of a signal per 1 Hz bandwidth. Mathematically, the PSD of any quantity $x(t)$ is defined as the square modulus of its Fourier Transform $X(f) = \mathcal{F}\{x(t)\}$. However, stationary random functions are not square integrable and thus their Fourier transform does not exist. In this case it is common to use the PSD defined by the Wiener-Khintchine-Theorem as the Fourier transform of the autocorrelation function $R_x(\tau)$ [48]:

$$S_x(f) = 2\int_0^\infty R_x(\tau)e^{-2\pi i f\tau}d\tau\,, \tag{4.28}$$

where the autocorrelation function of the time-varying quantity $x(t)$ is given by

$$R_x(\tau) = \langle x(t+\tau)x^*(t)\rangle\,, \tag{4.29}$$

in which the angled brackets denote the time average. In equation (4.28), $S_x(f)$ describes the one-sided spectral density defined as

$$S_x(f) = \begin{cases} 2\,S_x^d(f)\,, & f \geq 0 \\ 0\,, & f < 0 \end{cases} \tag{4.30}$$

where $S_x^d(f)$ is the double-sided PSD. By using the one-sided power spectrum, the negative frequencies are folded onto the positive frequency axis, which is reasonable in most physical measurements.
In the case that $x(t)$ is represented by the phase fluctuations $\phi(t)$ and the frequency fluctuations $f(t)$ of a signal, the two corresponding power spectral densities $S_\phi(f)$ and $S_f(f)$ are not independent, since phase and frequency are related by

$$f(t) = \frac{1}{2\pi}\frac{d\phi(t)}{dt}\,. \tag{4.31}$$

Hence, the relation between the spectral densities $S_\phi(f)$ and $S_f(f)$ is given by [32]

$$S_\phi(f) = \frac{S_f(f)}{f^2}\,. \tag{4.32}$$

The phase noise spectral density $S_\phi(f)$ of a signal as given in equation (4.26) can be calculated from the measured power spectrum $P_v(f)$ of the signal. In order to experimentally quantify the phase noise correctly, a careful interpretation of the different spectral power densities is necessary.

- The **signal power spectral density** $S_v^d(f)$ describes the power distributed around the center frequency f_0 of the oscillator signal in a 1 Hz bandwidth. In theory it is given by the Fourier transform of the autocorrelation function of $v(t)$. According to equation (4.26) it consists of a δ-peak at frequency f_0, which is broadened due to the presence of phase noise $\phi(t)$. The raw measured power spectrum $P_v(t)$ depends

on the settings of the spectrum analyzer (SA) and does not directly give the desired spectral density, since $S_v^d(f)$ describes the power in a 1 Hz bandwidth, whereas the resolution bandwidth (RBW) of the SA is usually considerably larger than 1 Hz. In order to obtain the true spectral density of the signal, one has to normalize the measured spectrum to the resolution bandwidth of the SA. If the amplitude is measured on logarithmic scale, this is done by subtracting $10\log(\text{RBW})$. This of course does not give a 1 Hz resolution, since the resolution is still set by the RBW of the SA, but is gives the power spectrum in units of dB/Hz.

- The **phase noise spectral density** $S_\phi(f)$, in contrast to the two-sided power spectral density $S_v^d(f)$ which is a direct measure of the physical signal $v(t)$, is typically a one-sided spectrum that describes the noise power relative to the total power in the carrier signal in a 1 Hz bandwidth at a frequency offset f from the carrier frequency f_0. Commonly it is expressed in units of dBc/Hz, or equivalently rad^2/Hz, and is widely used in PLLs to characterize the phase noise of a signal[2]. The spectrum $S_\phi(f)$ is obtained from the measured spectrum $P_v(f)$ as

$$S_\phi(f) = \frac{10^{\frac{P_v(f-f_0)}{10}}}{RBW \cdot 10^{\frac{P_v(f_0)}{10}}} \tag{4.33}$$

and afterwards using only the positive frequencies to obtain the one-sided spectrum. The term $P_v(f_0)$ denotes the power of the carrier, which is commonly the peak value of the spectrum. This is only an approximation to the correct power and it depends on the setting of the SA, especially on the RBW and the number of data points.

The phase noise variance is given by the root mean square (rms) of the phase fluctuations $\sigma_\phi^2 = \langle\phi(t)\phi^*(t)\rangle = \Delta\phi_{\text{rms}}^2$, and it can be determined by the integral of its power spectral density over all (positive) frequencies,

$$\sigma_\phi^2 = 2\int_0^\infty S_\phi(f)df\,, \tag{4.34}$$

in which the factor 2 takes into account that $S_\phi(f)$ is a one-sided spectrum. In the time domain, as illustrated in figure 4.5, phase noise is represented as timing jitter Δt_{jitter}, i.e. the zero crossing of the slope of the signal fluctuates in time [49]:

$$\Delta t_{jitter} = \frac{1}{2\pi}\frac{\sigma_\phi^2}{f_0}\,. \tag{4.35}$$

4.2.3. Spectrum of a phase stable laser field

In order to obtain the power spectrum of a phase-stabilized laser field, i.e. with small residual phase error, consider the electromagnetic field [48]

$$E(t) = E_0\exp[i(2\pi f_0 t + \phi(t))] \tag{4.36}$$

with negligible amplitude fluctuations and the stationary random phase fluctuations $\phi(t)$. The autocorrelation function of the signal is given by

$$R_E(\tau) = E_0^2\exp[2\pi i f_0\tau]\,\langle\exp[i\phi(t+\tau) - i\phi(t)]\rangle\,. \tag{4.37}$$

[2] dBc means "dB carrier", which is dB relative to the power of the carrier signal.

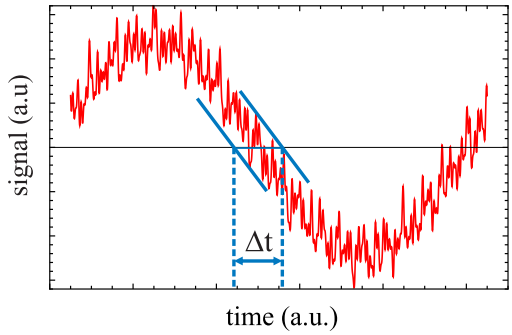

Figure 4.5.: Illustration of phase jitter in the time domain due to phase noise $\phi(t)$ of the carrier signal.

If $\phi(t)$ is represented by a Gaussian process, which is often assumed in the case of white noise sources, the latter term can be written as

$$\langle \exp[i\phi(t+\tau) - i\phi(t)] \rangle = \exp\left[-\frac{1}{2} \left\langle [\phi(t+\tau) - \phi(t)]^2 \right\rangle \right] \tag{4.38}$$

using the Gaussian moment theorem as outlined in reference [50]. The exponent on the right side of this equation can be written in terms of the autocorrelation function $R_\phi(\tau) = \langle \phi(t+\tau)\phi^*(t) \rangle$ of the phase fluctuations,

$$\exp\left[-\frac{1}{2} \left\langle [\phi(t+\tau) - \phi(t)]^2 \right\rangle \right] = \exp[-R_\phi(0) + R_\phi(\tau)] \,, \tag{4.39}$$

where $R_\phi(0)$ describes the phase noise variance $R_\phi(0) = \langle \phi(t)\phi^*(t) \rangle = \sigma_\phi^2$. Hence, the autocorrelation function of the laser field is given as

$$R_E(\tau) = E_0^2 \exp[2\pi i f_0 \tau] \exp[-R_\phi(0) + R_\phi(\tau)] \,. \tag{4.40}$$

With equation (4.28), the power spectrum $S_E(f)$ of the laser field is thus given by

$$S_E(f) = 2 \int_0^\infty R_E(\tau) \exp[-2\pi i f \tau] \, d\tau \tag{4.41}$$

$$= 2E_0^2 \int_0^\infty \exp[2\pi i (f_0 - f)\tau] \, \exp[-\sigma_\phi^2 + R_\phi(\tau)] \, d\tau \,. \tag{4.42}$$

For small phase fluctuations $\sigma_\phi^2 \ll 1$ it is justified to expand the second exponential term and keeping only the first terms [32]:

$$S_E(f) = 2 \int_0^\infty \exp[2\pi i (f_0 - f)\tau] \, [1 - \sigma_\phi^2 + R_\phi(\tau)] \, d\tau \,. \tag{4.43}$$

Thus, by using the definition of the Dirac delta function $\delta(f_0 - f)$, the spectrum of a phase stabilized beat signal can be expressed as

$$S_E(f) = 2E_0^2 \left[(1 - \sigma_\phi^2)\delta(f_0 - f) + S_\phi(f_0 - f) \right] \,. \tag{4.44}$$

Apparently the spectrum consists of the carrier signal at frequency f_0 and an additional noise term that describes the noise sidebands given by the phase noise spectral density

$S_\phi(f_0 - f)$ at an offset f from the carrier frequency.
The ratio between the carrier power $S_E(f_0)$ and the total power of the spectrum, which is the integral of the power spectrum over all frequencies, is given by

$$\eta = \frac{S_E(f_0)}{\int_{-\infty}^{\infty} S_E(f)df} \,. \tag{4.45}$$

This expression can also be estimated via the residual phase error as [46, 48]

$$\eta = e^{-\sigma_\phi^2} \,, \tag{4.46}$$

if the assumption of a small residual phase error $\sigma_\phi^2 \ll 1$ is valid, which is typically fulfilled in the case of a properly functioning OPLL.

4.2.4. Propagation of phase noise in an optical phase locked loop

Each device in the loop can superimpose phase noise to the signal. To begin with the reference oscillator, the phase noise of the microwave reference appears directly in the spectrum of the beat signal, and it puts a limit on its absolute phase stability, since the best achievable phase noise spectrum is that of the reference oscillator itself. Another source for additional phase noise is due to shot noise caused by the quantum nature of light in the detection process at the photodiode. Using a digital phase detector, shot noise is translated into phase noise, since amplitude noise causes the output of any digital counting device to have timing jitter, and the phase detector itself also intrinsically adds noise. These noise sources are referred to as additive noise sources, since they are not controlled by the feedback loop.
In contrast to the additive noise, the phase noise of the VCO is the one which the loop is trying to suppress. In a heterodyne OPLL the VCO is represented by the beat signal between the master and the slave laser. The phase noise of the unlocked beat signal, i.e. without any feedback applied, is determined by the input phase noise spectra of the master laser, $S_{\phi,\mathrm{m}}$, and that of the slave laser, $S_{\phi,\mathrm{s}}$. The output spectrum of a mixer, which in the case of optical signals includes the photodiode, is the sum of its two input noise spectra if those are uncorrelated [44]. Thus, the unlocked phase noise spectrum of the beat signal can be written as the sum of the two laser noise spectra,

$$S_{\phi,\mathrm{beat}}(f) = S_{\phi,\mathrm{m}}(f) + S_{\phi,\mathrm{s}}(f) \,. \tag{4.47}$$

To obtain an expression for the residual phase noise spectrum $S_{\phi,\mathrm{res}}$ of the phase locked beat signal dependent on the loop parameters, consider the noise model in figure 4.6. In this model the VCO, i.e. the beat signal, is considered to be the sum of a noise-free oscillator and an internal noise source which adds phase noise $\phi_{\mathrm{beat}}(t) = \phi_{\mathrm{m}}(t) + \phi_{\mathrm{s}}(t)$, where $\phi_{\mathrm{m}}(t)$ and $\phi_{\mathrm{s}}(t)$ are the phase fluctuations of the master and slave laser, respectively. The noise caused by all other components is merged together in one noise term $\phi_{\mathrm{add}}(t)$, describing all possible noise sources which cause additional phase noise at the error signal. The fact that negative feedback is applied is indicated by the negative sign of the control voltage output of the loop filter, and from system analysis the output of the VCO is obtained to be [51]

$$\Phi_{\mathrm{B}}(s) = \frac{G(s)}{1+G(s)}\,\Phi_{\mathrm{add}}(s) + \frac{1}{1+G(s)}\,\Phi_{\mathrm{beat}}(s) \,, \tag{4.48}$$

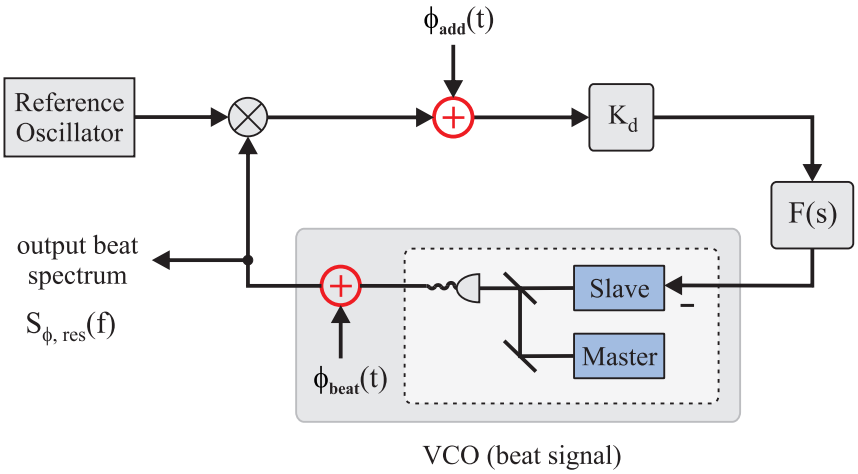

Figure 4.6.: Noise model for the OPLL. In this picture the VCO is represented by the beat signal. The gray box indicates that the beat signal is assumed to be the sum of an ideal noise-free oscillator and an internal noise source $\phi_{\mathrm{beat}} = \phi_{\mathrm{m}} + \phi_{\mathrm{s}}$, which contains the phase noise of both lasers. The quantity of interest is the residual phase noise spectrum $S_{\phi,\mathrm{res}}(f)$ at the output of the beat signal. The term ϕ_{add} combines all additive noise sources which can be present in the loop. The transfer functions of the phase detector and the loop filter are given by K_{d} and $F(s)$, respectively.

where the open-loop gain $G(s)$ is the product of all the transfer functions as described in section 4.2.1. The capital letters $\Phi_{\mathrm{add}}(s)$ and $\Phi_{\mathrm{beat}}(s)$ denote the Laplace transform of the respective phase fluctuations $\phi_{\mathrm{add}}(t)$ and $\phi_{\mathrm{beat}}(t)$. The first term in equation (4.48) indicates that all additive noise sources are not suppressed by the loop, since they propagate with the closed-loop transfer function $H(s)$ as given in equation (4.18). Since Φ_{add} also contains the phase noise of the reference oscillator, this shows that the best phase noise spectrum one can obtain is a direct replica of that of the stable reference.
However, the residual phase noise is normally determined by the lasers and in most cases it is not limited by the reference oscillator. The second term in equation (4.48) describes the suppression of the phase noise of the beat signal by the error transfer function $E(s)$, see equation (4.19). Usually the loop does not perfectly suppress this noise, and even in the locked condition the phase noise of the lasers dominates the residual phase noise spectrum $S_{\phi,\mathrm{res}}(f)$. Hence, one can neglect the additive noise part in equation (4.48) and $S_{\phi,\mathrm{res}}(f)$ is given by the input phase noise of the lasers as

$$S_{\phi,\mathrm{res}}(f) = \left| \frac{1}{1+G(s)} \right|^2_{s=2\pi i f} \left[S_{\phi,\mathrm{m}}(f) + S_{\phi,\mathrm{s}}(f) \right] , \tag{4.49}$$

in which relation (4.47) is used to express the phase noise spectrum of the beat signal. With equation (4.24) the open-loop gain $G(2\pi i f)$ can be modeled assuming a simple filter as explained in reference [46], and $G(s)$ can then be approximated by

$$G(2\pi i f) = K \frac{e^{-2\pi i f \tau}}{i f} , \tag{4.50}$$

where K is the overall linear gain of the loop. The input frequency noise spectrum $S_{f,\mathrm{in}}(f)$ of the lasers can be modeled as a superposition of white and $1/f$-frequency noise [46]:

$$S_{f,\mathrm{in}}(f) = (2\pi)^2 \left[C_\mathrm{w} + \frac{C_{1/f}}{2\pi f} \right] \tag{4.51}$$

with the coefficients C_w and $C_{1/f}$ for white and $1/f$-frequency noise, respectively. The phase noise spectrum is determined from the frequency noise by using the relation (4.32). Assuming equal frequency noise for both lasers, and combining equations (4.49), (4.50) and (4.51) yields the following expression for the residual phase noise spectrum of the beat signal:

$$S_{\phi,\mathrm{res}}(f) = \frac{1}{f^2} \left| \frac{if}{if + K\, e^{2\pi i f \tau}} \right|^2 (2\pi)^2 \left[C_\mathrm{w} + \frac{C_{1/f}}{2\pi f} \right] . \tag{4.52}$$

In figure 4.7 the single-sideband (SSB) phase noise spectrum is plotted for different values of K, where a constant delay time $\tau = 100\,\mathrm{ns}$ and equal coefficients $C_\mathrm{w} = C_{1/f}$ are assumed. Note, that this directly gives one the typical shape of a phase locked signal as depicted in figure 4.2, if one plots all negative and positive frequencies together with the delta function at f_0. In the case of no feedback, i.e. $K = 0$, the phase noise highly increases with decreasing frequency. The black dashed line in figure 4.7 shows the case of weak feedback, so that the noise at low frequencies is slightly suppressed, but the loop is not able to reduce any phase noise at higher frequencies. The red solid line illustrates the case of a properly adjusted loop gain, where the phase noise is suppressed up to frequencies of 1 MHz. In this model, the maximum loop bandwidth is limited by the phase shift due to the delay τ. This determines the position at which the servo bump occurs in the case of too large feedback gain, as indicated by the blue dashed line.

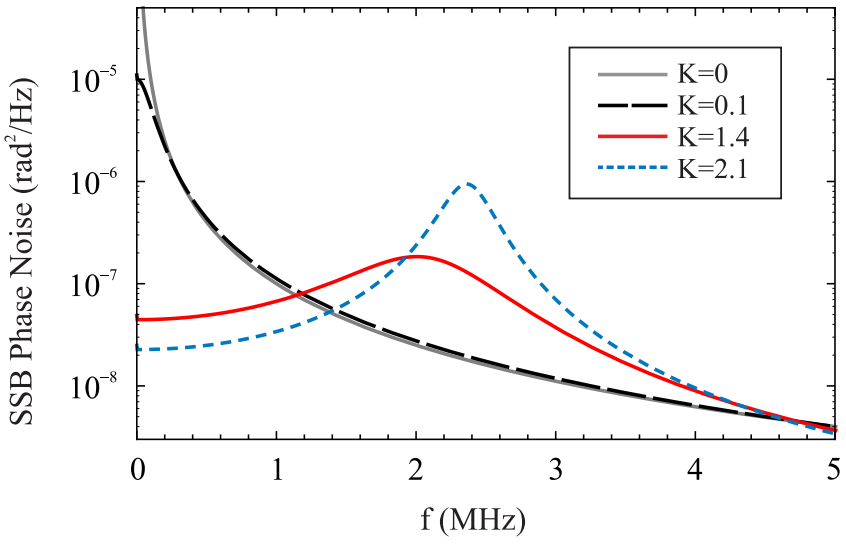

Figure 4.7.: Theory plots of the single sideband (SSB) phase noise of an oscillator signal containing white and $1/f$-frequency noise according to equation (4.52), plotted for different values of the linear gain K, where K has units of MHz/rad. The delay time is set to $\tau = 100\,\mathrm{ns}$ and it is assumed that the frequency noise of the unlocked beat signal is composed of equal parts of white and $1/f$-frequency noise, i.e. $C_\mathrm{w} = C_{1/f} = C_\mathrm{L}$.

5. Realization of an optical phase locked loop

In EIT experiments, the transparency and the width of the dark resonance depends highly on the coherence time τ between the two lasers needed for EIT. Thus, it is necessary that τ is on the order of the duration of an experimental sequence to ensure a fixed phase relation during the measurement. Furthermore, it is desired that one can perform several successive experiments without the need for relocking the system. Therefore, a phase locked loop should on the one hand be able to highly suppress the phase noise and reduce the linewidth of the beat signal to the sub-Hz regime, and on the other hand it should recapture lock in the case of large frequency fluctuations and thus ensure longterm stability. Since the free running linewidth of diode lasers is typically in the range of MHz, a fast feedback loop with a loop bandwidth of several MHz is necessary to meet the first requirement. Fast control demands a steep slope of the error signal provided by the phase detector at the locking point. Furthermore, the phase noise of the phase detector should be as small as possible in order to minimize the residual phase error, and a wide capture range is required to ensure a stable lock for several hours.
In this chapter, the realization of a heterodyne OPLL at a frequency offset of 9.192 GHz, corresponding to the hyperfine splitting of the cesium ground state, using a simple low noise digital phase frequency detector is described.

5.1. Experimental setup

This section describes the implementation of the laser system used to perform optical phase locking of two diode lasers for the use in EIT experiments on cesium atoms. In the first part, the lasers and the optical setup are presented. The optical detection of the beat signal and its processing through the loop is described in the second part.

5.1.1. Optical setup and laser system

Laser system

The two lasers are diode lasers named coupling and probe laser, corresponding to their use in EIT experiments. Regarding the OPLL the coupling laser serves as the master whereas the probe laser is used as the slave, which is stabilized to the master laser by the feedback loop. Diode lasers are particular suitable to realize a compact phase locked laser system, since they are small, inexpensive and their frequency can easily be controlled via the injection current.
The coupling laser is a home made diode laser in Littrow configuration, see section 3.4.1, whose design follows that described in reference [52] and is shown in figure 5.1[1]. A collimation tube[2] is used to collimate the divergent beam of the laser diode. Together with

[1] For this laser a SDL-5401 laser diode from Spectra Diode Labs operating at 852 nm is used
[2] LT220P-B from Thorlabs

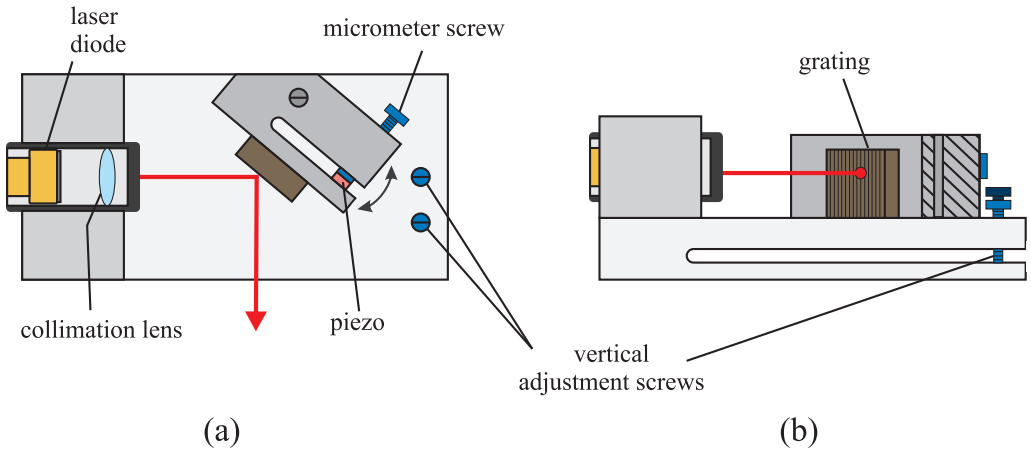

Figure 5.1.: Schematic drawing of the top (a) and side (b) view of the grating stabilized diode laser in Littrow configuration implemented in this theses.

the laser diode chip it is mounted to an L-shaped aluminum block. The diffraction grating used here[3] is made of 1800 lines per mm and is glued to an aluminum holder, which is screwed to the L-shaped aluminum block as depicted in figure 5.1. A micrometer screw can be used to tilt the grating, and two further screws allow for precise vertical adjustment of the back reflected beam into the laser diode. The angle of the grating can be tuned additionally with a piezoelectric actuator in order to select the desired wavelength and to scan the frequency of the laser.
The current of the laser diode is controlled by a home made laser controller. The threshold current is measured to be about 13 mA and the laser typically operates around 80 mA with an output power of about 60 mW. A peltier element is used to stabilize the temperature of the laser diode by controlling the temperature of the aluminum block. The entire construction is surrounded by a metal housing for acoustic shielding and mounted to a massive steel block to guarantee mechanical stability. Two cylindrical lenses are used to compensate for the ellipticity and the astigmatism of the laser diode beam.
The probe laser[4] is a diode laser in Littman-Metcalf configuration as explained in chapter 3.4.1. The angle of the tuning mirror can be adjusted with a piezoelectric actuator for wavelength adjustment. In the same as it is done for the coupling laser the temperature is stabilized using a peltier element. The laser typically operates at a current of −120 mA with an output power of about 40 mW.

Optical setup

The experimental setup of the optical system is sketched in figure 5.2. For each laser, a Faraday isolator with 60 dB isolation[5] prevents back reflections into the laser diode. In order to detect the beat signal, the beams are overlapped at a 50/50 beam splitter cube and afterwards focused on a fast photodiode. Two lenses with a long focal length are used to achieve better mode matching of the two beams. The laser beams are split into the different arms by using several polarizing beam splitter cubes (PBS) in conjunction with

[3] GR13-1850 from Thorlabs
[4] Sacher LION-SYS-500
[5] Linos DLI-1

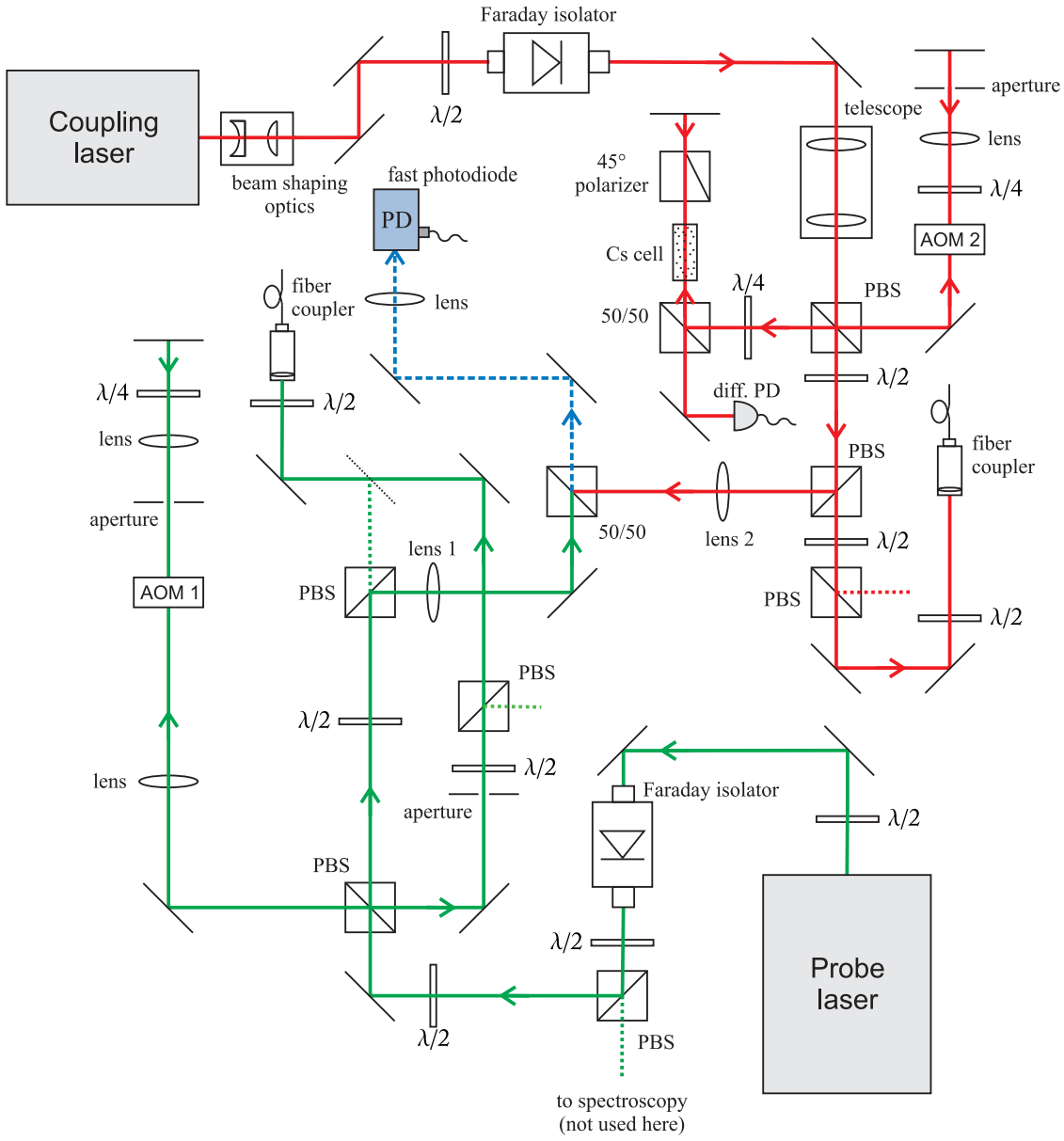

Figure 5.2.: Optical setup of the laser system used to implement the OPLL. The beat note detection is marked by the blue dashed beams, where the lenses 1 and 2 with a long focal length are used to obtain good mode matching of the two beams. Two acousto optic modulators both in double pass configuration are implemented, whereof AOM 1 provides the possibility to scan the frequency of the probe laser, and AOM 2 allows one to shift the frequency of the coupling laser before the beam enters the setup for polarization spectroscopy. For their use in the experiment both lasers are coupled into single mode fibers. In the case of the probe laser one can choose between the original beam and the one shifted by the AOM for this purpose.

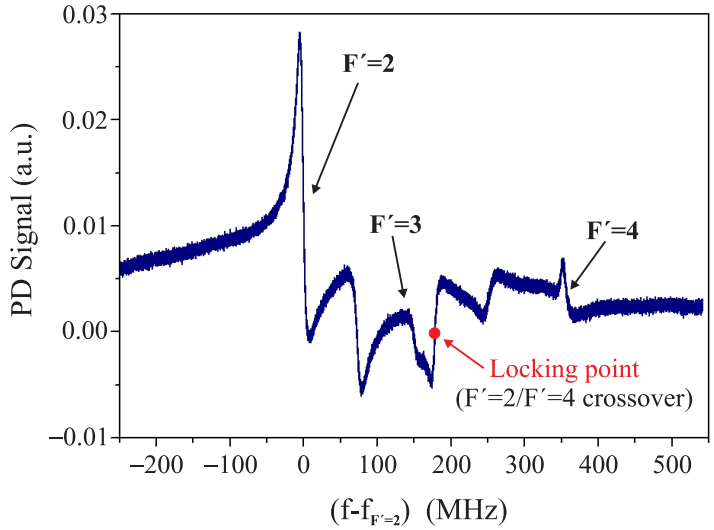

Figure 5.3.: Differential polarization spectrum of the coupling laser for the $|F = 3\rangle \rightarrow |F' = 4\rangle$ transition.

$\lambda/2$-plates, so that the powers can be adjusted individually. Concerning the probe laser, an acousto optic modulator (AOM) in double pass configuration [53] provides the possibility to scan its frequency across the EIT resonance by using a special AOM controller, which is phase stabilized to the same 10 MHz reference as the local oscillators used in the OPLL[6].

The frequency of the coupling laser is locked to an atomic transition using polarization spectroscopy as described in chapter 3.4.2. For EIT experiments on cesium atoms, the $|F = 3\rangle \rightarrow |F' = 4\rangle$ transition of the D_2 line in cesium is used, where F and F' are the hyperfine levels in the ground and excited states (the energy level structure of cesium is shown in appendix A.1). Before the coupling laser beam enters the spectroscopy setup, its frequency is shifted by an AOM again in double pass configuration. This allows one to lock at the crossover between the states $|F' = 2\rangle$ and $|F' = 4\rangle$ in order to be resonant with the $|F = 3\rangle \rightarrow |F' = 4\rangle$ transition. The frequency difference between the state $F' = 4$ and the crossover is 176.23 MHz, and thus the frequency of the AOM is tuned to approximately 88.11 MHz. Furthermore, the AOM allows one to precisely adjust the detuning of the coupling laser from resonance.

For polarization spectroscopy, the coupling laser beam is circularly polarized by a $\lambda/4$-plate after the double pass AOM and enters a 50 mm cesium gas cell. Thereupon it passes a 45°-polarizer realized by a PBS cube which is turned 45° with respect to the horizontal axes of the table. The back reflected beam, after again passing through the cesium cell, is detected by a differential photodiode consisting of a PBS and two photodiodes detecting the s- and p-components of the incident light. The difference between the two photodiode signals provides the error signal to lock the laser frequency. This simple compact setup for polarization spectroscopy has the disadvantage that the laser beam which is detected passes the cell twice. This leads to a reduced amplitude of the absorption signal

[6]Therefore, the voltage controlled oscillator (VCO) in the AOM controller is replaced by an external signal generator, which provides the possibility for external stabilization. Another possibility to scan the frequency of the probe laser would be to scan the local oscillator at the input of the phase detector of the OPLL.

at resonance, since the intensity of the probing laser depends on how much pump light is absorbed by the atoms. Additionally, this setup is susceptible to optical interferences due to reflections of vibrating optical elements. However, this setup is used here because of lack of space and provides a sufficiently stable error signal.
The differential polarization spectrum of the coupling laser is shown in figure 5.3, where the red dot indicates the locking point. The lock is stable for several hours even in a noisy environment and ensures longterm stability of the coupling laser. The locking bandwidth is approximately 1 kHz due to mechanical resonances of the piezo[7]. By measuring the time domain error signal in the locked condition, it is found that the mean frequency deviation of the laser is approximately 300 kHz.
Finally, one should note that the AOM 2 of the coupling laser does not disturb the phase relation between the coupling and probe lasers established by the OPLL, since both coupling beams, used for detection of the beat signal and EIT experiments, do not pass the AOM 2. In this configuration the AOM only affects the absolute stability of the coupling laser, but the relative stability between the two lasers is not influenced.

5.1.2. Detection and processing of the beatsignal

In order to detect the beat signal at a frequency difference of 9.192 GHz, a fast photodiode[8] with a specified bandwidth of more than 10 GHz is used. The current i at the photodiode is determined by the total optical power P incident on the photodiode chip and depends on the quantum efficiency η of the detector [54],

$$i = \frac{e\eta P}{hf}\,, \tag{5.1}$$

where e is the electron charge and hf the photon energy. The effect of the beating part of the light field on the photodiode is determined by the interference term in equation (4.6) by integration over the beam cross section area A [54],

$$P_{\text{beat}} = 2\epsilon_0 c \cos[\Delta\omega t + \Delta\varphi(t)] \iint \vec{E}_1(\vec{r}) \cdot \vec{E}_2(\vec{r})\, dA\,, \tag{5.2}$$

where $\vec{E}_1(\vec{r})$ and $\vec{E}_2(\vec{r})$ are the spatially dependent field amplitudes and $\Delta\varphi$ and $\Delta\omega$ are the phase and frequency difference of the lasers, respectively. In order to obtain a high value for the overlap integral in P_{beat}, careful mode matching of the beams is necessary. The quality of the beam overlap can be estimated by comparing the AC component of the photodiode signal with the DC component, where the modulation depth is given by the ratio of the peak-to-peak value of the modulation amplitude and the mean value of the AC signal [55]. Since no oscilloscope is available which can detect the desired frequency difference of 9.192 GHz, the lasers are locked to the same hyperfine ground state so that their frequency difference lies in the MHz range in order to measure the modulation depth. By carefully overlapping the two beams a modulation depth of 70 % at a frequency difference of 387 MHz is obtained. This value can differ by a small amount from the modulation depth at 9.192 GHz, since the modes of the laser beam can slightly change with frequency. However, it was tested that the change in the beam profile is small, and thus the measured value gives a good estimate for the modulation depth. In the case of accurate mode matching, the integral in equation (5.2) equals the product of the single

[7] This was tested by comparing the error signal of the lock-box in the locked and unlocked condition.
[8] ET-4000 GaAs PIN detector from EOT

fields, and the electrical power $P_{\mathrm{beat}}^{\mathrm{el}}$ of the beat signal measured at the load resistor R is given by

$$P_{\mathrm{beat}}^{\mathrm{el}} = \left\langle i_{\mathrm{beat}}^2 \right\rangle R = 2R \left(\frac{e\eta}{hf} \right)^2 P_1 P_2 \,, \tag{5.3}$$

where $\left\langle i_{\mathrm{beat}}^2 \right\rangle$ is the mean value of the squared current. An important quantity for the phase lock is the signal-to-noise ratio (SNR) of the beat signal. The optical powers $P_1 = \int I_1(\vec{r}) dA$ and $P_2 = \int I_2(\vec{r}) dA$ of the DC terms I_1 and I_2 in equation (4.6) do not contribute to the beat signal power, but they do contribute to the noise in the detection process.
There are mainly three effects which cause noise in the detector. One is Johnson-Nyquist noise due to the thermal motion of the charge carriers. Furthermore, shot noise is generated in a photodiode by random fluctuations of the flowing current, resulting on the one hand from the dark leakage current, which is independent of the signal, and more importantly from the photocurrent induced by the light detection. If the intensity of the light fields is chosen high enough, the thermal and dark current noise can be neglected and the noise current is determined only by the shot noise of the photocurrent i_{p} as

$$\left\langle i_{\mathrm{sn}}^2 \right\rangle = 2e i_{\mathrm{p}} B_{\mathrm{d}} \,, \tag{5.4}$$

where B_{d} is the bandwidth of the detector [42]. The photocurrent i_{p} is given by the total current caused by the incident optical powers P_1, P_2 and P_{12}. Since the oscillating beat part averages out over time, the shot noise current i_{sn} at the photodetector is only given by P_1 and P_2, yielding

$$\left\langle i_{\mathrm{sn}}^2 \right\rangle = \frac{2e^2 \eta B_{\mathrm{d}}}{hf} \left(P_1 + P_2 \right) . \tag{5.5}$$

With equation (5.3) the signal-to-noise ratio is then given by

$$\mathrm{SNR} = \frac{\left\langle i_{\mathrm{beat}}^2 \right\rangle}{\left\langle i_{\mathrm{sn}}^2 \right\rangle} = \frac{\eta}{hf\, B_{\mathrm{d}}} \, \frac{P_1 P_2}{P_1 + P_2} \,. \tag{5.6}$$

Thus, for a constant total power, the signal-to-noise ratio can be improved by using equally high powers for both laser beams. The damage threshold of the photodiode is 10 mW, thus the laser powers for the beat signal detection are set to $P = 4.5\,\mathrm{mW}$ for each beam. In this setup, amplitudes of the beat signal which are typically 40 dB above the noise floor are achieved.
In figure 5.4 the processing of the beat signal after its detection at the photodiode is shown. It is amplified by +34 dB in a first step using an ultra low noise pass band amplifier with a frequency range of 8 to 10 GHz. The amplifier exhibits excellent phase noise performance with a noise figure[9] of 1.05 dB @ 9 GHz. Thereupon a second amplifier adds another +12 dB to the signal, where the direction of the amplifiers is chosen so that the amplifier directly after the photodiode has the better noise performance. A DC-block is used to filter out the AC–signal, which afterwards is mixed down at a double balanced mixer[10] using a stable quartz oscillator. For this purpose, two oscillators with low phase

[9] The noise figure is defined as the ratio between the signal-to-noise ratio of the input signal, SNR_i, and that of the output signal, SNR_o. Note, that always $\mathrm{SNR}_o < \mathrm{SNR}_i$, and thus the noise figure will always be > 1 since every device intrinsically adds noise.

[10] The output of a normal unbalanced frequency mixer contains both input frequencies, the harmonics of the two input frequencies and all sum and difference frequencies which are possible between those frequencies. Instead, a double balanced mixer will suppress the two input frequencies and their harmonics.

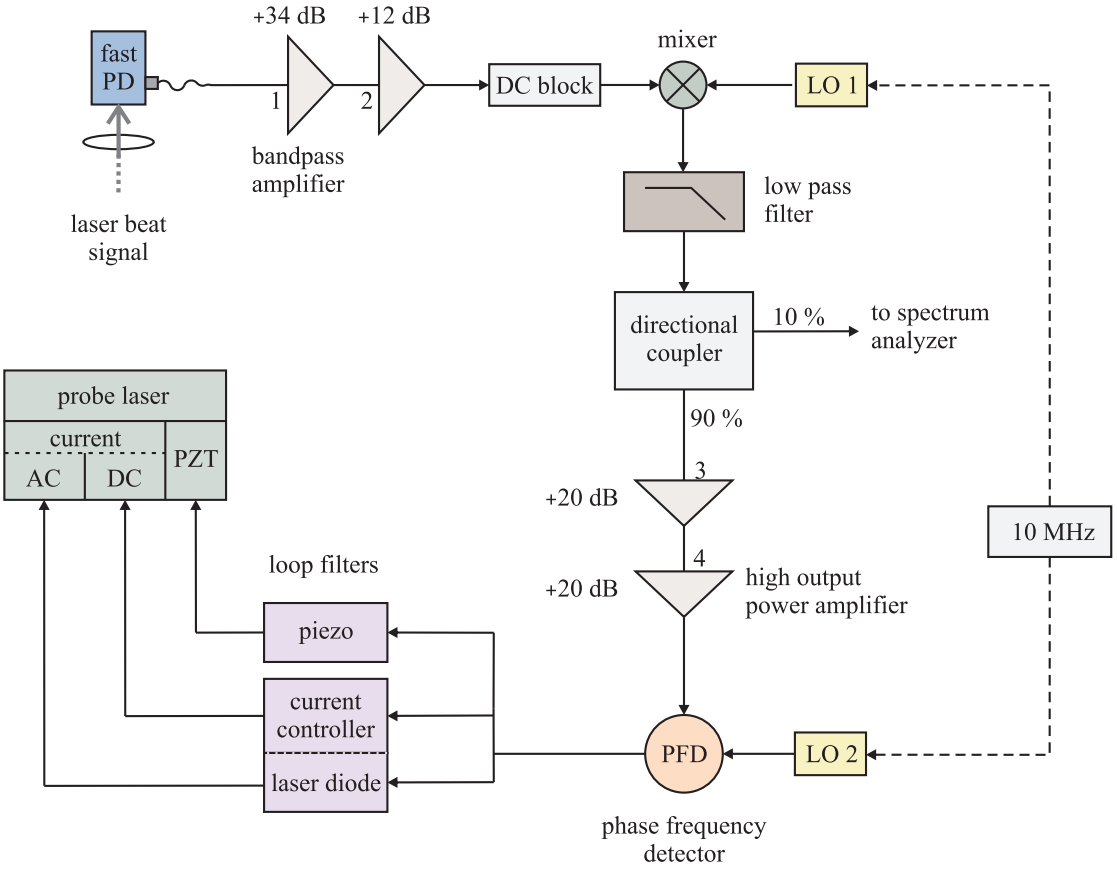

Figure 5.4.: Schematic of the beat signal processing after its detection with the fast photodiode. The used components are listed in table 5.1.

Components	Model	Company	Comment
Amplifier 1	AUL-8010	Microsemi	Bandpass 8-10 GHz
Amplifier 2	ZX60-14012L	Minicircuits	
Amplifier 3	ZFL-500LN	Minicircuits	
Amplifier 4	ZFL-500HLN	Minicircuits	High output power
DC Block	BLK-18	Minicircuits	
Directional Coupler	ZFDC-10-1	Minicircuits	
Frequency Mixer	ZMX-10G	Minicircuits	
Local oscillator 1	KU LO 92 PLL	Kuhne	@ 9.216 GHz
(two alternatives)	MKU LO 95 PLL	Kuhne	@ 9.486 GHz
Local oscillator 2	N5182A MXG	Agilent	Provides 10 MHz reference
Low pass filter	VLFX-500	Minicircuits	High rejection
Phase frequency detector	HMC439QS16G	Hittite	Ultra low phase noise

Table 5.1.: Components used for processing the beat signal.

noise performance of −110 dBc/Hz @ 100 kHz, each at a fixed frequency of 9.216 GHz and 9.486 GHz, respectively, are available and can be chosen depending on the desired frequency output of the mixer (see table 5.1). Both oscillators can be stabilized using the optional input for an external 10 MHz reference signal. Since the output of the mixer oscillates at both the sum and difference frequencies of the input signals, a high rejection low pass filter is used to block the unwanted high frequency part. A −10 dB directional coupler splits the beat signal into two parts, whereof 10 % can be used for monitoring the beat signal with the spectrum analyzer (SA). The remaining 90 % are further amplified using two low noise amplifiers, each with a gain of +20 dB. Thereof the last one is a high power amplifier with a large possible output power of +16 dBm. Altogether, the beat signal is amplified to a level of about +5 dBm, i.e. 3.2 mW in a 50 Ω–system, and finally sent into the phase frequency detector, which will be characterized in detail in the next section. A second local oscillator LO2 provided by a vector signal generator is used as the reference input of the phase detector. The internal 10 MHz reference of this signal generator is used to stabilize the phase of the two local oscillators LO1 and LO2. All components are directly connected by SMA adapters and no cables are used in order to avoid long signal tracks and large phase delays at higher frequencies. In fact, the delay time has been estimated to be less than 10 ns, which causes a negligible small phase delay of less than 10 mrad @ 1 MHz.

5.2. The phase frequency detector

5.2.1. Introduction to phase detectors

In the OPLL the most important component is the phase detector, which is required to provide the error signal. In chapter 4.2.1 the phase detector was assumed to be a perfectly linear device whose output voltage is proportional to the phase difference, i.e. $v(t) = K_\mathrm{d}\Delta\phi(t)$, with the linear gain K_d. However, no such ideal phase detectors exist, and every physical detector has a maximum possible output voltage and a limited dynamic range inside which phase excursions are tracked.
The phase detector defines a number of important parameters of the OPLL. The capture range is the maximum frequency difference Δf of the input signals at which the PLL is still able for initial phase–lock acquisition. It is mainly determined by the behavior of the phase detector and should not be confused with the phase detection range, that is the linear dynamic range of the phase detector. The bandwidth of a properly working loop should be a few times the linewidth of the (RF) beat signal, which is typically several hundreds of kHz up to a few MHz. In order to obtain the desired stability and bandwidth, it is of great importance to lock at a frequency which significantly exceeds the desired loop bandwidth, i.e. usually more than several tens of MHz for an OPLL. Furthermore, if it is desired to scan the frequency of the slave laser by scanning the local oscillator at the phase detector input, a phase detector with a wide operating bandwidth is required. Finally, the phase noise floor of the phase detector should be as low as possible to reduce additional noise in the loop.

Analog phase detectors

The best performance regarding noise and fast control is offered by an analog phase detector, which is a simple analog frequency mixer. They are fast low noise devices whose noise is mainly determined by shot noise of the electric current and some flicker noise at

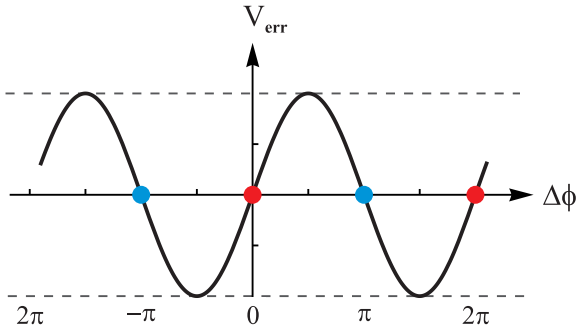

Figure 5.5.: Error output voltage of an analog phase detector depending on the phase difference of its two input signals. The red and blue dots indicate two types of locking points, depending on the polarity of the signal.

low frequencies [56]. Since the analog phase detector multiplies its two input signals, the output varies sinusoidal with phase as shown in figure 5.5. The blue and red dots indicate two different, in each case indistinguishable, locking points depending on the polarity of the phase difference. Due to the sinusoidal shape, the monotonic range is $\pm\pi/2$ and the output is linear only for a phase differences of $\Delta\phi < 1\,\mathrm{rad}$. Unless the phase error is very small, cycle slips occur very likely for phase excursions which exceed $\pi/2$. Since the capture range of analog phase locked loops is typically on the order of the loop bandwidth [56], frequency changes of more than the bandwidth will cause the loop to lose track of the signal. Likewise, if the PLL is initially out of lock and the signal frequency difference exceeds the loop bandwidth, the error signal averages to zero, what makes it impossible for the loop to acquire lock. This makes it rather difficult to lock a fairly noisy input signal, as it is in the case of the beat signal of two lasers, without any pre-stabilization of the signal.

Digital phase detectors

Digital phase frequency detectors are intrinsically noisier and the analog to digital conversion of the signal can be highly susceptible to amplitude-to-phase noise conversion. Additionally, the loop bandwidth can be limited due to substantial delay times of the comparators, which are typically several ns compared to the fast response in the range of hundred ps of analog phase detectors. Nevertheless, digital phase detectors are often used in PLL applications since they provide a wide capture range, a small cycle slip rate and good longterm stability.
There are several types of digital phase detectors, and the most common three examples are shown in figure 5.6, namely the folding (a), periodic (b) and the saturating (c) type. The folding type is usually implemented by an EXOR gate and is similar to the analog type. The phase tracking is limited to the range $-\pi/2 < \Delta\phi < \pi/2$, however with a constant linear gain K_d, and the locking point depends on the polarity of the signal. The periodic phase detector, as depicted in figure 5.6 (b), changes its sign when it reaches the maximum (or minimum) output voltage. This detector type also suffers from multiple locking points, but the periodic behavior allows for sideband selection, i.e. only one of the possible polarities of the phase difference leads to a stable lock. It can be realized using an edge-triggered JK-flip-flop [57], wherewith a phase error range of $-\pi < \Delta\phi < \pi$

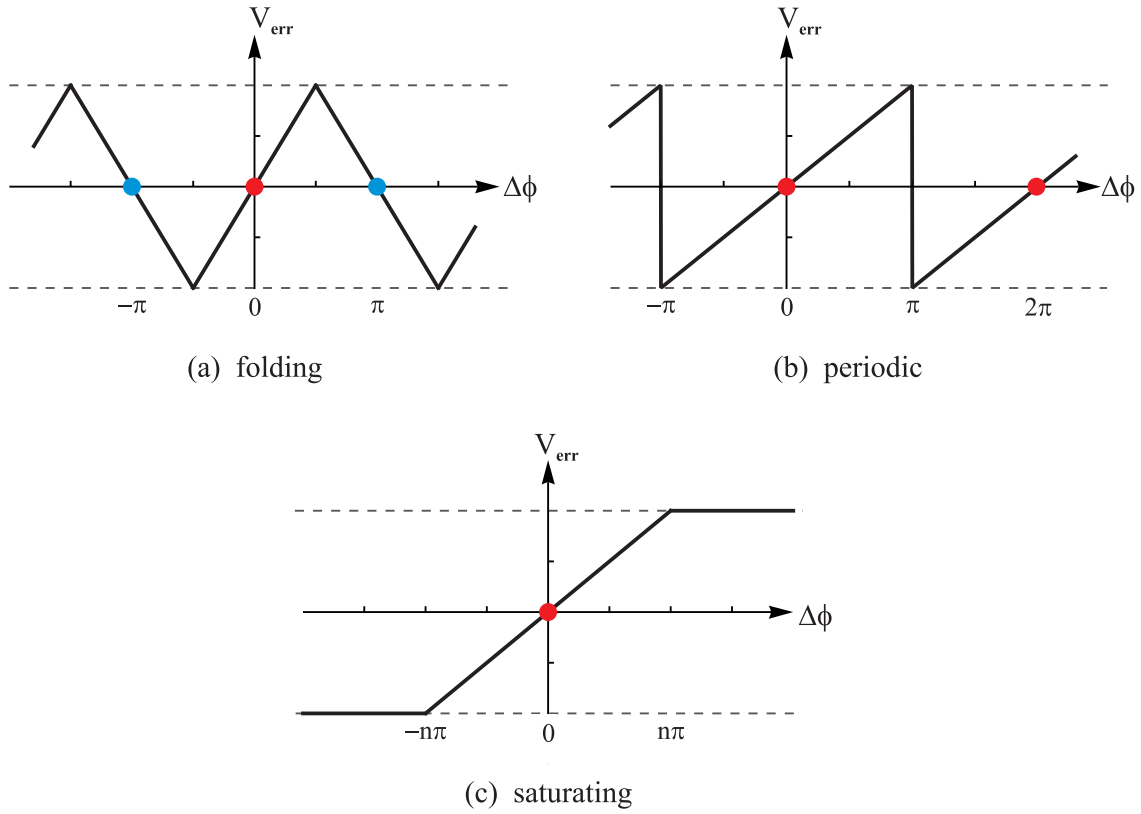

Figure 5.6.: Error output voltage of (a) a folding, (b) a periodic and (c) a saturating digital phase detector depending on the phase difference of the two input signals. The dots indicate the locking points, whereby in (a) two types exist corresponding to the polarity of the phase difference.

is achieved. The bandwidth of such digital phase detectors is limited by the maximum toggle frequencies of the flip-flops. In contrast to the previous types, the output of the saturating phase detector shown in 5.6 (c) remains at the respective maximum and the minimum voltage level after reaching the edges of its linear range. This behavior has the advantage of a well-defined locking point. If the phase escapes the dynamic range, the detector is not able to detect the phase difference anymore, but the sign of the output voltage still indicates in which direction the frequency has to be adjusted. One possible implementation is a phase counter [46], for which the linear range is only limited by the number of bits of the counters. This allows the loop to recapture lock even for large phase excursions without losing the phase information. However, these phase counters are not sensitive to phase fluctuations smaller than 2π, since they count the phase difference between the input signals in multiples of 2π, leading to a stepwise error function. Consequently, information about phase changes within one period are lost and fast phase fluctuations around the locking point cannot be detected.

5.2.2. Implementation of a phase frequency detector

Several designs of phase locked laser systems using all kinds of phase detector implementations can be found in the literature, some examples are given in [46, 56, 58]. It depends on the specific application of the laser system what is the primary goal of the OPLL. In the fields of optical frequency standards and metrology, it is of great importance that no

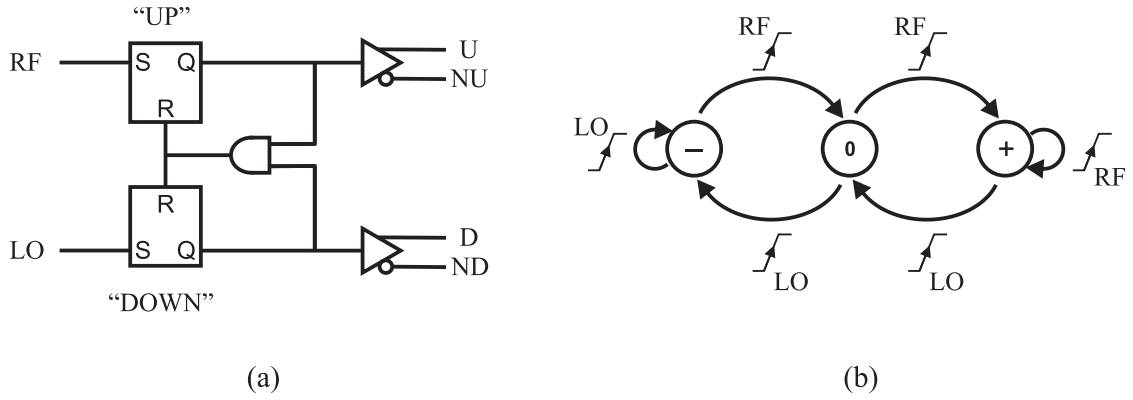

Figure 5.7.: Logic diagram (a) and state diagram (b) of a common three state phase frequency detector.

cycle slips occur for a very long time interval. A digital phase counter as presented in the previous chapter allows for cycle-slip free measurements even in the presence of significant residual phase errors. In order to additionally reduce the phase noise, combined analog-digital phase detectors are developed using a digital frequency counter in conjunction with a fast analog phase detector. However, these systems are rather complex and require a careful interplay between the two detectors, and their scan range is often limited to some tens of MHz. In this thesis a digital phase frequency detector[11] (PFD) with excellent phase noise performance and an ultra low noise floor of -153 dBc/Hz @ 10 kHz offset is used to implement an OPLL. Although it is a digital device, it has a very large operating bandwidth from 10 to 1300 MHz, which allows for a wide scanning range of the slave laser frequency.

The behavior of a PFD differs from normal phase detectors, since it does not only detect the phase difference of its two input signals but also their difference in frequency. A common type of phase frequency detector is a three state sequential PFD, which is a digital logic circuit whose output depends linear on the phase error within a dynamic range of $\pm 2\pi$. In figure 5.7 (a) the logic diagram of the simplest type of a three-state PFD often found in PLL applications is shown [57, 59]. It consists of two D-flip-flops in conjunction with a simple AND-gate. The two flip-flops are named "UP" and "DOWN" and their possible outputs are the two logic states 0 and 1, accordant to a low and high voltage level, respectively. The AND-gate is used to disable the unstable situation when both outputs are in the high state 1 by resetting both flip-flops to the low state 0. Thus, all together there are three possible output states of the PFD circuit:

$$+1: \quad \mathrm{U} = 1,\ \mathrm{D} = 0 \tag{5.7}$$

$$0: \quad \mathrm{U} = 0,\ \mathrm{D} = 0 \tag{5.8}$$

$$-1: \quad \mathrm{U} = 0,\ \mathrm{D} = 1\,. \tag{5.9}$$

The output signals of the flip-flops are additionally inverted, so that altogether the PFD circuit provides four possible outputs U, NU, D and ND. The input signals are the beat signal (RF) and the local oscillator (LO), respectively, and the output states Q of the flip-flops are set by the rising slopes of the input signals. A low Q output will transition high on the next positive edge of its input, whereas a high Q output will stay high. The

[11] Hittite HMC439QS16G

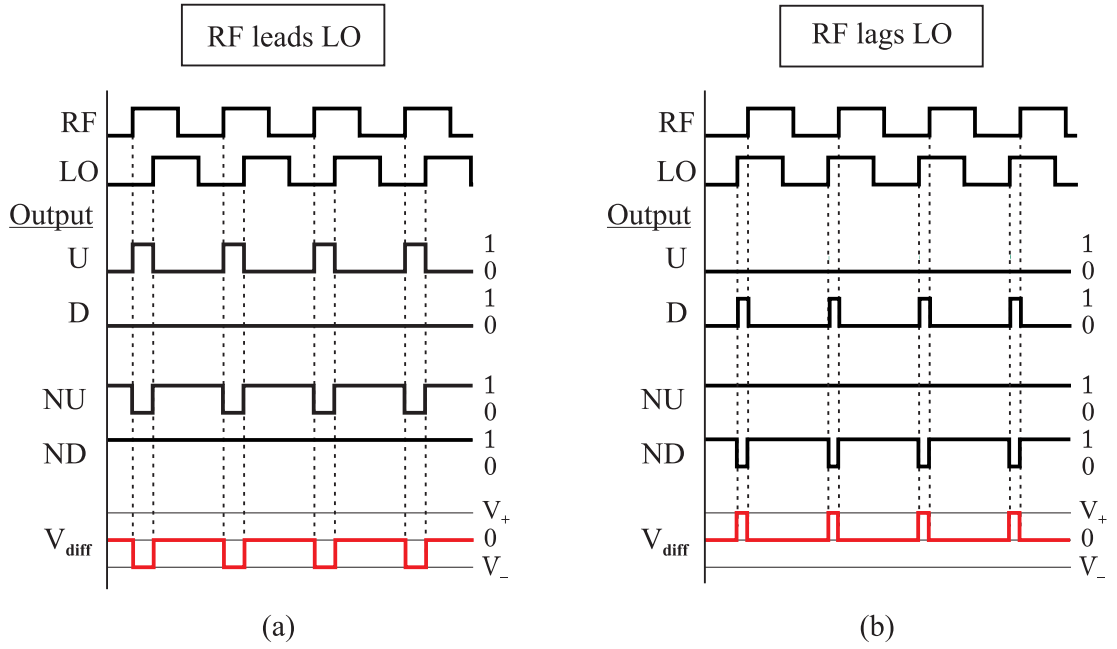

Figure 5.8.: Timing diagram for the different output signals U, NU, D and ND of the PFD together with the difference V_{diff} between NU and ND, depending on the input signals RF and LO. In (a) RF leads LO whereas in (b) RF lags the LO. This leads to a sign of the difference voltage which depends on the phase relation between RF and LO.

state diagram of the PFD is shown in figure 5.7 (b). According to this, a positive slope of the RF signal transfers the PFD in the next "higher" state, unless it is already in state +1, whereas the LO signal does the opposite.
Figure 5.8 shows the timing diagram of the PFD outputs for equal frequencies $f_{\text{LO}} = f_{\text{RF}}$. The difference between the inverted outputs NU and ND is the relevant output of the PFD which will provide the error signal. The case that RF leads LO, i.e. $\Delta\phi = \phi_{RF} - \phi_{LO} > 0$, is shown in figure 5.8 (a), where it is assumed that the PFD circuit is initially in state 0. As soon as the RF signal arrives, it forces the "UP" flip-flop and thus the U output in the high voltage state, whereas the D output stays at its low level, thus the PFD circuit is transferred into state +1. The delayed LO signal then brings the PFD back into state 0, since the transfer of the "DOWN" flip-flop into 1 causes the AND to reset both flip-flops. Hence, the output of U continuously switches between its low and high level whereas the D output always stays at its low level, and the PFD circuit toggles between the states 0 and +1. As a result, one obtains negative output pulses of the differential signal $V_{\text{diff}} = \text{NU} - \text{ND}$, whose duration depend on the phase difference. The averaged voltage $\overline{V}_{\text{diff}}$ will thus increase (negative) with increasing phase difference. The opposite situation when RF lags LO, i.e. $\Delta\phi < 0$, is shown in figure 5.8 (b), which leads to positive differential output pulses and thus a positive averaged error voltage. This swapping between the pair of "toggling states" as $\Delta\phi$ changes sign is essential for the circuit to act as a phase detector.
To demonstrate the phase characteristics of the PFD used in this theses, figure 5.9 shows the averaged voltages $\overline{\text{NU}}$ and $\overline{\text{ND}}$ and their difference $\overline{V}_{\text{diff}}$ depending on the phase differ-

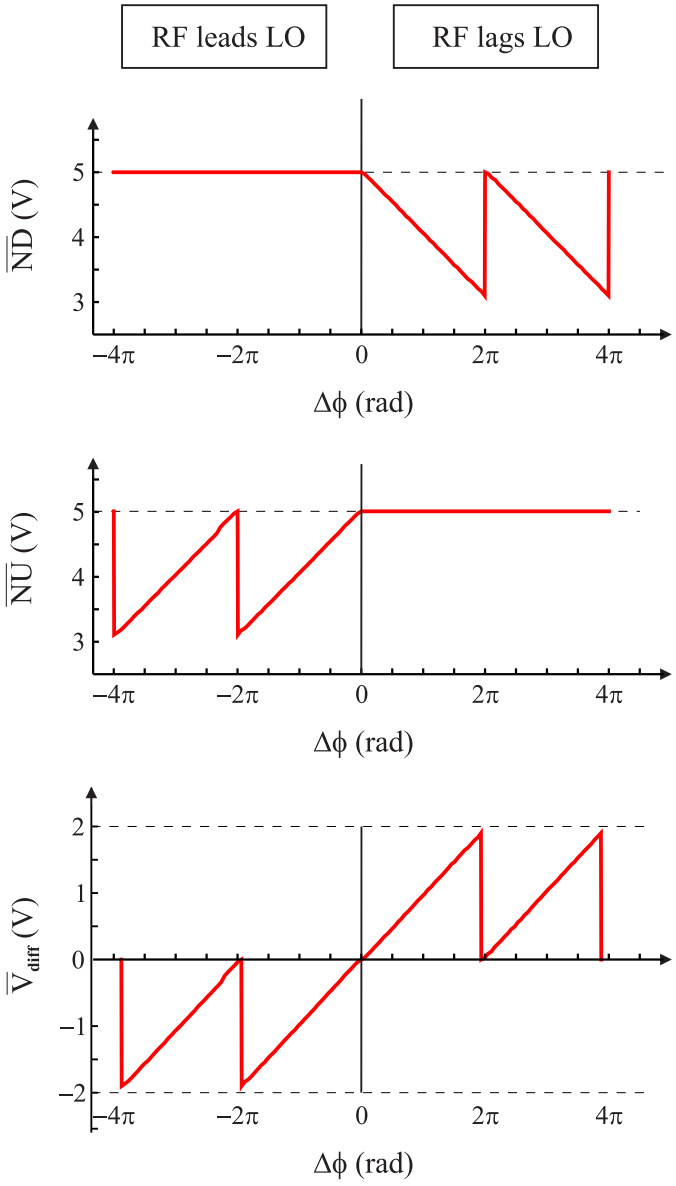

Figure 5.9.: Averaged output voltages of the phase frequency detector measured with two signal generators. The graphs show the outputs $\overline{NU}$ and $\overline{ND}$ and their difference $\overline{V}_{diff}$.

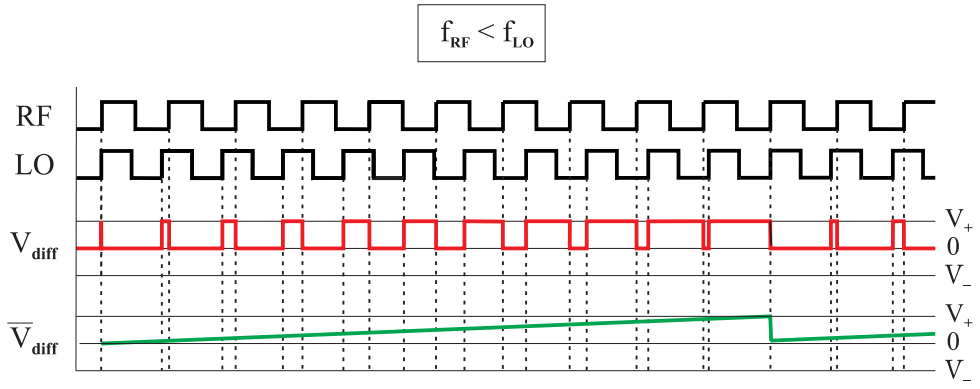

Figure 5.10.: Timing diagram of the differential output V_{diff} of the PFD in the case of slightly different frequencies of RF and LO. Here, the case of $f_{\text{RF}} < f_{\text{LO}}$ is shown, where the pulses of V_{diff} are positive. The average voltage $\overline{V}_{\text{diff}}$ is then a sawtooth function with the periodicity given by the frequency difference.

ence between input signals of the PFD[12]. It is measured by independently adjusting the phase of the RF and the LO signal using two signal generators which are both stabilized to the same 10 MHz reference[13]. If RF leads LO, the $\overline{\text{ND}}$ output stays at a constant level of 5 V whereas the $\overline{\text{NU}}$ voltage is a sawtooth function with an amplitude between 3 V and 5 V and a periodicity of 2π. In the contrary situation the $\overline{\text{NU}}$ output is at a constant voltage of 5 V, and the output $\overline{\text{ND}}$ varies between 3 V and 5 V. Thus, the differential voltage is a multivalued sawtooth function with an amplitude either between 0 and the positive voltage +2 V or the negative voltage -2 V, whose sign depends on the phase relation between the RF and the LO signal.
The sign swapping of the output as $\Delta\phi$ crosses zero does not occur if the two input signals have different frequencies. In figure 5.10 the timing diagram is shown for the situation that $f_{\text{RF}} < f_{\text{LO}}$. In this case the duration of the output pulses is not constant but increases with time, with a periodicity depending on the frequency difference. Since the rising slopes of the LO signal always arrive "earlier" than that of the RF signal, the sign of the phase difference does not change until the frequencies will be equal, and thus the sign of the output pulses will always be the same. As a result, the average output voltage $\overline{V}_{\text{diff}}$ shows a sawtooth shape with a periodicity given by the inverse of the frequency difference. In this case the PFD acts as a frequency detector, and the sign of the output indicates in which direction the frequency has to be adjusted. This kind of PFD can acquire lock even for large frequency differences of the input signals, which is in principle only limited by the operating bandwidth of the PFD.
The electrical circuit of the surface mount PFD chip which is used in the OPLL is shown in appendix A.2. The error signal is obtained using an additional differential amplifier[14] to subtract the NU and ND outputs. The transfer function K_{d} of the PFD after the amplifier is measured in the linear range between $\pm\pi$ by adjusting the relative phase between the RF and the LO signal, and the result in shown in figure 5.11. By fitting a line this gives

[12]This data is measured with a PFD which is equivalent to that used in the OPLL, but on an evaluation board, to demonstrate the operating principle of the PFD. In the OPLL an individual surface mount chip of the same PFD is used instead.
[13]This is necessary to have full control of the phase relation between the two signal generators.
[14]OpAmp THS4031ID

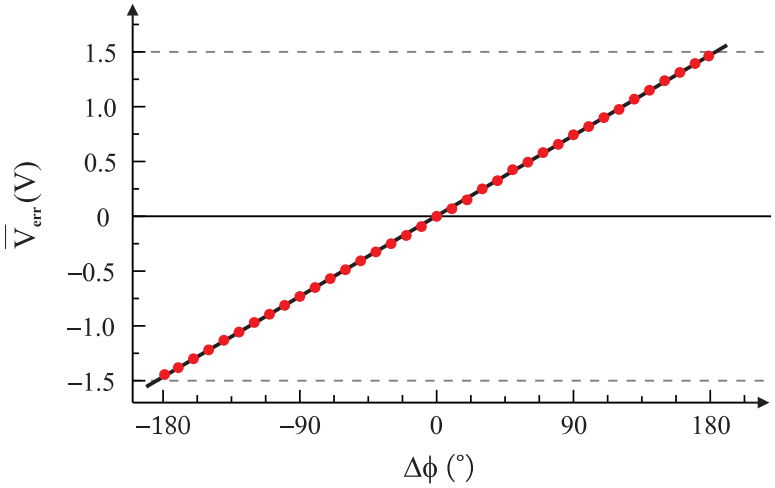

Figure 5.11.: Linear gain of the PFD including the differential amplifier. The sensitivity is obtained by fitting a line (black) to the measured data (red dots).

a sensitivity of the PFD of

$$K_{\mathrm{d}} = 0{,}467\ \frac{\mathrm{V}}{\mathrm{rad}}\,. \tag{5.10}$$

5.3. Implementation of the feedback

5.3.1. Introduction

In order to build a stable phase lock it is essential to have slow and fast control of the slave laser frequency, and three different feedback paths are combined to obtain the desired loop bandwidth. The piezoelectric actuator used to tilt the grating can compensate slow frequency variations and longterm drifts in the frequency range below several kHz, and thus provides the slow feedback path of the system. The medium and fast frequency fluctuations are both controlled via the injection current. The medium path uses the DC-coupled modulation input of the laser controller[15], wherefore the bandwidth is limited by the electronic bandwidth of the device. The fast path uses a Bias-T[16] to directly modulate the injection current of the laser diode. The bandwidth of this path is limited by the high frequency cutoff of the Bias-T, which is about 100 MHz, and the low frequency cutoff of the AC-coupled input of the Bias-T.
The bandwidth of all three paths is measured by modulating the probe laser frequency with a sinusoidal signal and measuring the peak frequency deviation $\Delta\Omega$ in units of $^{\mathrm{MHz}}/_{\mathrm{mV}}$ for different modulation frequencies and for a constant modulation amplitude, see section 3.2. Since modulation of the probe lasers frequency directly appears at the output spectrum of the beat signal, the frequency deviation of the beat signal is used to measure the response of the probe laser. The frequency of the coupling laser is thereby stabilized to an atomic transition as described in section 5.1.1, and a spectrum analyzer (SA) is used to measure the spectrum of the modulated beat signal. The value obtained for the peak deviation

[15] MLD-1000 from Sacher
[16] BT25-V2 from Sacher

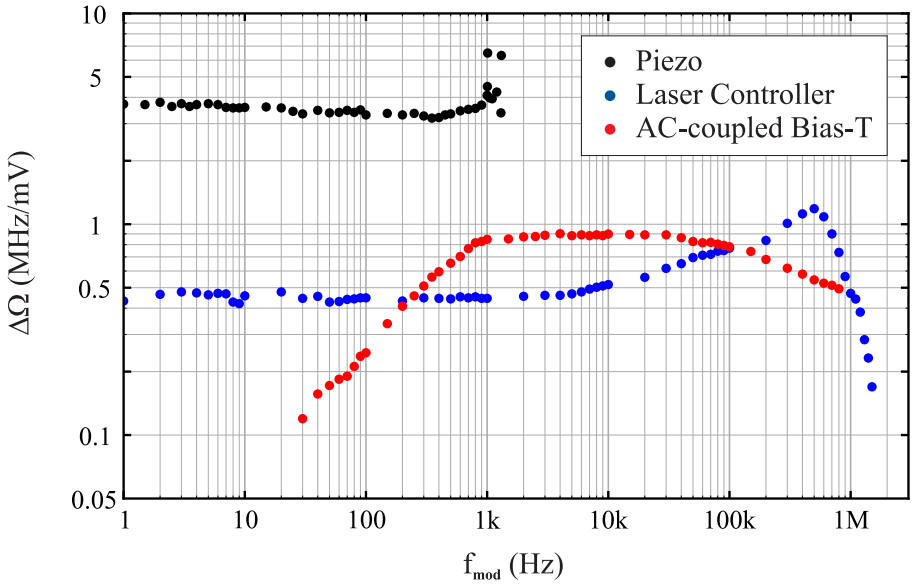

Figure 5.12.: Peak frequency deviation $\Delta\Omega$ of the beat signal dependent on the modulation frequency in the range between 1 Hz and 1 MHz. The frequency of the probe laser is modulated via the piezoelectric actuator (black) and the injection current using the laser controller (blue) and the direct modulation input of the laser diode (red).

is only a rough estimate, but still gives some useful results in terms of the bandwidth and sensitivity of the different modulations paths. The settings of the spectrum analyzer, and especially the sweep time, have to be chosen carefully so that the displayed spectrum is consistent with the real frequency modulated (FM) spectrum of the input signal. The signal must be monitored for a period of time which is long enough to ensure that the peak deviations on both sides of the signal really occur, i.e. the modulation frequency has to be at least twice the sweep frequency of the SA. In fact, the modulation frequency should be significantly larger than the sweep frequency in order to measure a meaningful spectrum[17]. Hence, the sweep time is always set to an appropriate value depending on the modulation frequency. Accordant to chapter 3.2.1 the modulation amplitude is chosen so that the modulation index is always larger than 100 in order to measure $\Delta\Omega$. Additionally, since the probe laser frequency is not stabilized and thus slowly drifts in time, a large modulation amplitude ensures that $\Delta\Omega$ considerably exceeds the drift of the beat signal on time scales of the SA sweep.

In figure 5.12 the peak frequency deviation $\Delta\Omega$ is plotted on a logarithmic scale versus the modulation frequency for the three different feedback paths. The sensitivity of each path can be estimated by fitting a line to the data points in the flat linear range. For the slow path, the voltage of the piezoelectric actuator is modulated around its DC value. The first mechanical resonance is observed at a modulation frequency of about 1 kHz, which limits the bandwidth of the slow path to less than 1 kHz, and the sensitivity is found

[17] The Fourier spectrum of a time varying periodic signal can only be properly displayed by the SA, if the modulation frequency is too fast for the input band pass filter to "see" the instantaneous frequency, i.e. it is not able to measure a single line on each data point in the spectrum. The SA will then display the time independent Fourier components of the input signal, which correspond to the Bessel functions explained in chapter 3.2.1.

to be 3.49 $^{\mathrm{MHz}}/_{\mathrm{mV}}$. To measure the frequency deviation for the medium and fast path, the frequency of the probe laser is modulated via the injection current. For the medium path using the laser controller, the DC current has to be smaller than the upper limit of the operating current of −121 mA, since the controller automatically disables at larger currents to prevent any damage of the laser diode. Otherwise the modulation will be asymmetric, and hence the DC current is set to −115 at which the laser is still in single mode operation. The response of the medium path is shown by the blue data points in figure 5.12, and it is flat from DC up to frequencies of about 10 kHz with a sensitivity of 0.45 $^{\mathrm{MHz}}/_{\mathrm{mV}}$. A resonance is observed at 500 kHz, and the OPLL the bandwidth of this path will be restricted to frequencies up to 100 kHz, since this path is only needed to cover the intermediate frequencies in the range of several tens of kHz. Since this path goes down to DC, it is not implicitly necessary to use the slow path. However, the maximum frequency deviation of the current is limited by mode hops, whereas the external grating provides a tuning range of several GHz. Thus, it is reasonable to use the piezo rather than the DC-coupled current path at low frequencies to compensate for large frequency drifts.
In the case of the fast feedback path one is primarily interested in the lower cutoff frequency of the AC input of the Bias-T. The plot clearly shows the corner frequency in the range of 1 kHz, indicating the high-pass behavior of the Bias-T. The curve is flat in the frequency range between 1 kHz and 30 kHz, and in this range the sensitivity is about 0.88$^{\mathrm{MHz}}/_{\mathrm{mV}}$. At higher frequencies the peak deviation slowly starts to decrease according to the low pass shape of the thermal current-to-frequency transfer function in the FM signal of a laser diode, given in equation (3.29). To account for this effect, the feedback gain of the OPLL should be increased for larger frequencies in order to achieve a locking bandwidth in the range of several MHz.
The measurements shown in figure 5.12 are performed at a fixed modulation amplitude in each case, and a linear dependence of $\Delta\Omega$ on the amplitude according to equation (3.20) is assumed. In order to verify this linear behavior, $\Delta\Omega$ was also measured at a fixed modulation frequency but for different amplitudes. For all three paths, it is found that the voltage-to-frequency conversion is linear up to the largest measured modulation amplitude of 200 mV.

5.3.2. Loop filter design

The error output of the PFD is send into three filters, which provide the control voltage for the different feedback paths according to their specific bandwidth and sensitivity. The quality of the loop is highly sensitive to the correct design of the loop filters. If multiple feedback is used, crosstalk between the different paths can lead to spurious components in the output spectrum, which can significantly reduce the quality of the lock. Thus, special care has to be taken at the crossover frequencies of the filters in order to avoid crosstalk. Furthermore, one has to make sure that all control signals have the same polarity and correct the frequency in the right direction.

Piezo loop filter (slow path)

The loop filter of the slow part is implemented as shown in figure 5.13 (a). The error signal is integrated by a proportional-integral (PI) controller [43] to adjust the length of the external cavity. The integrator ensures high gain at low frequencies, and the cut-off-frequency is about 160 Hz. A voltage divider is used to reduce the feedback voltage to an appropriate level, and a potentiometer can be used to adjust the overall gain. The

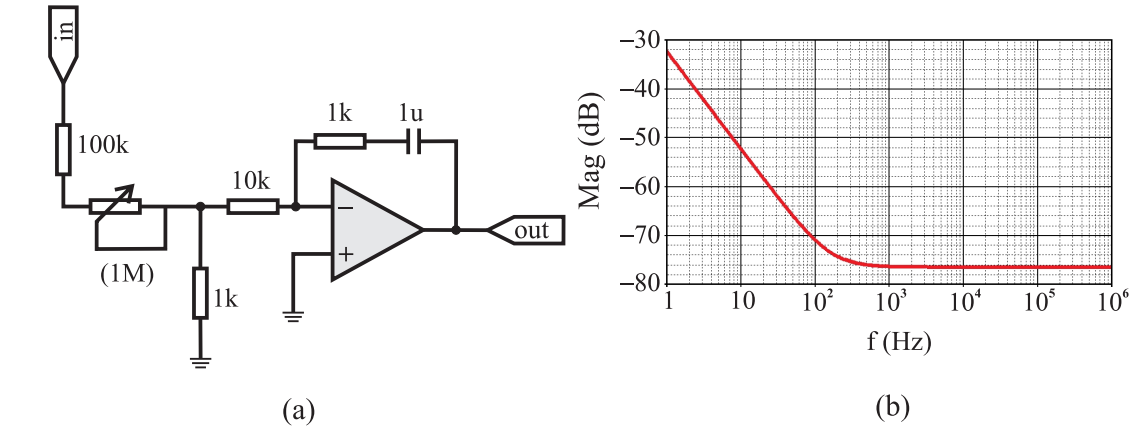

Figure 5.13.: Schematic circuit diagram (a) of the filter used for feedback to the slow grating path and the corresponding magnitude plot of the frequency response (b).

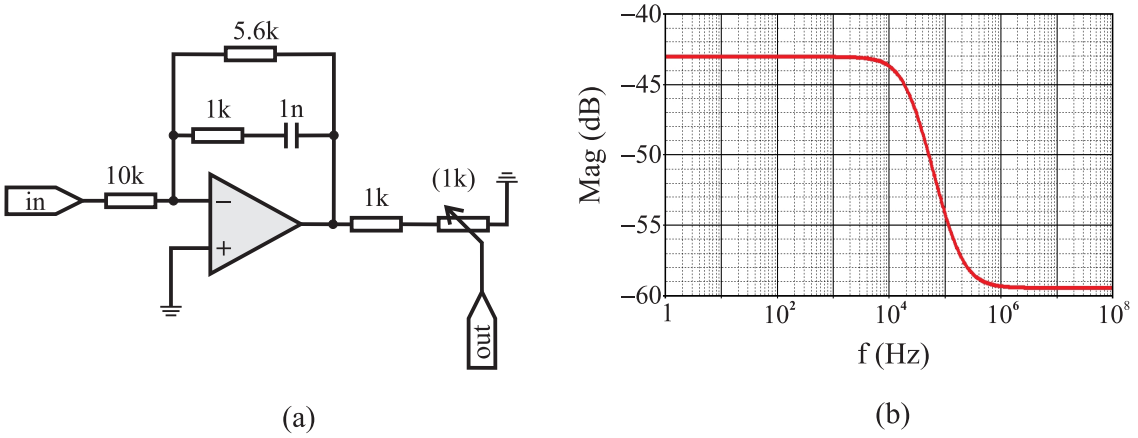

Figure 5.14.: Schematic circuit diagram (a) of the filter used for the medium feedback path via DC-coupled current modulation at the laser controller. In (b) the corresponding magnitude plot of the frequency response is shown.

magnitude of the filter transfer function is plotted in figure 5.13 (b)[18], where the actual values of the magnitude in the OPLL can differ slightly from the plotted values, depending on the exact setting of the voltage divider. After the filter, a summing amplifier adds the output of the PI controller to the constant DC voltage of the piezo (see appendix A.2).

Laser controller loop filter (medium path)

The medium path is used to control frequencies between several 100 Hz up to 100 kHz. The filter is realized using a PI controller with an extra resistor, which is connected parallel to the PI part in the feedback of the controller, as shown in figure 5.14 (a). The additional P-part cuts off the integrator at a frequency of about 10 kHz, so that the response is flat down to DC, as depicted in figure 5.14 (b). This ensures that the slow integration part dominates the frequency control at low frequencies. The upper cut-off-frequency is about 160 kHz to make sure that the resonance found for the laser controller at 500 kHz does

[18] All plots are obtained using the student version 9.1. of the simulation program PSpice.

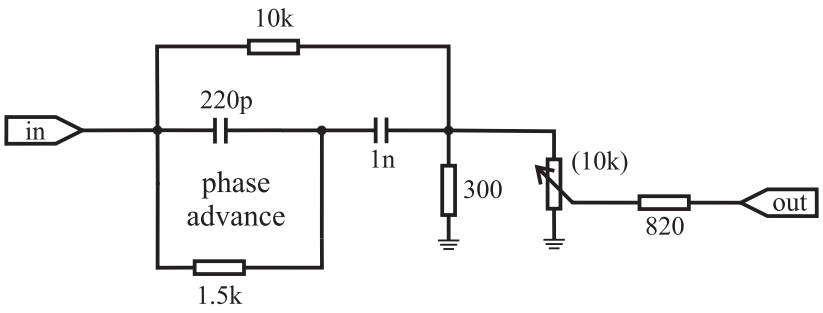

Figure 5.15.: Schematic circuit diagram of the laser diode loop filter to implement the fast feedback path. The key element is a phase advance circuit which shifts the phase and thus widens the loop bandwidth.

not affect the loop. Again, a voltage divider including a potentiometer is used to adjust the overall gain, and the exact values of the magnitude depend on the specific ratio of the voltage divider ratio.

Laser diode loop filter (fast path)

The fast feedback path is the most important one in order to reduce the phase noise of the beat signal and to achieve the desired loop bandwidth of several MHz. The slow and medium paths are mainly used to stabilize the signal to the range of the phase detector. The design of the laser diode filter is more challenging since it has to account for the phase shift of the laser diode in the range between 100 kHz and 1 MHz.
In order to build the perfect filter it would be necessary to have full information about the transfer function of the system, i.e. the open-loop gain given in equation (4.17) without the filter $F(s)$. One could then easily design a filter $F(s)$ which leads to the desired closed-loop and error transfer function, respectively. According to equation (4.23) the system transfer function includes the phase detector sensitivity K_d, the delay time τ and the transfer function of the laser diode. The linear gain K_ld of the laser diode, as written in equation (4.24), is given by the sensitivity of the probe laser, which was measured in the previous section. However, the last term in equation (4.24) is the particularly important one, since it describes the pole of the transfer function of the laser diode. In principle, one could measure this transfer function with a network analyzer (NWA), which measures the frequency response of a device by comparing the magnitude and phase between the output voltage and the input of the device for different signal frequencies. In order to measure the frequency response of the laser diode, an output voltage which is proportional to the frequency modulation of the laser field is required. For this purpose one could in principle measure the output of the PFD versus current modulation. However, this only works if the beat signal is already phase locked and thus within the linear range of the PFD. Therefore, the filter is designed empirically based on the filter described in reference [46], and with the help of PSpice it was possible to design an appropriate filter for the laser diode feedback.
The final version of the loop filter is shown in figure 5.15 and the Bode plot in figure 5.16 shows the magnitude and phase of the filter frequency response. The key element to achieve the desired loop bandwidth is a phase advance filter, which shifts the phase in the frequency

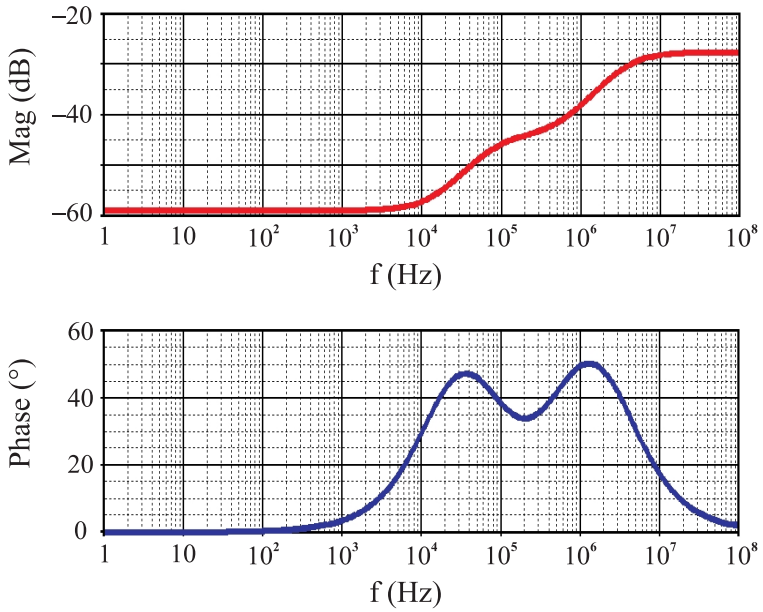

Figure 5.16.: Bode Plot of the frequency response of the fast feedback filter. The phase advance circuit shifts the phase in the range around 1 MHz and also increases the gain in this region.

range between 500 kHz and 3 MHz and also highly increases the gain for large frequencies. The second capacitor in series with the phase advance is used to increase the gain at lower frequencies in the range between 10 kHz and 100 kHz. The extra resistor parallel to the phase advance (10 kΩ) mainly determines the gain at lower and intermediate frequencies up to 1 MHz. Finally, the resistor which is connected parallel to ground primarily influences the amount of the phase shift caused by the phase advance, which is about 50° in the case of a 300 Ω resistor. In the end, the chosen values in the circuit in 5.15 are found to be the best ones to obtain a stable lock with the widest possible loop bandwidth. Since the fast feedback path is build without any active device, which would add extra noise and possibly limit the bandwidth, the polarities of the slow and medium paths are adjusted according to the polarity of this path.

The crossover frequencies of the three filters can be estimated on the basis of the plots in figures 5.13, 5.14 and 5.16 of the filter transfer functions, and they are found to be around 10 Hz for the slow and medium path, whereas the filters of the medium and fast paths cross around 100 kHz. The plots do not include the different sensitivities of the three feedback paths measured in the previous chapter, and thus the actual crossover frequencies differ slightly from these values. However, in the end the gain of each filter is adjusted so that no crosstalk components are present at the output of the beat signal.

5.3.3. Phase lock performance

In this subsection the performance of the OPLL is examined in terms its capability to initially acquire lock, its scanning range, and its longterm stability. The residual phase noise and thus the ability of the loop to suppress the phase noise of the beat signal is characterized in more detail in section 5.4.

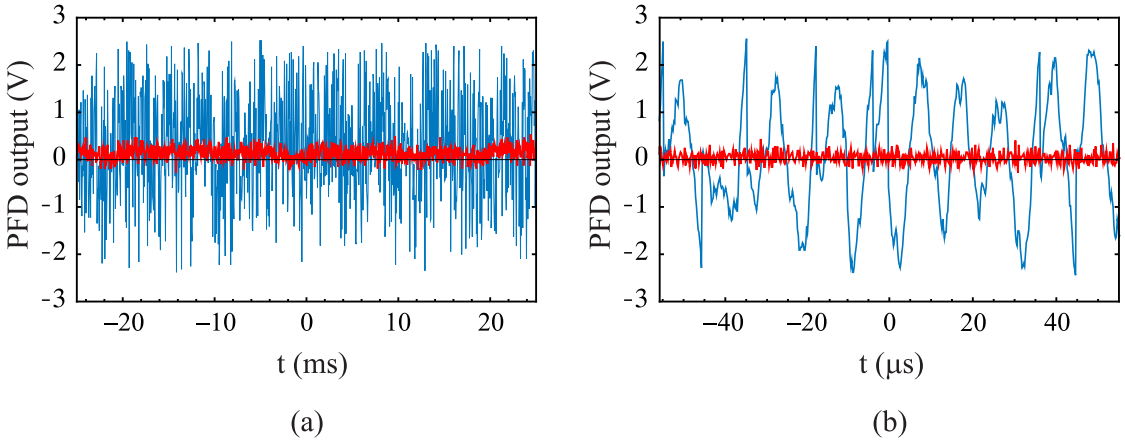

Figure 5.17.: Error voltage of the PFD measured in the time domain in the case of a weakly locked beat signal using only the slow and medium feedback (blue line), and in the locked condition (red line). In (a) a scan over 50 ms is shown and (b) shows a measurement over 100 μs.

Phase lock acquisition

In order to acquire lock the spectrum analyzer (SA) is usually used to watch the frequency of the beat signal. The DC voltage of the piezoelectric actuator can be adjusted so that the beat signal is within the capture range of the phase detector, and the feedback for the three paths is enabled by switching on the corresponding filters one by one. The spectrum displayed by the SA provides a convenient measure for the lock performance of the loop. Alternatively, the output voltage of the PFD can be used as an indicator to detect if the loop is in its locked condition. If the frequency of the beat signal is outside the linear range of the PFD, the output voltage will be either positive or negative in sign. Once the slow PZT and medium current feedback paths are switched on, the beat signal is stabilized to the LO frequency, but still exceeds the linear range of the PFD. The output voltage of the PFD in this condition is shown by the blue curve in figures 5.17 (a) and (b) for different scanning times, where one can see that the noisy beat signal drives the PFD out of its linear range. As soon as the fast feedback is included, the beat signal stays within the linear range of the PFD and the output voltage is zero plus some residual noise, as shown by the red lines in figure 5.17.

Scanning range

The operating bandwidth of the PFD is specified from 10 MHz to 1.3 GHz, and in principle the scanning range is limited to this range. However, it is found that the phase detector used here does not work properly in the frequency range below 100 MHz. The reason for this behaviour could not be identified. Nevertheless, in the frequency range above 100 MHz the loop works properly up to frequencies of at least 700 MHz. This is the cutoff frequency of the high rejection low pass filter which is used after the mixer in figure 5.4. Within this frequency range, one can scan the frequency of the slave (probe) laser by scanning the frequency of the LO input of the PFD. This is tested by using a stepwise frequency sweep of the signal generator used as LO2. By replacing the low pass filter with one which has a a larger cutoff frequency, one could probably increase the operating bandwidth of the loop to the high frequency limit of the PFD of 1.3 GHz.

Longterm stability

Several factors determine the longterm stability of the OPLL. First of all, the frequency lock of the master (coupling) laser has to be stable for several hours in order to ensure a longterm stable phase lock, which is typically the case when locking the master laser to an atomic resonance using polarization spectroscopy as described in section 5.1.1. A second important factor is the operating current of the probe laser. It is observed that the stability of the OPLL is highly dependent on the exact setting of the probe laser current, and even if it is in single mode operation, a slight change in the operating current can cause an unstable lock. Finally, it is the ability of the slow feedback path to recapture lock in the case of large frequency changes which determines the longterm stability of the OPLL. If the corresponding loop filter is adjusted properly, it is found that the lasers stay phase locked over several hours even in a noisy laboratory environment.

Finally, it is checked that the OPLL does not affect the intensity fluctuations of the probe laser. Since the current of the laser is modulated, this could additionally cause unwanted intensity modulation. However, corresponding to equation (3.31) and for small modulation currents it is expected that the intensity is not influenced much by the OPLL. This is verified by measuring the output of a photodiode over a time intervall of 200 s, and no change in the maximum intensity fluctuation could be detected.

5.3.4. In-loop measurements

Once the loop is working and the signal stays within the range of the PFD, one can measure the frequency response of the feedback loop, i.e. the closed-loop transfer function $H(s)$ and the error transfer function $E(s)$, and also the transfer function of the optical system including the laser diode using the network analyzer. For this purpose, the NWA signal has to be injected in the loop as an error signal. The propagation of this noise through the feedback loop describes the different transfer functions of the system. The position at which one has to measure the output signal in order to obtain the different transfer functions, e.g. $H(s)$ and $E(s)$, depends on the position at which the noise is added in.
Figure 5.18 illustrates the measurement setup. The NWA[19] signal V_{in} is injected in the loop directly after the phase detector and before the loop filter of the fast feedback path by using a differential amplifier[20], whose output voltage is named V_1. The slow (PZT) and medium feedback paths (DC), indicated by the light gray colored filters, are used to lock the beat signal, but they are not included in the loop through which the NWA signal propagates. The output voltage of the fast path (AC) loop filter is named V_2, and V_3 denotes the error voltage directly after the PFD (K_{d}). From system analysis, the transfer functions can be obtained by the following relations:

$$E(2\pi if) = \frac{V_1}{V_{\mathrm{in}}} \qquad H(2\pi if) = \frac{V_3}{V_{\mathrm{in}}} \tag{5.11}$$

$$G(2\pi if) = \frac{V_3}{V_1} \qquad S(2\pi if) = \frac{V_3}{V_2}\,, \tag{5.12}$$

where i is the imaginary unit and $S(2\pi if)$ is the system transfer function, that is the open-loop gain $G(2\pi if)$ without the (AC) loop filter. These ratios are measured with the NWA, which displays the ratio S/R of its reference (R) and signal input (S). The

[19] 3577A from Hewlett Packard
[20] AD844 with a bandwidth of 60 MHz

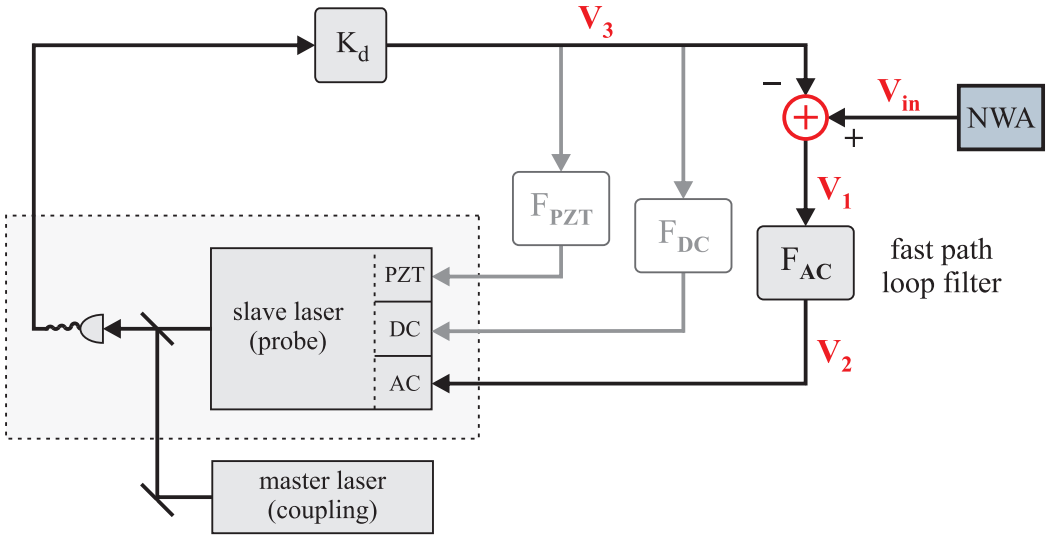

Figure 5.18.: Schematic setup for measuring the transfer functions with the network analyzer. The dashed box indicates that the master (coupling) laser is not directly included in the loop, but it is the transfer function of the slave laser diode which determines the frequency response.

input signals are provided by the voltages measured at the different positions in the loop, depending on the desired transfer function. For these measurements, the OPLL was in its locked condition using a first version of the fast laser diode loop filter. At this stage, the filter parameters have not been perfectly adjusted yet and the loop bandwidth was approximately 1 MHz, which is sufficient to be in the linear range of the PFD.
In figure 5.19 the magnitudes of the error and closed-loop transfer functions $E(2\pi if)$ and $H(2\pi if)$ are plotted in the frequency range between 10 kHz and 10 MHz. For frequencies up to 1 MHz the magnitude $|H(2\pi if)|$ of the system transfer function is at zero dB, corresponding to the expected unity gain within the loop bandwidth, and decreases very rapidly for frequencies larger than 1 MHz. Conversely, the error transfer function $|E(2\pi if)|$ shows the expected high pass filtering behavior, meaning that the loop is able to suppress noise for frequencies up to 1 MHz. In both plots the bandwidth is indicated by the bump around 1 MHz, which is more pronounced for the error transfer function, where one can see the effect of noise enhancement in the vicinity of the loop bandwidth. These plots confirm the characteristic behavior of the PLL transfer functions as explained in section 4.2.1.
The system transfer function $S(2\pi if)$ includes the PFD transfer function K_d and the transfer function of the probe laser diode, whereas the delay time can be neglected since it is sufficiently small. The phase and magnitude of the frequency response is shown in figure 5.20. The magnitude $|S(2\pi if)|$ decays almost linearly, similar to that of an integrator. That is expected since the PFD transfers the frequency output of the beat signal into phase. However, the measured response decreases more rapidly than one would expect from a pure integrator, which decays 20 dB per decade and whose linear frequency response is indicated by the dashed black line in figure 5.20. Thus, the actual magnitude of the transfer function of the laser system starts to drop off at frequencies between 10 kHz and 100 kHz, which is in agreement with the frequency response measured in section 5.3.1.

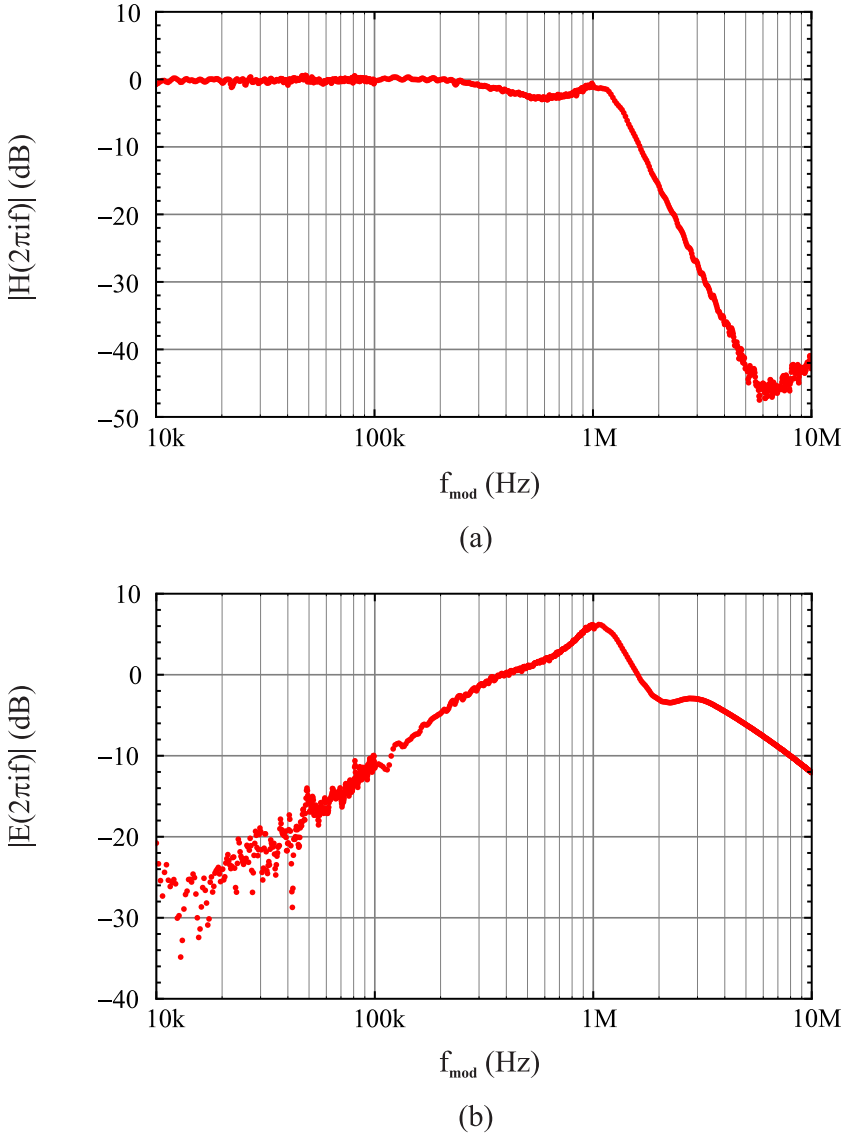

Figure 5.19.: Magnitude Bode Plots of the system (a) and error transfer function (b). The system transfer function has unity gain (0 dB) up to 1 MHz and decreases with higher frequencies. The error transfer function in (b) demonstrates that the loop is able to suppress phase noise with a bandwidth of around 1 MHz, indicated by the servo bump.

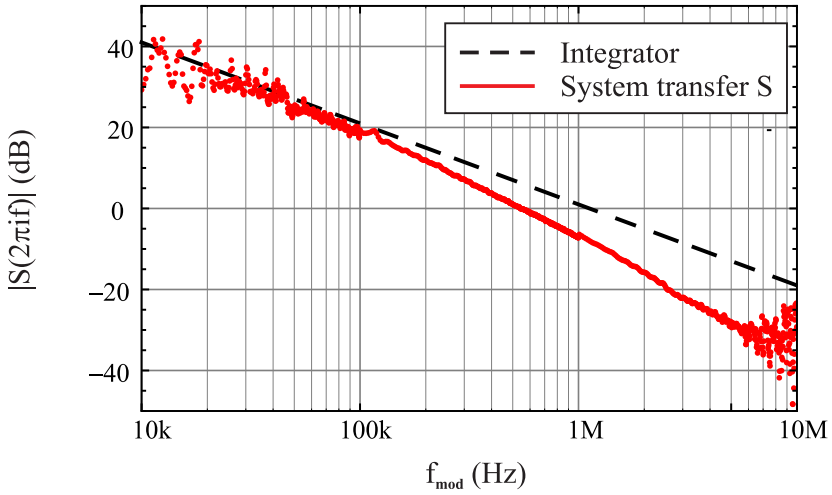

Figure 5.20.: Magnitude of the transfer function of the system consisting mainly of the phase detector and the probe laser diode. The loop filter is not included in this measurement. From the PFD one expects the shape of an integrator, indicated by the black dashed line.

The effect of the loop filter on the system transfer function is shown in figure 5.21, where the phase and magnitude of the system transfer function are plotted together with the open-loop gain $G(2\pi if)$, which is $S(2\pi if)$ multiplied by the filter. As can be seen in the amplitude plot, the filter decreases the overall gain which is due to the voltage divider used to adjust the feedback voltage to an appropriate level. The effect of the phase advance filter starts to appear around 400 kHz, which increases the gain for higher frequencies as explained in the previous section. Simultaneously, the phase of the system is shifted about 45° between 100 kHz and 1 MHz. According to the integrator included in the transfer function, the phase of the system starts at -90°, drops of at higher frequencies and it converges -180° in the range of several 100 kHz. At the same time the amplitude of S crosses zero, and without the phase shift due to the phase advance the system would get unstable. The bandwidth of the loop is limited to 1.2 MHz where the phase approaches $-180°$, and for frequencies around 1 MHz one obtains noise enhancement, since in this region the phase is already very close to 180° and the amplitude of G is smaller than 1. This noise enhancement causes the servo bump mentioned above, which is most pronounced in the error transfer function in figure 5.19.

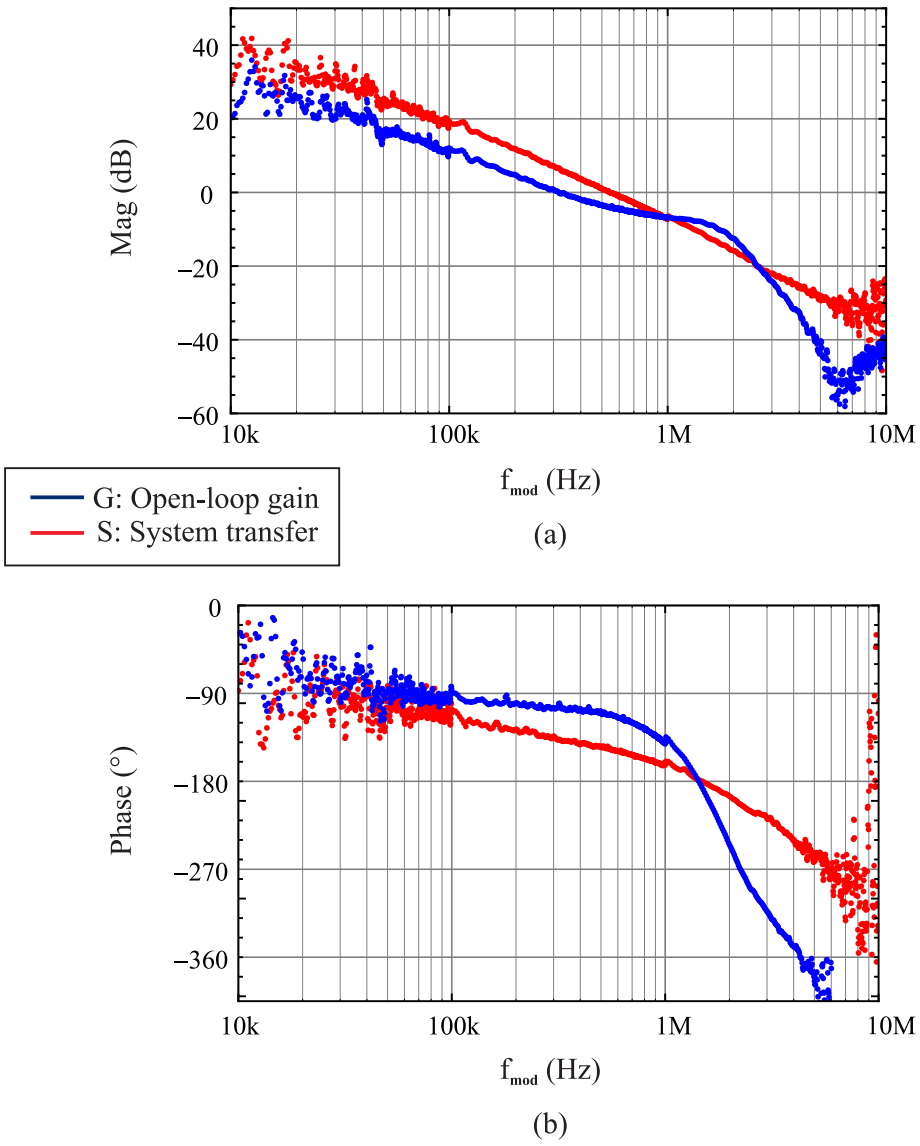

Figure 5.21.: Effect of the loop filter on the system transfer function S by comparison with the open-loop gain G. In (a) the magnitude is plotted and one can see that the filter increases the gain at higher frequencies to account for the thermal low pass behavior of the laser diode. In (b) the phase of S and G is shown, and the phase shift caused by the phase advance filter becomes apparent.

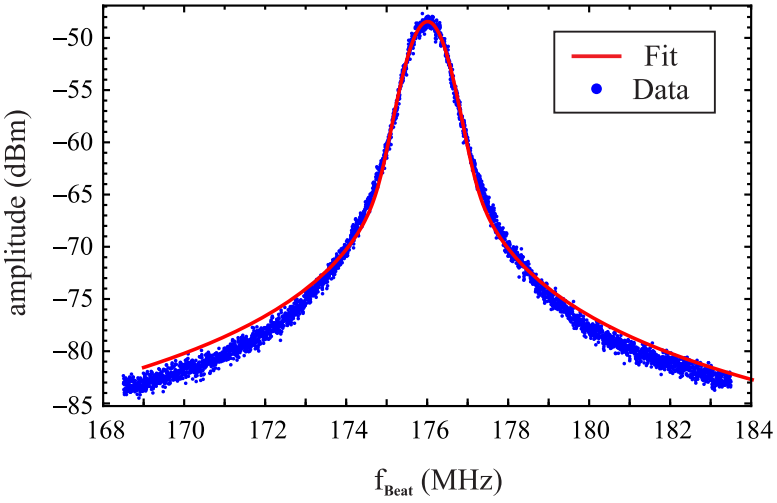

Figure 5.22.: Beat note signal between the two lasers locked at 176 MHz using only the slow and medium feedback path. The red line shows the fit of a Voigt profile on the spectrum.

5.4. Phase noise analysis of the beat signal

The quality of the OPLL concerning the phase stability between the two lasers is characterized by the phase noise spectral density of the beat signal. The beat note spectra are measured in the locked condition while the master laser is frequency stabilized as explained in section 5.1.1. The frequency of the beat signal is set by adjusting the local oscillator LO2 at the phase detector input. For the measurements described here, the oscillator at 9.216 GHz is used as the LO1 to mix down the beat signal, and the frequency of LO2 is set to 176 MHz.
In order to estimate the linewidth of the weakly locked beat signal, figure 5.22 shows the beat note spectrum in the case that only the slow and medium feedback paths are used. According to section 3.3, the line shape of a single mode semiconductor laser in the presence of 1/f-frequency noise can be described by a Voigt profile, and it is found that the latter fits the measured spectrum best. The linewidth of the beat signal is thus estimated by fitting a Voigt function on the spectrum. The linewidth $\Delta\nu_\mathrm{v}$ of the Voigt profile is determined by the corresponding Gaussian width σ and Lorentzian widths γ, respectively, by [60]

$$\Delta\nu_\mathrm{v} = 0.5346\,\gamma + \sqrt{0.2169\,\gamma^2 + \sigma^2}\,. \tag{5.13}$$

The fit values are $\gamma = 142.30\,\mathrm{kHz}$ and $\sigma = 287.52\,\mathrm{kHz}$, resulting in a linewidth of $\Delta\nu_\mathrm{B} = 371{,}142\,\mathrm{kHz}$ of the weakly locked beat signal. Since still a considerable amount of noise is contained in the wings of the spectrum, which spread over a frequency range of several MHz, it is necessary for the loop bandwidth to exceed the linewidth of the beat signal by a significant fraction.
By including the fast feedback path using the filter from section 5.3.2, the phase noise is highly reduced and figure 5.23 shows the resulting beat note spectrum for different spans of the SA. The narrow 500 Hz scan spectrum in 5.23 (e) is measured using an analog spectrum analyzer[21] with a minimum resolution bandwidth (RBW) of 10 Hz. The spectra (a)

[21] 8568B from Hewlett Packard

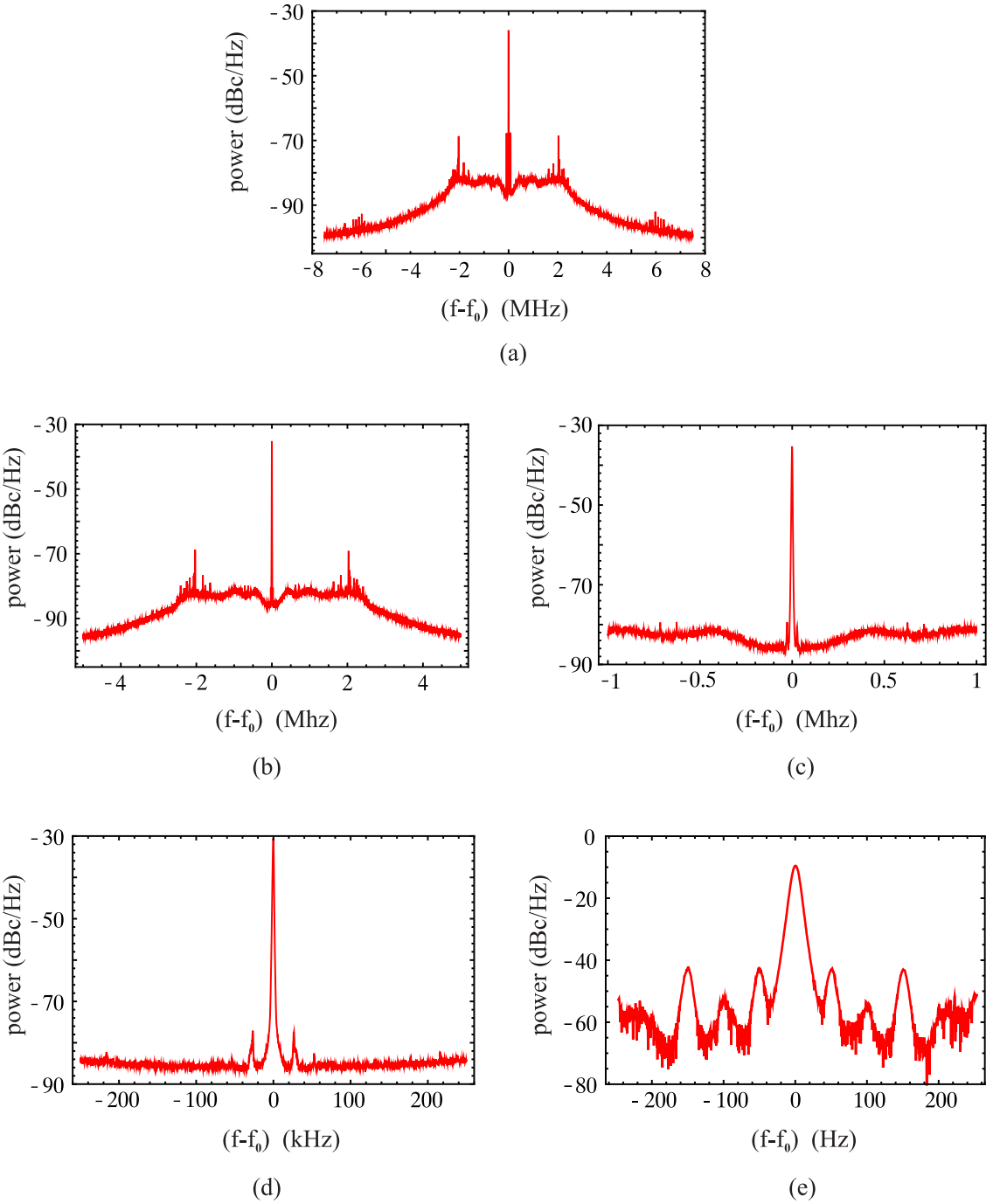

Figure 5.23.: Power spectra of the phase locked beat signal, normalized to the RBW of the SA and the power in the carrier signal. (a): 15 MHz span, 3 kHz RBW. The noise suppression is about 40 dB compared to the carrier signal. (b): 10 MHz span, 3 kHz RBW. (c): 2 MHz span, 3 kHz RBW. In (b) and (c) one can see that the noise suppression is even better in the vicinity of several 100 kHz around the carrier. (d): 500 kHz span, 1 kHz RBW. One observes a flat noise suppression in this frequency range. (e): 500 Hz span, 10 Hz RBW. The resolution is limited by the RBW of the analog SA.

to (d) are measured with a digital spectrum analyzer[22] whose RBW is limited to 1 kHz, which is sufficient for large scan ranges. The digital spectra are averaged over 100 scans, whereas the analog spectrum is an average over 5 scans. All spectra are normalized to the RBW of the SA and to the power $P(f_0)$ contained in the carrier frequency corresponding to equation (4.33). Since in all scans the carrier signal consists of more than one data point, the peak value is only an (under) estimation of the total power. It is determined more accurately by integrating the RBW-normalized power spectral density over the frequency range of the carrier.
From the spectra one obtains that the noise suppression compared to the carrier is approximately 40 dB. If the gain is increased, servo bumps occur at the corners of the flat plateau, indicating a loop bandwidth of 2.4 MHz. The spurious peaks at 2 MHz in figures 5.23 (a) and (b) should not be confused with the servo bumps, since their amplitude is independent from the loop gain and they are too narrow. The origin of these peaks is not clear, however, they are suppressed by more than 30 dB compared to the carrier and thus contribute only by a small amount to the residual phase noise. In the scan in (a), two spurious peaks close to the carrier at 80 kHz are also observed. These peaks arise from the power supply of the ion pump in the laboratory, which is turned off for all other scans.
In the frequency range of ±400 kHz around the carrier, as one can see in the scans in figures 5.23 (b) and (c), the phase noise is even more suppressed and is 50 dB below the peak amplitude of the carrier signal. If the gain of the medium feedback path is increased, bumps appear in the range of 300 kHz due to crosstalk between the medium and the fast feedback path. Figure 5.23 (d) shows a scan of 500 kHz around the carrier signal, where another spurious component at 26.5 kHz is observed, however they are suppressed by more than 40 dB compared to the carrier. This unwanted signal is present at any signal measured in the laboratory and probably arises due to some digital power supply, whose switching frequencies typically lie in the range of several kHz up to several 100 kHz.
The last scan with a span of 500 Hz is shown in figure 5.23 (e), where a 50 Hz oscillation and its harmonics are observed. The peaks at 50 Hz and 150 Hz are the most pronounced ones and they are suppressed by approximately 35 dB. The resolution in this scan is limited by the RBW of the SA of 10 Hz, and the shape of the carrier signal as well as that of the spurious peaks is that of the reference oscillator of the SA. Hence, the width of the phase locked beat signal cannot be resolved and is less than 10 Hz. This is not a surprising result, since according to equation (4.44) in section 4.2.3 the beat note spectrum of the two lasers is composed of a delta function at the carrier frequency f_0, plus an additional noise term which describes the residual phase noise of the signal.

The phase noise variance σ_ϕ^2 of the phase locked beat signal is determined as the integral of the single sideband (SSB) phase noise spectrum. In order to obtain the phase noise spectrum in the range between 40 Hz and 7.5 MHz, several beat note spectra are combined to one phase noise spectrum, so that one has information about the phase noise over a wide frequency range. Therefore, two more spectra with a span of 100 kHz and 1 kHz are used in addition to the spectra shown above. Since the 15 MHz scan spectrum in 5.23 (a) only contributes to the SSB phase noise in the range between 5 MHz and 7.5 MHz (below 5 MHz the SSB phase noise spectrum is determined by the other spectra), the presence of the perturbation of 80 kHz is not included in the calculation of σ_ϕ^2.
The resulting SSB phase noise spectrum $S_\phi(f)$ is shown in figure 5.24, where the noise power per 1 Hz bandwidth, given in $\mathrm{rad}^2/\mathrm{Hz}$, is plotted against the frequency offset from

[22] E4407B from Agilent

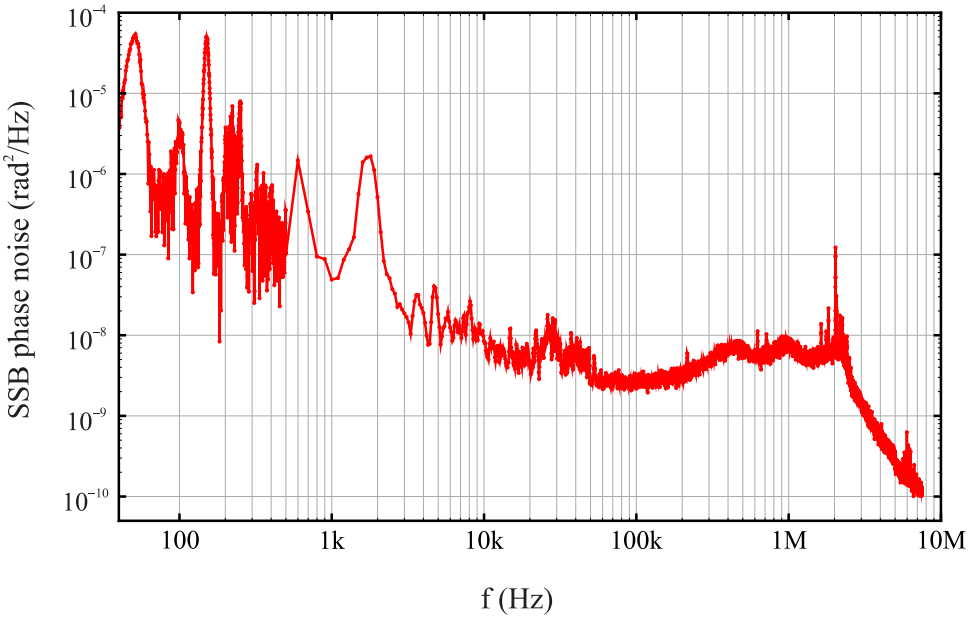

Figure 5.24.: SSB phase noise of the phase locked beat signal in the frequency range between 40 Hz and 7.5 MHz, plotted on a logarithmic scale.

the carrier frequency on a logarithmic scale. The spurious peaks at 50 Hz plus harmonics, 26 kHz (weak), 2 MHz and 6 MHz are clearly visible, and additionally another oscillation at 1.6 kHz is observed which arises due to electronic noise in the laboratory.
Integrating $S_\phi(f)$ and including the factor of 2 to account for the negative frequencies, the residual phase error in the frequency range between 100 Hz and 7.5 MHz is found to be

$$\sigma_\phi^2 = 0.038\,\mathrm{rad}^2\,, \tag{5.14}$$

which gives an average phase deviation of 197 mrad. From this value, the fraction of power in the carrier can be determined using the formula given in equation (4.46), which yields

$$\eta = 96.08\,\%\,. \tag{5.15}$$

For comparison, the fractional power in the carrier is also determined using equation (4.45) for the spectrum measured with a span of 15 MHz, which yields

$$\eta = 95.97\,\%\,. \tag{5.16}$$

which gives almost the same result. This shows that the fraction of power in the carrier can be determined by the residual phase noise in the case of $\sigma_\phi^2 \ll 1$. Thus, more than 95% of the power in the beat signal is available to coherently excite the two-photon transition in the EIT experiment.
According to reference [61, 62], the average time between two cycle slips can be estimated from the residual phase error σ_ϕ^2 by

$$t_{\mathrm{av}} \approx \frac{1}{\mathrm{BW}} \exp\left(\frac{0.6\,\theta}{\sigma_\phi^2}\right)\,, \tag{5.17}$$

where the factor θ is given by the linear range of the PFD in units of π, thus here it is $\theta = 2$. Using this formula, the average time between to cycle slips is determined to $t_{\mathrm{av}} = 9.6\,10^6\,\mathrm{s}$, which is negligible large. In fact, it can be seen from equation (5.17) that the probability for a cycle slip becomes negligible small if the residual phase error is significantly smaller than the range of the phase detector.

In conclusion, this phase locked laser system allows to stabilize the relative phase between two diode lasers with a residual phase noise of less than $0.04\,\mathrm{rad}^2$. This value is comparable to those obtained in the literature, where a residual phase noise between $0.01\,\mathrm{rad}^2$ and $0.08\,\mathrm{rad}^2$ is typically achieved [46, 56, 58, 63]. Thus, more than 95 % of the power of the beat signal can be stored in the narrow carrier signal with a linewidth of less than 10 Hz.

6. Electromagnetically induced transparency on cesium atoms

The small linewidth of dark resonances, as predicted for electromagnetically induced transparency (EIT), makes them particular attractive for applications in precision spectroscopy [21]. In real atomic media, it is essential for an effective quantum interference that the atomic coherence is maintained during the interaction of the atom with the two required laser fields. Any dephasing of the coherence will lead to a reduction and eventually to total destruction of the dark resonance.
The important parameter responsible for the reduced absorption in EIT is the ground state coherence γ_{21} between the states $|1\rangle$ and $|2\rangle$ as explained in chapter 2. The lifetime of the dipole-forbidden transition between the two ground states is negligibly large. Therefore, the coherence is mainly determined by several experimental parameters, such as the simultaneous excitation of several closely spaced hyperfine or Zeeman levels, spontaneous decay of the upper state $|3\rangle$, Doppler broadening, collisions between the atoms, and the phase- and frequency stability of the laser fields. Hence, these parameters need to be controlled carefully in order to obtain a narrow dark resonance.

6.1. EIT and decoherence on atomic cesium gas

In this thesis first measurements of EIT were performed on an atomic cesium vapor cell. In cesium the $6^2S_{1/2}$-ground states with $|F = 3\rangle$ and $|F = 4\rangle$ can be used as the two lower states $|1\rangle$ and $|2\rangle$ of the Λ-system as shown in figure 2.4. In both the D_1- and the D_2-line the excited state $|3\rangle$ can be realized by either of the upper hyperfine states $|F' = 3\rangle$ and $|F' = 4\rangle$, since the transition rules allow both to couple to the two ground states. In the presence of magnetic fields, each of the hyperfine states is split into $(2F + 1)$ magnetic sublevels [64], which leads to the formation of multiple Λ-systems. This leads to a broadening of the EIT resonance due to the simultaneous excitation of several sublevels, depending on the polarization of the lasers and the direction of the magnetic field [42].
For experiments on atomic vapor one also has to take into account several decoherence mechanisms due to the motion of the atoms. The Doppler-broadening due to the different velocities of the atoms can be calculated by

$$\Delta\nu_{\mathrm{D}} = \frac{1}{\lambda_0}\sqrt{\frac{8k_{\mathrm{B}}T\ln 2}{m}}\,, \tag{6.1}$$

where λ_0 is the transition wavelength, m the atomic mass, k_{B} the Boltzmann constant and T the temperature [65]. For a cesium gas at room temperature, one obtains a Doppler-broadened linewidth of 357 MHz for the D_1-line and 374 MHz for the D_2-line. As a consequence of the Doppler-shift, there are two velocity classes that can form a Λ-system for a certain detuning of the coupling laser, i.e., the classes which are on resonance with the $|F' = 3\rangle$ state and the ones resonant to the upper state $|F' = 4\rangle$.
For the D_2-line at 852 nm in cesium [64], off-resonant single photon excitation from the

ground states to the excited levels $|F' = 2\rangle$ and $|F' = 5\rangle$ can occur due to the Doppler-broadening. This causes significant background absorption, and therefore 100 % transparency cannot be achieved using the cesium D_2-line [42]. Additionally, the non-zero coupling to hyperfine states which do not contribute to the Λ-system leads to atomic decoherence and broadening of the EIT resonance. Since the largest transition strength of the D_2-line is that of the $|F = 4 \rightarrow F' = 5\rangle$ transition, it is reasonable to use the $|F = 3 \rightarrow F' = 4\rangle$ ground state for the probe laser transition in order to minimize background absorption. However, there is still considerable background absorption to the $|F' = 2\rangle$ state. For the D_1-line at 894 nm, on the other hand, there are only the two upper hyperfine states $|F' = 3\rangle$ and $|F' = 4\rangle$, which both contribute to the Λ-system but do not contribute to any background absorption or decoherence.
Another effect in an atomic gas is time-of-flight (TOF) broadening of an atomic resonance. The transit time of the atoms passing the laser beam contributes to the linewidth of the atomic transition, if the lifetime of the excited state is longer than the transit time. The linewidth due to time-of-flight broadening for a Gaussian beam profile can be estimated by

$$\Delta\nu_{\mathrm{TOF}} = \frac{4.7}{2\pi}\,\frac{\overline{v}}{d}\,, \tag{6.2}$$

where $\overline{v}$ is the mean velocity of the atoms and d is the beam diameter [65]. For example, at room temperature and for a beam diameter of 1 mm, an atomic resonance in cesium is broadened by 208 kHz due to the transit time of the atoms. Finally, collisions of atoms in a dense atomic vapor cell lead to collisional broadening due to the interatomic dipole-dipole interaction.
It is still not certain which effect dominates the width of an EIT resonance in atomic vapor [66]. As explained in chapter 2.2.3, the Doppler-broadening can be avoided by choosing co-propagating beams in the case of a Λ-system. However, all other linewidth broadening effects can still contribute to the decoherence of the atomic system.

6.2. First experimental results for EIT on atomic cesium gas

The experimental setup to measure EIT on a cesium vapor cell is shown in figure 6.1. The measurements were performed using the D_2-line at 852 nm, since parts of the laser system were already available in the lab.
Since it is advisable to use the $|F = 3\rangle$ ground state for the probe laser, as explained above, the coupling laser is locked to the $|F = 4 \rightarrow F' = 4\rangle$ transition for these measurements. Both lasers are overlapped on a polarizing beam splitter cube (PBS) so that they have orthogonal polarizations. The width of the EIT resonance can be broadened by several MHz due to the residual Doppler-shift if there is only a slight angle of several mrad between the two laser beams [67]. Therefore, both lasers are coupled into the same polarization maintaining (PM) single mode fiber in order to guarantee perfect mode matching of the two beams. Afterwards, the beams have a diameter of approximately 1 mm and are sent through a 2.5 cm long cesium vapor cell. The cell is positioned in a box made of μ-metal for magnetic shielding in order to prevent broadening of the EIT resonance due to Zeeman-shifts of the m_F-sublevels. The intensity of the probe beam is detected with a photodiode[1] which measures the transmission through the cesium cell. The coupling laser is separated from the probe beam using a second PBS.

[1] MFL250907A01

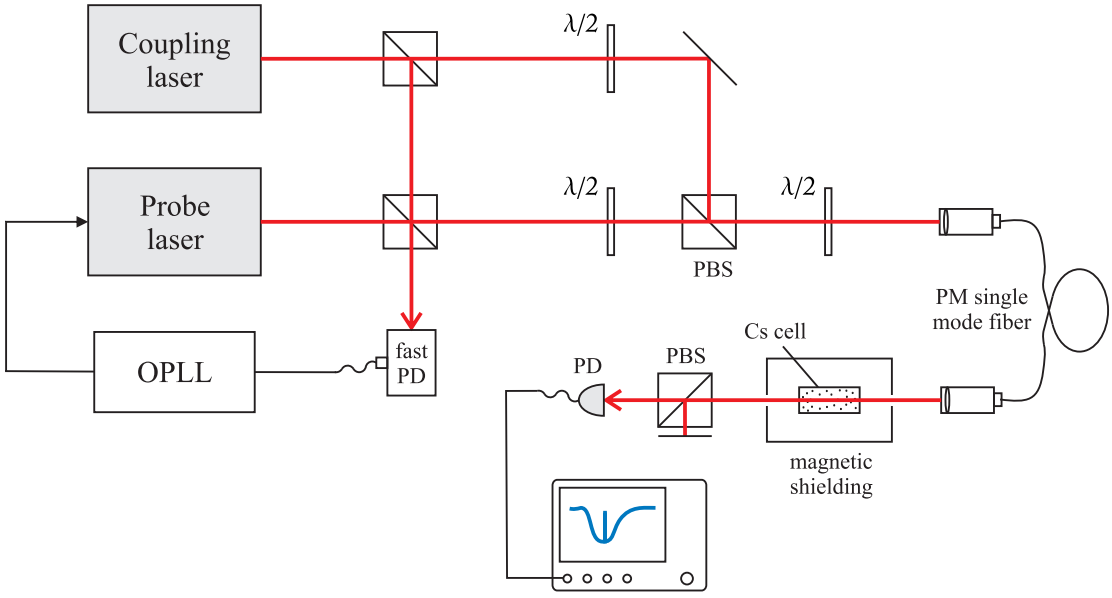

Figure 6.1.: Optical setup to measure EIT on a cesium vapor cell. The coupling and probe lasers are overlapped on a polarizing beam splitter cube (PBS) and afterwards coupled into a polarization maintaining (PM) single mode fiber. The two lasers can be phase locked by the optical phase locked loop (OPLL) described in chapter 5.

The probe laser can be scanned across the whole Doppler-profile of the upper hyperfine states using the piezoelectric actuator. Furthermore, the optical phase locked loop (OPLL) allows to scan the probe laser within a certain frequency range as explained in chapter 5.

Probe absorption profile in the presence of the coupling laser

In order to measure the Doppler-broadened absorption profile, the frequency of the probe laser is scanned with the piezo, i.e., the lasers are not phase locked in this case. Figure 6.2 shows the probe transmission for different powers of the coupling laser at a probe power of $50\,\mu$W. Without the coupling laser, one observes the usual Doppler-broadened absorption profile as shown by the black transmission line.
In the presence of the coupling laser, two velocity classes of atoms are optically pumped via the $|F' = 3\rangle$ and $|F' = 4\rangle$ states, leading to an enhanced absorption at five resonances in the spectrum. In figure 6.3 the pumping is illustrated using the energy level scheme. Assuming a resonant coupling beam, atoms with velocity zero are optically pumped via the $|F' = 4\rangle$ state into the $|F = 3\rangle$ ground state, see figure 6.3 (a). This leads to an enhanced absorption of the probe laser when it is on resonance with one of the $|F' = 2{,}3{,}4\rangle$ hyperfine states, and one observes three corresponding enhanced absorption resonances in the transmission spectrum (see (1), (2) and (4) in figure 6.2). Additionally, the coupling laser pumps atoms via the $|F' = 3\rangle$ state whose Doppler-shift is equal to the frequency difference Δ_{34} between $|F' = 3\rangle$ and $|F' = 4\rangle$, see figure 6.3 (b). This leads to enhanced absorption resonances which are shifted by $\Delta_{34} = 201.24\,$MHz compared to the non shifted resonances. Thus, altogether one obtains five resonances, since the two labeled with (4) in figures 6.2 and 6.3 occur at the same probe frequency. Inside this resonance one observes an increased transmission: the EIT transparency window.

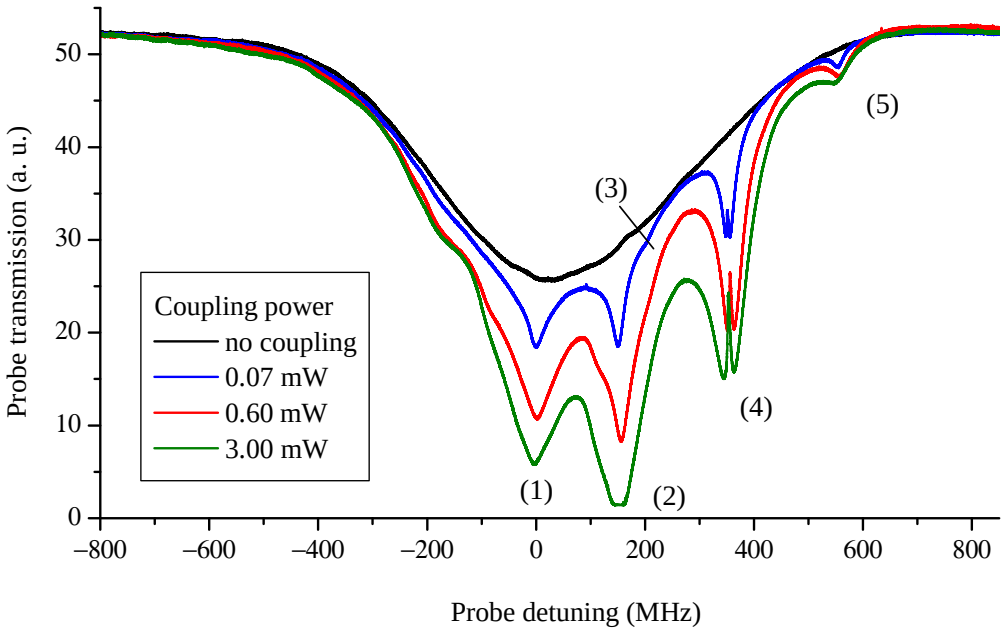

Figure 6.2.: Probe transmission for different values of coupling powers. The probe laser is scanned across the upper hyperfine states and the coupling laser is locked to the $F = 4 \rightarrow F' = 4$ transition. The enhanced absorption resonances can be identified as optical pumping as illustrated in figure 6.3. Inside resonance (4) one observes the EIT transmission peak.

Even at very small coupling powers the EIT resonance is observed inside the corresponding absorption resonance, see blue spectrum in figure 6.2 with a coupling power of 70 μW, and it becomes more pronounced with increasing coupling power. For optimized conditions it is expected that the transmission increases even above the Doppler background [42]. The width of the enhanced absorption resonances increases with increasing coupling power due to power broadening. One should note that these spectra are measured with an unlocked probe laser, which demonstrates the high frequency stability of the diode lasers.
The transparency of the EIT resonance is estimated by measuring the ratio of the EIT peak height compared to the total transmission without the EIT resonance. The probe transmission in the absence of the EIT peak is estimated by the mean value between the lowest transmission measured on both sides of the EIT resonance. This gives an underestimation of the transparency, since the enhanced absorption resonance is in fact more pronounced as it is in the presence of the EIT peak. The error is calculated by the Gaussian propagation of uncertainty. Transparencies between 12 % and 25 % could be obtained in these measurements. Its dependence on the coupling power is shown in figure 6.4. One clearly observes that the amount of transparency increases with coupling power and saturates for powers larger than 3 mW. In references [68, 69], a similar dependency was observed, although in both cases for rubidium atoms. Starting from low coupling powers, the power has to be chosen high enough so that induced coherence exceeds the decoherence rate to observe reduced absorption. At some point, increasing the coupling power only broadens the EIT resonance, but the transparency is limited by the decoherences of the system.

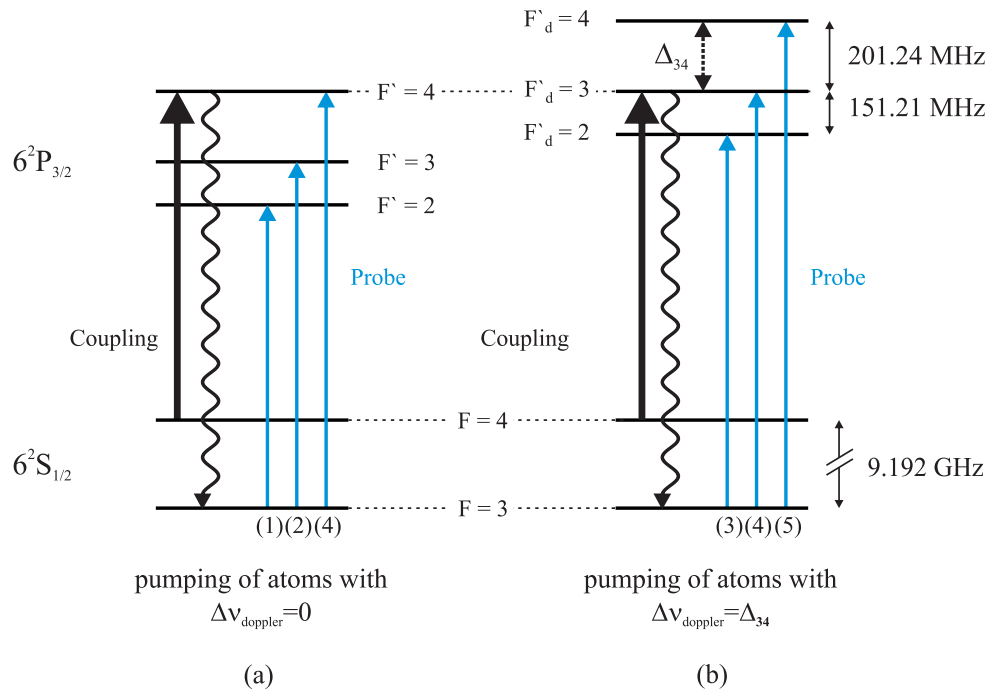

Figure 6.3.: Energy level diagram of the cesium D_2-line to illustrate optical pumping due to the coupling laser. The black arrow denotes the coupling laser, and the curly arrows indicate the spontaneous emission. The fact that the probe laser is scanned across all upper hyperfine states is indicated by the blue arrows. (a) Pumping of atoms with velocity zero via the $F' = 4$ state. (b) Pumping of atoms with a Doppler-shift $\Delta\nu_{\mathrm{doppler}} = \Delta_{34} = 201.24\,\mathrm{MHz}$.

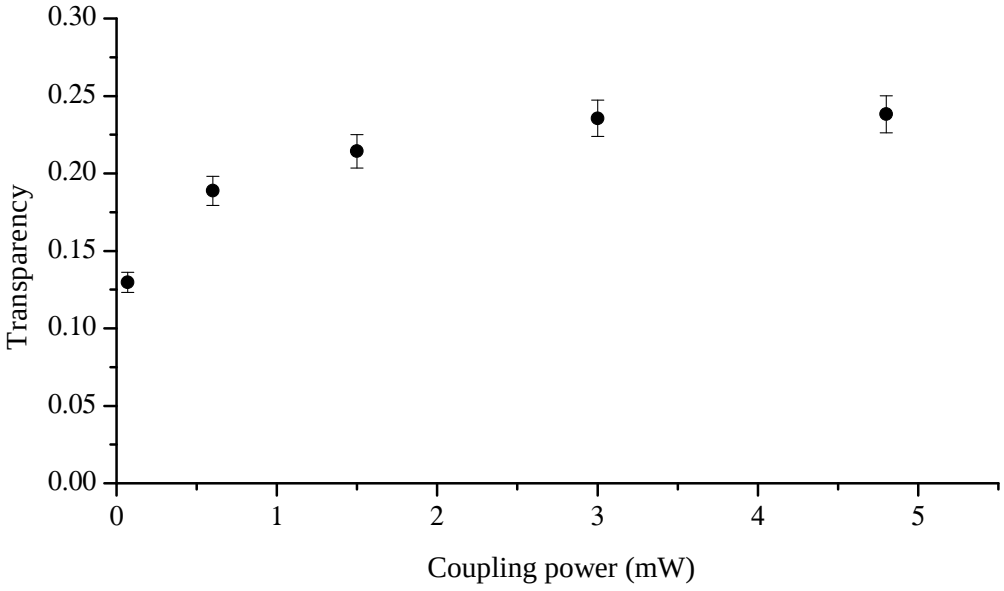

Figure 6.4.: Transparency of the EIT resonance dependent on the coupling power at a beam diameter of 1 mm and 50 μW probe power.

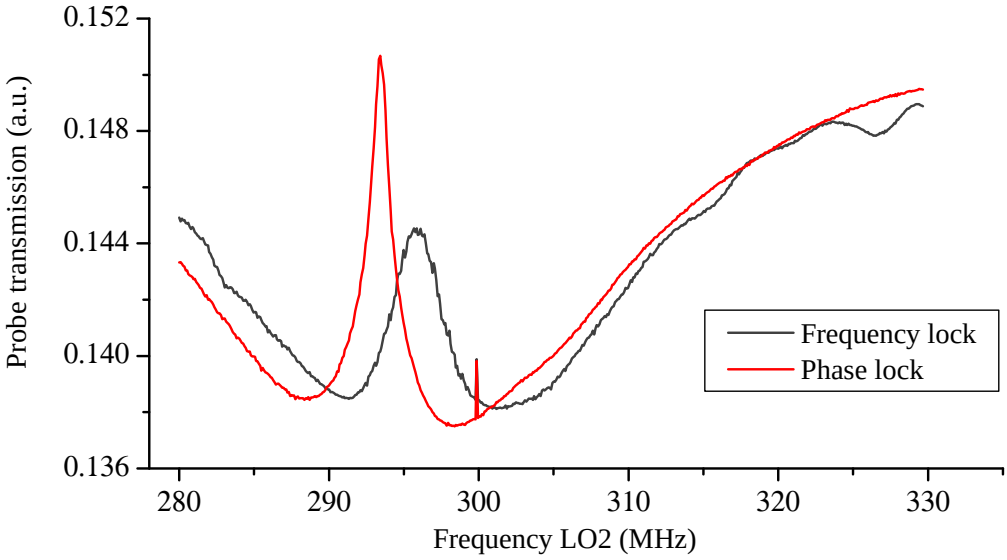

Figure 6.5.: Scan of the probe laser across the EIT resonance by scanning the local oscillator (LO2) at the phase detector input. The black spectrum shows the case that both lasers are not phase locked, whereas the red line shows the scan while the lasers are phase locked.

Measurement of the EIT linewidth using the OPLL

In order to investigate how the optical phase locked loop (OPLL) influences the EIT resonance, the probe laser is stabilized to the master laser using the OPLL described in chapter 5. To scan the frequency of the probe laser across the EIT resonance, the LO2 at the input of the phase detector, see section 5.1.2, is scanned using the stepwise sweep function of the signal generator. For the measurements performed here, the oscillator MKU LO 95 PLL is chosen as LO1, and no AOM is included in the setup. The frequency of LO2 is swept over the expected EIT resonance at 294 MHz, in the case of a resonant coupling laser, in a range from 280 MHz to 330 MHz, and the power of the probe laser is set to 50 μW.
In figure 6.5 the EIT absorption spectrum with a coupling power of 100 μW is shown. In gray line shows the spectrum when the lasers are frequency offset locked using only the slow piezo and current paths of the OPLL as explained in section 5.3.2. The second spectrum (red curve) shows the case where the lasers are phase locked including the fast feedback path. One can clearly see the strong effect of the OPLL on the EIT line shape. The OPLL causes an increase of the probe transmission by about a factor of two compared to the absorption background of the enhanced absorption resonance. In addition to the increased transmission, the width of the EIT resonance is considerably narrowed by the OPLL.
One observes that the center frequency of the EIT resonance is shifted by approximately 2.3 MHz. In the phase locked condition the EIT peak is located at an LO frequency of 293.5 MHz, whereas it is at 295.8 MHz in the frequency offset locked condition. This discrepancy could be explained by an inaccurate operation of the OPLL. A measurement supporting this assumption showed that the beat signal is locked with an offset of -1 MHz

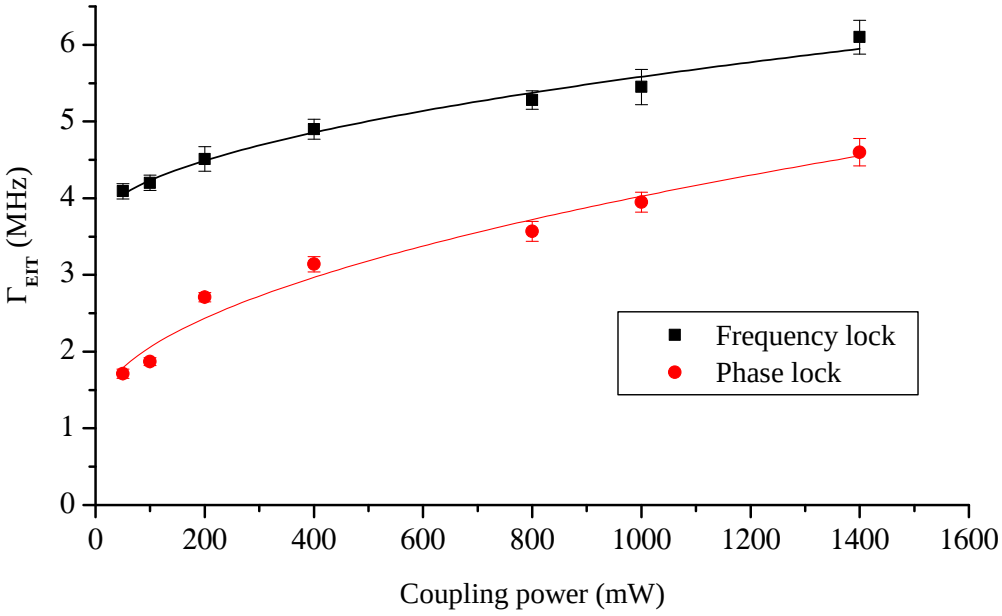

Figure 6.6.: Dependence of the EIT linewidth Γ_{EIT} on the pump power. The red dots show the obtained linewidth in the case of phase locked lasers, whereas the black squares are measured for the case that the lasers are offset frequency locked. In both cases a square root function is fitted on the data.

to the frequency set by the LO2, if the fast path is not included in the loop. Such an offset could cause the scan of the OPLL to start at a different frequency than expected and could therefore in principle account for an offset of the two EIT peaks. A further future investigation of the OPLL should resolve this issue.
The EIT transmission spectrum is measured for different coupling powers, in each case both for frequency and phase locked lasers. In order to investigate the dependency of the EIT linewidth Γ_{EIT} on the coupling power, a Lorentzian is fitted to the EIT peak. This is justified in the case of small coupling powers [66]. In figure 6.6, the dependency of Γ_{EIT} on the coupling power is shown, where the errors of the linewidth are obtained from the fit. First of all, it is observed that the EIT linewidth can be reduced by approximately 1.5 MHz using the fast feedback of the OPLL and keeping the lasers phase locked. Furthermore, in both cases the linewidth increases more rapidly at lower coupling powers.
From equation (2.51) one expects a linear dependence of Γ_{EIT} on the Rabi frequency Ω_{c}, which gives a square root dependence on the coupling power. The measured data shows a good agreement with the expected behavior, as can be seen from the fitted square root functions.

In summary, it could be shown that the optical phase locked loop is well suitable for EIT measurements on cesium atoms. Both the transparency and the linewidth of the EIT resonance could be improved by phase locking the lasers. Although there is still need for further investigations, this laser system meets all requirements to perform highly coherent spectroscopy on cesium atoms.

7. Summary and outlook

Within the scope of this thesis, a phase locked laser system at a frequency offset of 9.192 GHz corresponding to the hyperfine splitting of the cesium ground state has been successfully implemented and characterized. Such highly coherent lasers are an essential tool for future experiments on coherent spectroscopy of cesium atoms, such as electromagnetically induced transparency and slow light.

Using the technique of heterodyne optical phase locking, it was achieved to synchronize the phases of two diode lasers so that their relative phase does not vary by more than 197 mrad. The quality of the phase locked loop was characterized by measuring the beat note spectrum between the two lasers, where the residual phase noise was found to be less than $0.04\,\mathrm{rad}^2$, which is comparable to the values obtained in the literature [46, 56, 58, 63]. The linewidth of the beat signal was measured to be less than 10 Hz. The true linewidth could not be resolved due to the limited resolution of the spectrum analyzer. It was found that more than 95 % of the power are contained in the narrow carrier signal, which is the power available for coherent excitation of two-photon processes.
Using a digital phase frequency detector, a wide locking bandwidth of 2.4 MHz together with excellent phase noise suppression has been achieved. Due to the all-digital phase and frequency detection, the loop provides excellent longterm stability, a wide capture range and it can be used to scan the slave laser frequency over a wide range of several hundreds of MHz. One of the big challenges during the implementation of the phase locked loop has been the realization of the required locking bandwidth of several MHz in order to efficiently reduce the phase noise of the beat signal. Besides the phase frequency detector, the design of the fast feedback path, where one directly modulates the current of the laser diode, has been the key element in this context.
In the last part of this thesis, the applicability of the laser system for coherent spectroscopy on cesium atoms has been demonstrated by performing first experiments of EIT on cesium vapor. In these measurements it was shown that the transparency of the EIT resonance can be considerably improved by using a phase locked loop to stabilize the two lasers. It was also achieved to narrow the linewidth of the EIT signal by a factor of 2, and an EIT linewidth in the low MHz range could be measured.

Throughout the development of the laser system, several issues have been observed that could be improved in the future. The phase frequency detector which was implemented in this thesis exhibits a so far unexplained behavior at frequencies below 100 MHz which limits the scanning range of the loop. This problem can probably be solved using the evaluation board of the same detector type which was used to measure the phase detector characteristics in chapter 5.2. This could additionally avoid the problem that an offset is observed in the frequency of the beat signal when using only the slow feedback path of the loop. Furthermore, the scanning range of the lock is limited by the high pass filter in the feedback loop. Choosing a filter with a higher cut-off frequency probably allows one to expand the scanning range to more than 1 GHz.

The EIT measurements in this thesis were performed on the D_2-line in cesium. This has the disadvantage of background absorption and broadening of the EIT resonance due to the upper $F' = 2$ and $F' = 5$ hyperfine states. For future applications of EIT such as precision spectroscopy in the sub-kHz regime, it is advisable to use the D_1-line of cesium, since no such loss channels are present in this case. It should be possible without any difficulty to readjust the phase locked loop for phase locking of two different diode lasers. In principle, it is only the filter which has to be adjusted according to the specific response of the laser diode which is used as the slave laser.

The longterm goal of this laser system is to perform coherent spectroscopy on fiber-coupled cesium atoms [13]. The trapping of cold cesium atoms close to the surface of an optical nanofiber allows for direct integration of laser-cooled atoms inside optical fiber networks. The high optical density of this system makes it particular attractive for the investigation of nonlinear coherent effects such as slow light [7, 8], the storage of light pulses [9], quantum memories [10] and quantum repeater [11]. The laser system implemented in this thesis forms the basis for a variety of those applications.

A. Appendix

A.1. Cesium level diagram

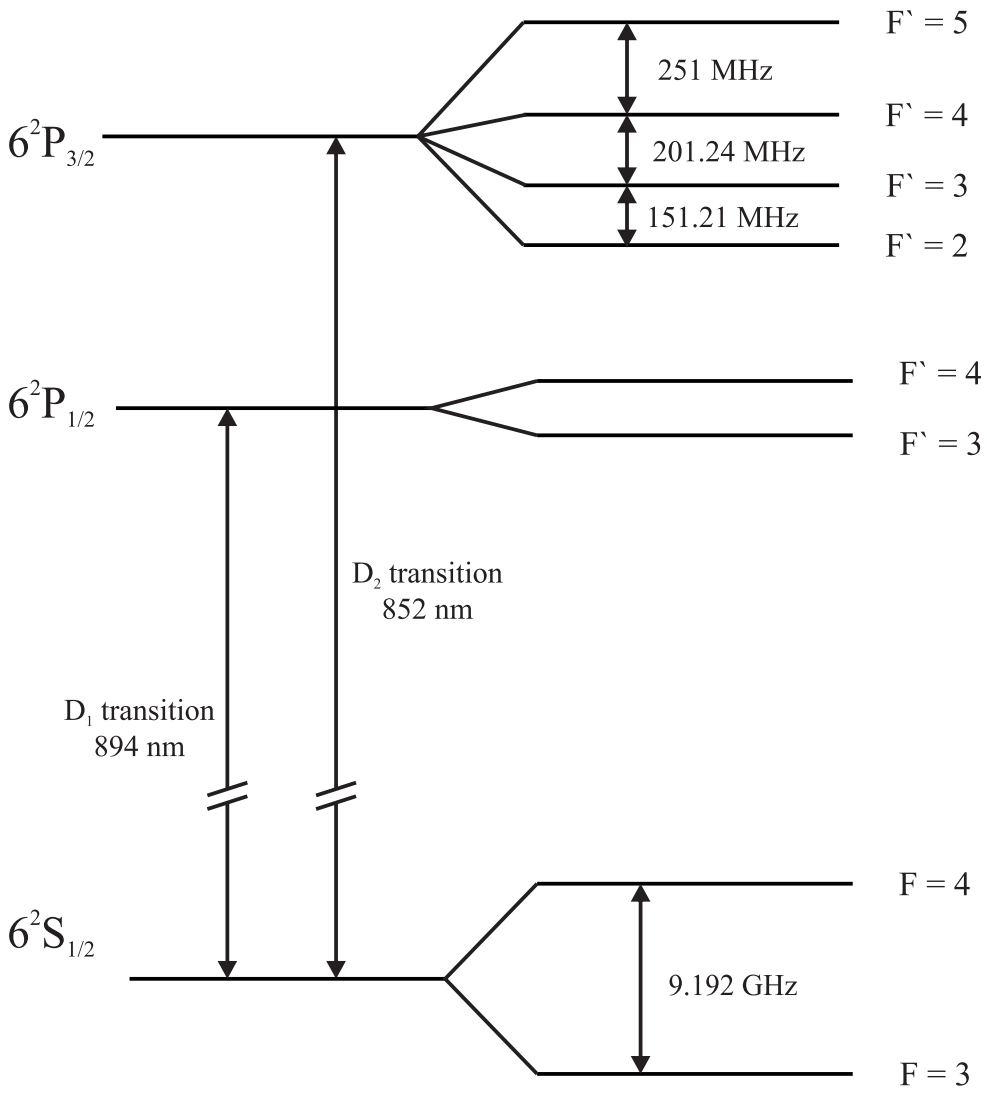

Figure A.1.: Energy level diagram of ^{133}Cs

A.2. Electrical circuits

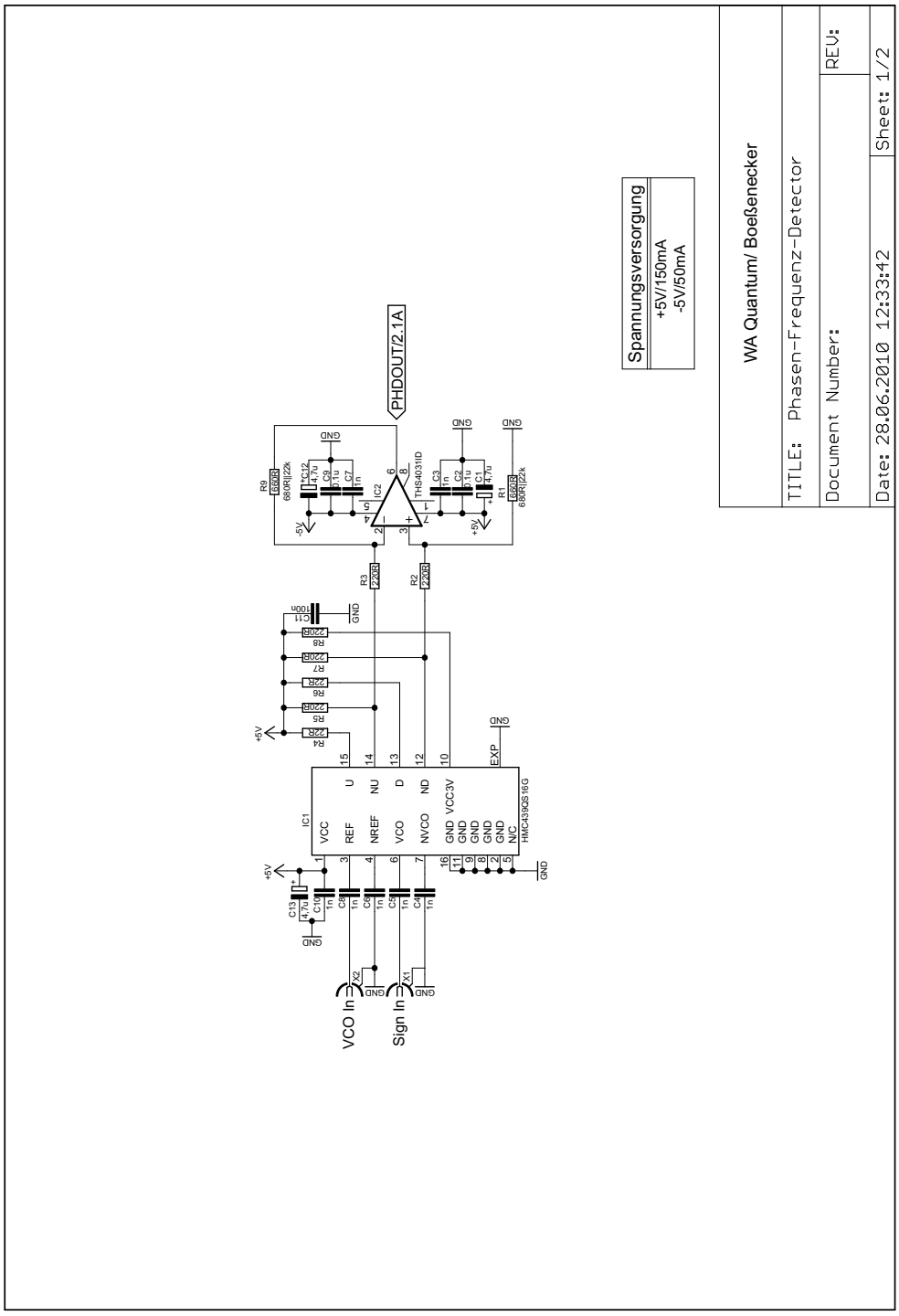

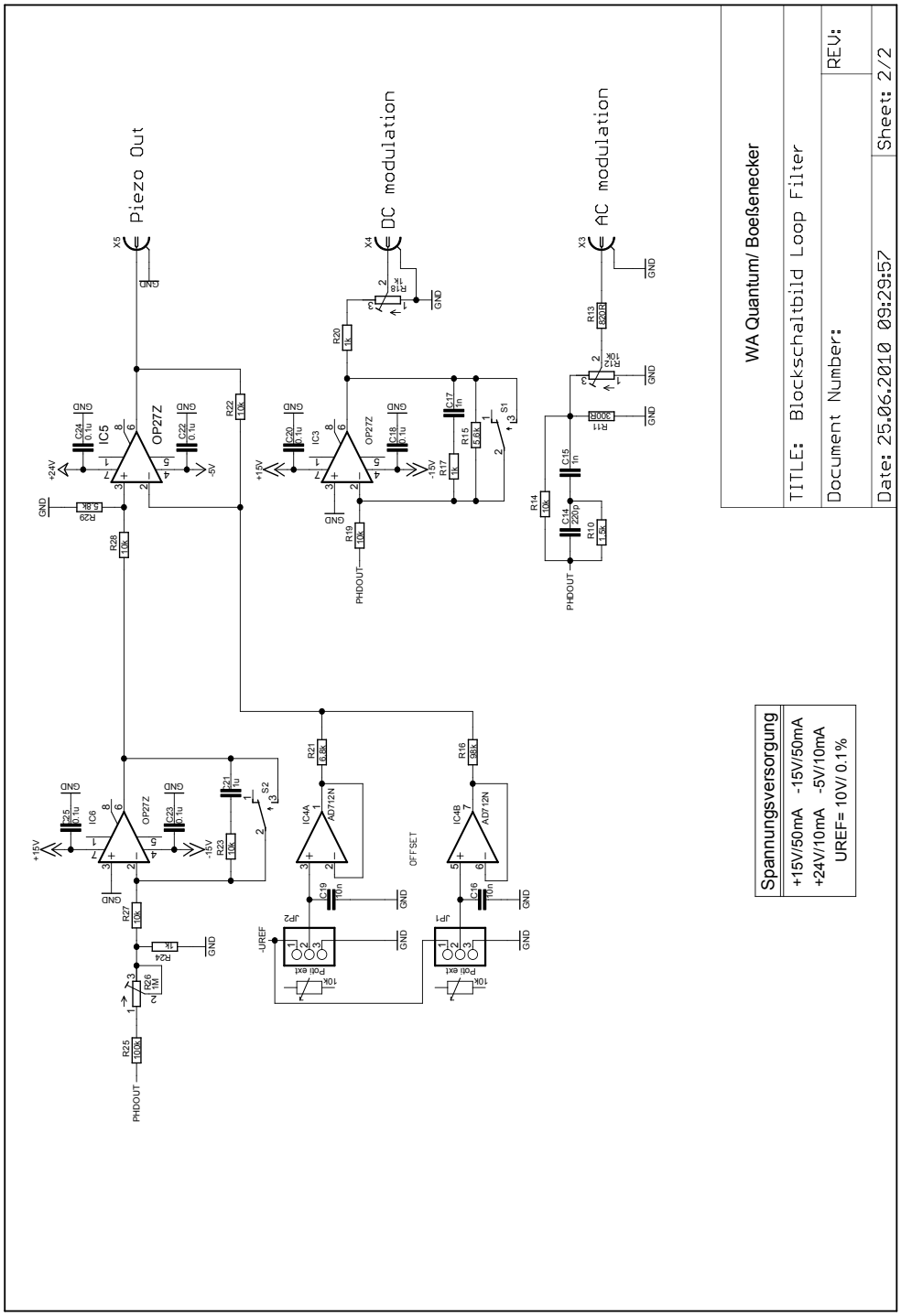
Piezo Out
DC modulation
AC modulation
X5
X4
X3
IC5
IC6
IC3
IC4A
IC4B
OP27Z
AD712N
R29 5.8k
R28 10k
R27 10k
R24 1k
R25 100k
R22 10k
R23 10k
R21 6.8k
R16 98k
R20 1k
R19 10k
R17 1k
R15 5.6k
R13 500Ω
R14 10k
R10 1.6k
C24 0.1u
C22 0.1u
C25 0.1u
C23 0.1u
C21 1u
C20 0.1u
C18 0.1u
C17 1n
C15 1n
C14 220p
C19 10n
C16 10n
S1
S2
JP1
JP2
OFFSET
-UREF
PHIDOUT
GND
+24V
-5V
+15V
-15V
WA Quantum/ Boeßenecker
TITLE: Blockschaltbild Loop Filter
Document Number:
REV:
Date: 25.06.2010 09:29:57
Sheet: 2/2
Spannungsversorgung
+15V/50mA -15V/50mA
+24V/10mA -5V/10mA
UREF= 10V/ 0.1%

Bibliography

[1] T. H. Maiman. Stimulated Optical Radiation in Ruby. *Nature*, 187:493–494, 1960.

[2] G. Alzetta, A. Gozzini, L. Moi, and G. Orriols. An Experimental Method for the Observation of R.F. Transitions and Laser Beat Resonances in Oriented Na Vapour. *Nuovo Cimento B*, 36:5–20, 1976.

[3] E. Arimondo. Coherent population trapping in laser spectroscopy. In *Progress in optics*, volume 35. Elsevier, 1996.

[4] S. E. Harris. Lasers without inversion: Interference of Lifetime-Broadened Resonances. *Phys. Rev. Lett.*, 62:1033–1036, 1989.

[5] S. E. Harris. Electromagnetically Induced Transparency. *Phys. Today*, 50:36–42, 1997.

[6] L. H. Enloe and J. L. Rodda. Laser phase locked loop. *Proc. IEEE*, 53:165–166, 1965.

[7] L. V. Hau, S. E. Harris, Z. Dutton, and C. H. Behroozi. Light speed reduction to 17 metres per second in an ultracold atomic gas. *Nature*, 397:594–598, 1999.

[8] M. M. Kash, V. A. Sautenkov, A. S. Zibrov, L. Hollberg, G. R. Welch, M. D. Lukin, Y. Rostovtsev amd E. S. Fry, and M. O. Scully. Ultraslow Group Velocity and Enhanced Nonlinear Optical Effects in a Coherently Driven Hot Atomic Gas. *Phys. Rev. Lett.*, 82:5229–5232, 1999.

[9] D. F. Phillips, A. Fleischhauer, A. Mair, R. L. Walsworth, and M. D. Lukin. Storage of Light in Atomic Vapor. *Phys. Rev. Lett.*, 86:783–786, 2001.

[10] M. Fleischhauer and M. D. Lukin. Quantum memory for photons: Dark-state polaritons. *Phys. Rev. A*, 65:022314, 2002.

[11] Z. Yuan, Y. Chen, B. Zhao, S. Chen, J. Schmiedmayer, and J. Pan. Experimental demonstration of a BDCZ quantum repeater node. *Nature*, 454:1098–1101, 2008.

[12] F. Warken. *Ultradünne Glasfasern als Werkzeug zur Kopplung von Licht und Materie*. PhD thesis, Rheinische Friedrich-Wilhelms-Universität Bonn, 2007.

[13] E. Vetsch, D. Reitz, G. Sagué, R. Schmidt, S. T. Dawkins, and A. Rauschenbeutel. Optical interface created by laser-cooled atoms trapped in the evanescent field surrounding an optical nanofiber. *Phys. Rev. Lett.*, 104:203603, 2010.

[14] F. L. Kien, V. I. Balykin, and K. Hakuta. Atom trap and waveguide using a two-color evanescent light field around a subwavelength-diameter optical fiber. *Phys. Rev. A*, 70:063403, 2004.

[15] R. Schmidt. Fangen und Speichern von neutralen Cäsium-Atomen in einer faseroptischen Dipolfalle. Diplomarbeit, Johannes Gutenberg-Universität Mainz, 2009.

[16] K. J. Boller, A. Imamoglu, and S. E. Harris. Observation of electromagnetically induced transparency. *Phys. Rev. Lett.*, 66:2593–2596, 1991.

[17] U. Fano. Effects of Configuration Interaction on Intensities and Phase Shifts. *Phys. Rev.*, 124:1866–1878, 1961.

[18] R. P. Madden and K. Codling. New Autoionizing Atomic Energy Levels in He, Ne, and Ar. *Phys. Rev. Lett.*, 10:516–518, 1963.

[19] A. Imamoglu and S. E. Harris. Lasers without inversion: interference of dressed lifetime-broadened states. *Opt. Lett.*, 14:1344–1346, 1989.

[20] S. H. Autler and C. H. Townes. Stark Effect in Rapidly Varying Fields. *Phys. Rev.*, 100:703–722, 1955.

[21] R. Wynands and A. Nagel. Precision spectroscopy with coherent dark states. *Appl. Phys. B*, 68:1–25, 1999.

[22] M. Fleischhauer, A. Imamoglu, and J. P. Marangos. Electromagnetically Induced Transparency: Optics in Coherent Media. *Rev. Mod. Phys.*, 77:633–673, 2005.

[23] M. Mücke, E. Figueroa, J. Bochmann, C. Hahn, K. Murr, S. Ritter, C. J. Villas-Boas, and G. Rempe. Electromagnetically induced transparency with single atoms in a cavity. *Nature*, 465:755–758, 2010.

[24] J. Appel, E. Figueroa, D. Korystov, M. Lobino, and A. I. Lvovsky. Quantum Memory for Squeezed Light. *Phys. Rev. Lett.*, 100:093602, 2008.

[25] M. Fleischhauer and M. D. Lukin. Dark-State Polaritons in Electromagnetically Induced Transparency. *Phys. Rev. Lett.*, 84:5094–5097, 2000.

[26] A. Yariv. *Quantum electronics.* Wiley, 3rd edition, 1989.

[27] C. Cohen-Tannoudji, J. Dupont-Roc, and G. Grynberg. *Atom-Photon Interactions.* Wiley, 1st edition, 1992.

[28] H. Lee, Y. Rostovtsev, C. J. Bednar, and A. Javan. From laser-induced line narrowing to electromagnetically induced transparency: closed system analysis. *Appl. Phys. B*, 76:33–39, 2003.

[29] N. G. Basov, O. N. Krokhin, and Y. M. Popov. Production of negative-temperature states in p-n junctions of degenerate semiconductors. *Sov. Phys. JETP*, 13:1320–1321, 1961.

[30] R. N. Hall, G. E. Fenner, J. D. Kingsley, T. J. Soltys, and R. O. Carlson. Coherent Light Emission From GaAs Junctions. *Phys. Rev. Lett.*, 9:366–368, 1962.

[31] K. Petermann. *Laser diode modulation and noise.* Springer-Verlag, 1st edition, 1991.

[32] F. Riehle. *Frequency Standards.* Wiley, 1st edition, 2004.

[33] Agilent Technologies. *Spectrum Analysis Amplitude and Frequency Modulation.* Application Note 150-1.

[34] J. Huang and L. W. Casperson. Gain and saturation in semiconductor lasers. *Opt. Quantum Electron*, 25:369–390, 1993.

[35] A. L. Schawlow and C. H. Townes. Infrared and Optical Masers. *Phys. Rev.*, 112:1940–1949, 1958.

[36] M. W. Fleming and A. Mooradian. Fundamental line broadening of single-mode (GaAl)As diode lasers. *Appl. Phys. Lett.*, 38:511–513, 1981.

[37] C. H. Henry. Theory of the Linewidth of Semiconductor Lasers. *IEEE J. Quantum Electron*, 18:259–264, 1982.

[38] G. M. Stéphan, T. T. Tam, S. Blin, P. Besnard, and M. Têtu. Laser line shape and spectral density of frequency noise. *Phys. Rev. A*, 71:043809, 2005.

[39] K. C. Harvey and C. J. Myatt. External-cavity diode laser using a grazing-incidence diffraction grating. *Opt. Lett.*, 16:910–912, 1991.

[40] C. P. Pearman, C. S. Adams, S. G. Cox, P. F. Griffin, D. A. Smith, and I. G. Hughes. Polarization spectroscopy of a closed atomic transition: applications to laser frequency locking. *J. Phys. B: At. Mol. Opt. Phys.*, 35:5141, 2002.

[41] C. Wieman and T. W. Hänsch. Doppler-Free Laser Polarization Spectroscopy. *Phys. Rev. Lett.*, 36:1170–1173, 1976.

[42] R. Wynands. Precision Spectroscopy With Coherently Coupled Lasers. Habilitationsschrift, Universität Bonn (1998).

[43] U. Tietze and Ch. Schenk. *Halbleiter-Schaltungstechnik*. Springer-Verlag, 11th edition, 1999.

[44] F. M. Gardner. *Phaselock Techniques*. Wiley, 3rd edition, 2005.

[45] M. Meyer. *Signalverarbeitung: Analoge und digitale Signale, Systeme und Filter*. Vieweg+Teubner Verlag, 5th edition, 2008.

[46] M. Prevedelli, T. Freegarde, and T. W. Hänsch. Phase locking of grating-tuned diode lasers. *Appl. Phys. B*, 60:241–248, 1995.

[47] D. R. Stephens. *Phase-locked loops for wireless communications: digital, analog, and optical implementations*. Kluwer Academic Publishers, 2nd edition, 2002.

[48] M. Zhu and J. L. Hall. Stabilization of optical phase/frequency of a laser system: application to a commercial dye laser with an external stabilizer. *J. Opt. Soc. Am. B*, 10:802–816, 1993.

[49] Maxim Integrated Products. *Clock (CLK) Jitter and Phase Noise Conversion*. Application Note 3359.

[50] D. S. Elliott, R. Roy, and S. J. Smith. Extracavity laser band-shape and bandwidth modification. *Phys. Rev. A*, 26:12–18, 1982.

[51] M. Ohtsu. *Highly coherent semiconductor lasers*. Artech House, 1st edition, 1992.

[52] L. Ricci, M. Weidemüller, T. Esslinger, A. Hemmerich, C. Zimmermann, V. Vuletic, W. König, and T. W. Hänsch. A compact grating-stabilized diode laser system for atomic physics. *Opt. Comm.*, 117:541–549, 1995.

[53] E. A. Donley, T. P. Heavner, F. Levi, M. O. Tataw, and S. R. Jefferts. Double-pass acousto-optic modulator system. *Rev. Sci. Instr.*, 76:063112, 2005.

[54] Thomas Udem. *Phasenkohaerente optische Frequenzmessungen am Wasserstoffatom. Bestimmung der Rydberg Konstanten und der 1S Lamb Verschiebung.* PhD thesis, Ludwig Maximilians Universität Muenchen, 1997.

[55] R. Paschotta. *Encyclopedia of Laser Physics and Technology.* Wiley, 1st edition, 2008.

[56] L. Cacciapuoti, M. de Angelis, M. Fattori, G. Lamporesi, T. Petelskiand, M. Prevedelli, J. Stuhler, and G. M. Tino. Analog+digital phase and frequency detector for phase locking of diode lasers. *Rev. Sci. Instr.*, 76:05311, 2005.

[57] R. E. Best. *Phase-Locked Loops: Design, Simulation, and Applications.* McGraw-Hill Professional, 6th edition, 2007.

[58] J. Appel, A. MacRae, and A. I. Lvovsky. A versatile digital GHz phase lock for external cavity diode lasers. *Meas. Sci. Technol.*, 20:0553302, 2009.

[59] Paul Shockman. *Phase Lock Loop General Operations.* On Semiconductor. Application Note AND8040/D.

[60] J. J. Olivero and R. L. Longbothuma. Empirical fits to the Voigt line width: A brief review. *J. Quant. Spectrosc. Radiat. Transfer*, 17:233–236, 1977.

[61] A. N. Luiten. *Frequency measurement and control: advanced techniques and future trends.* Springer-Verlag, 1st edition, 2001.

[62] H. R. Telle. *Absolute Measurement of Optical Frequencies in Frequency Control of Semiconductor Lasers.* Wiley, 1st edition, 1996.

[63] D. Höckel, M. Scholz, and O. Benson. A robust phase-locked diode laser system for EIT experiments. *Appl. Phys. B*, 94:429–435, 2009.

[64] D. A. Steck. *Caesium D line data.* http://steck.us/alkalidata/, 2009.

[65] W. Demtröder. *Laser spectroscopy: Experimental techniques.* Springer-Verlag, 4th edition, 2008.

[66] E. Figueroa, F. Vewinger, J. Appel, and A. I. Lvovsky. Decoherence of electromagnetically induced transparency in atomic vapor. *Opt. Lett.*, 31:2625–2627, 2006.

[67] P. R. S. Carvalho, L. E. E. de Araujo, and J. W. R. Tabosa. Angular dependence of an electromagnetically induced transparency resonance in a Doppler-broadened atomic vapor. *Phys. Rev. A*, 70:063818, 2004.

[68] B. Lü, W. H. Burkett, and M. Xiao. Electromagnetically induced transparency with variable coupling-laser linewidth. *Phys. Rev. A*, 56:976–979, 1997.

[69] X. Feng, G. Rui-Min, C. Shuai, Z. Yu, L. Lu-Ming, and C. Xu-Zong. Observation of Electromagnetically Induced Transparency in a Zeeman-Sublevel System in Rubidium Atomic Vapour. *Chin. Phys. Lett.*, 20:1257–1260, 2003.

Danksagung

An dieser Stelle möchte ich die Gelegenheit nutzen mich bei all denjenigen zu bedanken, die zum Gelingen dieser Diplomarbeit beigetragen haben und die mich in meiner Zeit als Diplomandin unterstützt haben. In dem Jahr in der Gruppe von Arno Rauschenbeutel konnte ich viele wertvolle Erfahrungen auf dem Gebiet der Quantenoptik sammeln, wobei die angenehmen Arbeitsbedingungen das eigenständige Experimentieren wesentlich erleichterten. Durch das freundschaftliche Arbeitsklima in der Gruppe bin ich auch zu Zeiten, in denen nicht alles so funktionierte wie geplant, immer wieder gerne zur Arbeit gekommen.

Allen voran danke ich Prof. Arno Rauschenbeutel für die Aufnahme in seine Gruppe und die Vergabe des interessanten Themas, wodurch er mir die Arbeit an einem überaus spannenden Forschungsprojekt ermöglichte. Weiterhin danke ich Klaus Wendt dafür, dass er sich die Zeit nahm das Zweitgutachten für diese Arbeit zu erstellen.
Ein großer Dank gilt meinen Betreuern und Kollegen Daniel Reitz, Samuel Dawkins, Rudolf Mitsch und Eugen Vetsch, die mir während des letzten Jahres immer mit wertvollen Tipps und Ratschlägen zur Seite standen. Meinem Doktoranden Daniel danke ich hierbei besonders für die tolle Einweisung in die experimentellen Grundlagen der Quantenoptik, insbesondere in der schwierigen Anfangsphase, in der er immer ein offenes Ohr für meine Fragen hatte. Unserem Postdoc Sam möchte ich vor allem für die tatkräftige Unterstützung bei der Realisierung der Phasenregelung danken. Die vielzähligen Diskussionen mit Sam haben mir immer wieder neue Denkanstösse gegeben und so wesentlich zum Gelingen des Phasenregelkreises beigetragen.
Für das Korrekturlesen meiner Arbeit möchte ich mich ebenfalls bei Daniel, Rudi und Sam bedanken, und besonders bei Sam für die hilfreichen Hinweise, wenn mal ein englisches Wort zu offensichtlich in Leo nachgeschaut wurde. Weiterhin möchte ich auch Ariane Stiebeiner für die Korrektur des letzten Kapitels danken, bei dem sie mir mit hilfreichen Tipps in der nervenaufreibenden letzten Nacht zur Seite stand. In diesem Zusammenhang danke ich auch Sebastian und Daniel für das „Händchenhalten" in den letzten Tagen vor der Abgabe, sowie Christian Hauswald für den gegenseitigen Beistand in den stressigen Wochen des Zusammenschreibens.
Den restlichen Rauschis möchte ich für ein Arbeitsklima danken, das ich in Zukunft sehr vermissen werde, ebenso wie die zahlreichen Kuchen, der nicht wegzudenkende Kaffee nach der Mittagspause und die schönen Kinoabende.
Weiterhin bedanke ich mich bei Christine Best und Elvira Stuck-Kerth für die gute Betreuung in allen organisatorischen Anliegen, mit denen ich während meiner Arbeit konfrontiert wurde. Auch geht ein besonderer Dank an unseren Elektroniker Michael Boeßenecker für die Unterstützung bei der Realisierung der elektrischen Schaltungen. Herrn Lenk möchte ich außerdem für die stetige Hilfe danken, wenn mal wieder eine unbeantwortete Frage zur Elektronik in meinem Kopf schwirrte, sowie für die Bereitstellung des Netzwerkanalysators und anderer diverser kleiner Hilfsmittel, die meine Arbeit im Labor erleichterten.
Auch gruppenübergreifend bin ich stets auf freundliche Unterstützung gestoßen. So möchte ich der Elektronengruppe von Herwig Ott danken für die sofortige Bereitstellung von

Bauteilen für meinen Diodenlaser, als dieser versehentlich in Wärmeleitpaste ertrank. Weiterhin danke ich Stefan Ulmer aus der AG Walz für die Hilfe mit Labview und dem Auslesen des NWA. Auch geht ein besonderer Dank an Prof. Oliver Benson und David Höckel dafür, dass ich ihre Gruppe in Berlin besuchen durfte, wodurch ich mit neuer Motivation an meinem Projekt weiterarbeiten konnte. Ein besonderer Dank gilt auch Jürgen Appel für seine hilfreichen Ratschläge bei meinen ersten EIT-Messungen.
Zu guter Letzt danke ich meiner Familie, meinem Freund Sebastian, meiner WG und meinen Freunden für die zahlreiche Unterstützung während des letzten Jahres. Allen voran danke ich meinen Eltern dafür, dass sie mir durch ihre, nicht nur finanzielle, Unterstützung das Studium ermöglicht haben. Insbesondere möchte ich meiner Mutter und auch meiner Schwester Christine danken, dass sie immer ein offenes Ohr für mich hatten. Ein besonderer Dank gilt auch Sebastian für sein Verständnis und seine Geduld, wenn es mal wieder etwas später wurde im Labor und wir uns nicht so oft sehen konnten, und für die vielen lieben Aufmunterungen in schwierigeren Phasen des letzten Jahres.